THE UNIVERSITY
of EDINBURGH

Raman Studies on Hot Dense Hydrogen

Philip Dalladay-Simpson

A thesis submitted in fulfilment of the requirements
for the degree of Doctor of Philosophy
to the
University of Edinburgh

February 2016

Abstract

The study of hydrogen and the understanding of its response to extended pressure and temperatures is of great importance due to its significant universal abundance. Hydrogen is currently not well understood in these extended regimes due to it being inherently difficult to work with experimentally as well as having a poor response to a wide range of diagnostics. Consequently, there have been long standing predicted phenomena which still remain experimentally elusive: (1) melting driven by large zero point oscillations [Brovman 72] and (2) adopting a purely atomic state at higher pressures [Wigner 35].

Coupling high-pressure, high-temperature techniques with *in-situ* optical diagnostics, the stability of the solid phases of hydrogen were evaluated over an extended pressure-temperature regime. The first ever H_2 solid-solid transitions above 300 K are reported and the evolution of the I-IV phase line after the III-IV-I triple point is constrained. A transition which could be attributed to melting is observed at 480 K and 225 GPa, the lowest known melting temperature for any material under these conditions. A new triple point between phase I-IV-Liquid is identified, the third known triple point in the phase diagram and the first on the melting curve. The possible continuations of the melting line are discussed, ultimately revising the melting transition at 300 K and at 0 K to much higher pressures than previously thought [Bonev 04].

The contributing work also marks a new high pressure achievement, obtaining some of the highest ever recorded static pressures in the laboratory. Hydrogen and its heavier isotopes hydrogen deuteride and deuterium were compressed to pressures of 384 GPa, 388 GPa and 380 GPa respectively. These experimental data are indicative that above 325 GPa H_2 and HD adopt a new solid phase, phase V. Analysis of the spectra over the IV-V transition is suggestive that under

compression the molecular bonding in the G-layers of the *Pc* structure lengthen and symmetrise, evolving into the *Ibam* structure. It is speculated that this phase could be a precursor to the elusive, purely atomic $I4_1/amd$ structure predicted to be stable at higher pressures (>400 GPa) [McMahon 11, Azadi 14].

Declaration

Except where otherwise stated, the research undertaken in this thesis was the unaided work of the author. Where the work was done in collaboration with others, a significant contribution was made by the author.

P. Dalladay-Simpson

June 2015

Acknowledgements

I would like to record my thanks to all those who have helped me in the course of this work. In particular, the following:

Prof. E. G. Gregoryanz for introducing me to the field of high-pressure and his next to constant availability for guidance, assistance, encouragement, and occasional outings on the bike.

Dr. R. T. Howie and Dr. C. Guillaume for their encouragement and guidance through the good and the bad and for their unfaultering patience in mentoring me in the tricks of the trade.

M. Frost for experimental assistance in the laboratory and companionship at conferences.

To the technical staff at the University of Edinburgh, who without which a lot of the experiments conducting in the contributing work could not be realised.

To EPSRC and the CM-CDT for financial support.

and to my parents, for their unfailing love, encouragement and support throughout and to whom this thesis is dedicated.

Contents

List of Figures

Chapter 1

Introduction

1.1 Introduction and motivation

Hydrogen, the universe's simplest and most abundant elemental configuration exists in vastly different environmental (pressure-temperature-volume) conditions. Varying from the cold vacuum of space to the heart of giant astrophysical structures such as the Jovian planets ($\sim$ 4x10^4 K and $\sim$4 TPa [Elkins-Tanton 06]). Since hydrogen's discovery by Robert Boyle in 1671, it has been very well characterised at ambient terrestrial conditions as a flammable colourless gas finding its place at the head of the periodic table. Ambient conditions however are a seemingly unique environment for hydrogen to exist, as with all matter, it is more commonly found in a much hotter denser state. It is therefore paramount to understand a material's response, particularly hydrogen, to these extended pressure-temperature conditions, to have a clearer understanding of the structures and phenomena present throughout the universe.

As a thermodynamic parameter, pressure has already unveiled a wealth of new physics from the emergence of electride structures, turning metals into insulators [Ma 09], extreme complexity [Loa 12] and - quite recently - high temperature superconductivity [Drozdov 15]. Hydrogen is also believed to have a remarkable response to pressure and it has long been theorised to undergo pressure-induced melting [Brovman 72] and metallisation [Wigner 35] perhaps even concomitantly. There has also been theoretical evidence that metallic hydrogen may represent a

completely novel state of matter, which could display rich properties such as high T_c superconductivity and superfluidity depending on the magnetic fields applied [Babaev 05, Babaev 04, Ashcroft 68].

The narrative in achieving metallic properties in hydrogen is perhaps best reflected by the endeavors made by the great experimentalists of the 19^{th} century in attempts to liquefy the same system. The liquefication of hydrogen, dubbed by James Dewar as"Mount Hydrogen," [Dewar 01] was a considerable challenge of its time. Largely due to the existing technological limitations in reaching the low temperatures required, coupled with hydrogen being an experimental nuisance. The endeavors however were not in vain and contributed to the discovery of fascinating phenomena such as the dissapationless flow of matter [Kapitza 38] and electricity [Onnes 11] in the early 20^{th} Century. Just like its liquification, the metalisation of hydrogen has also proven to be experimentally challenging. For 80 years and despite significant developments in the field high pressure achieving ever-higher compressions, notably with the invention of the Diamond Anvil Cell (DAC) in the 60s [Weir 63, Weir 59], the existence of this phase still remains experimentally unconfirmed, thus making it the "Mount Hydrogen" of modern times.

Conventionally a material's melting temperature is found to increase in response to increasing pressure, first experimentally realised by Perkins in 1826 observing the crystallisation of acetic acid (the main component of vinegar) around 1 kbar at room temperature [Perkins 26]. Although a typical response, some systems can exhibit constrasting behaviour famously shown by two prominent scientists of the 19th century, Lord Kelvin and Faraday, observing that water could melt purely by compression alone [Thomson 50, Faraday 59]. Hydrogen, is also believed to be in this renegade group of systems, exhibiting a falling melting temperature with increasing pressure, the nature however is drastically different to that seen in water. Abrikosov in 1960 proposed a mechanism in which pressure could enhance the zero-point motion so that it would be sufficient in destabilising any crystalline phase. A mechanism that could be particularly pronounced in hydrogen, due to its light mass, resulting in very unusual melting characteristics such as melting at 0K [Brovman 72].

Recent endeavors to reach the elusive previously described states within

hydrogen have largely been unsuccessful, perhaps - if he was still alive - invoking Dewar's greatest sympathies. The effort however has not been in vain and has produced novel, surprising and highly motivating phenomena. Recent experimental investigations up to 310 GPa and at room temperature [Howie 12a, Eremets 11], a significant improvement on the existing experimental limits ($\sim$ 180 GPa [Baer 07, Baer 09]), resulted in the discovery of a new phase, phase IV [Howie 12a]. Perhaps the most interesting property of phase IV is that its rich vibrational structure is indicative of two very distinct bonding environments. With a wonderful interplay of theoretical structure searching and direct experimental insight, the rich vibrational characteristics were finally attributed to a "mixed" *Pc* structure consisting of alternating weakly and strongly bonded layers. With the discovery of this new phase came a new narrative of metalisation in hydrogen; perhaps instead direct tranistion from a molecular to a monatomic state there could be intermediary phases which possess a degree of both.

The objectives of the contributing work is to conduct high temperature measurements on the Hydrogen system to: (1) constrain and extend our current understand of its melt line, (2) Assess the possibility of the evolution of phase IV into a fully metallic state at higher pressures. All whilst simultaneously putting De Beers famous slogan,"A diamond is forever" to the test.

Chapter 2

Raman Spectroscopy

2.1 Introduction to Optical Diagnostics

Optical diagnostics have become prolific in modern day research and a vast range of the electromagnetic spectrum has found application in some kind of diagnostic or experimental technique. A review of some relevant light-matter interactions are presented in figure 2.1 from microwaves up to the ultraviolet, however spectroscopies do exist over a much wider range (for example X-ray spectroscopy for analyses of electronic structures). It is clear from figure 2.1 that as the photon energy increases, we probe more energetic excitations in the system, beginning from rotational modes up to electronic excitations.

Great success has been made in the field of structure refinement of solids at high pressures using x-rays, however due to H_2's low number of valence electrons, its scattering cross section is heavily reduced and therefore is limited to studies in which thicker lower pressure samples are used <150 GPa [Akahama 10c, Akahama 10a, Loubeyre 96]. H_2 is also unfavourable for microwave and infrared measurements at low pressures because of the absence of a permanent molecular dipole, however its infrared activity significantly increases at higher pressures suggesting a modification in the intermolecular bonding and electronic distribution.

The electromagnetic regime which has had the most success to date in exploring H_2 under extended P-T conditions is visible light corresponding to the Raman scattering mechanisms 2.1. This light-matter interaction is composed of

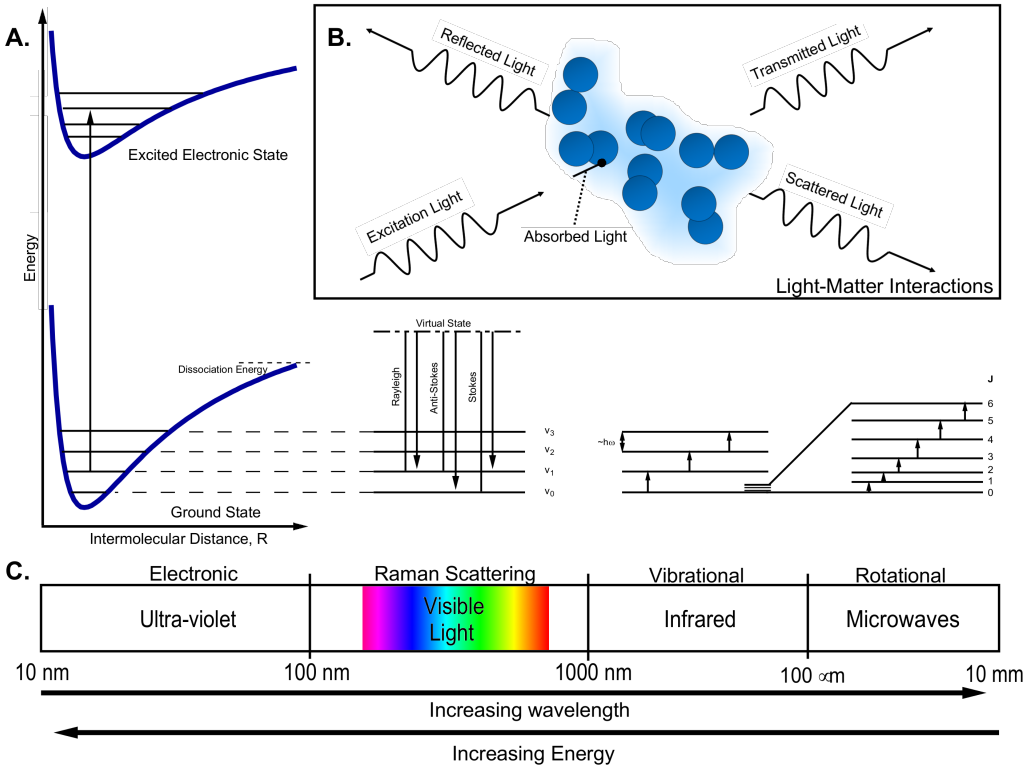

Figure 2.1: **(A)** Schematics of a range of excitations: electronic, Raman, vibrational and rotational. Corresponding to the light-matter interactions **(B)** of different regions of the electromagnetic spectrum **(C)**

both elastic (Rayleigh) and inelastic (Stokes, anti-Stokes) scattering phenomena via the transition through a virtual state figure 2.1A. Analysis of these signals can give information about both about characteristic vibrational and rotational structure of a system, and therefore also can allude to molecular arrangements in solid structures and consequently being considerably sensitive to phase transitions.

As Raman Spectroscopy was the main diagnostic in the contributing work the proceeding chapters 2.2, 2.3 and 2.4 will serve as a theoretical and experimental review.

2.2 Classical Theory of Raman Spectroscopy

The first theoretical treatment for the Raman process was conducted by Smekel in 1923 [Smekal 23], the first physical evidence however was found independently in 1928 by two groups: Raman and Krishnan in India [Raman 28a, Raman 28b]; Mandelshtam and Landsberg in Russia [Landsberg 28]. Since, it has been the first author of the former group which has recieved most of the credit, including being the sole recipient of the Nobel Prize for the discovery as well as his name being attributted to the phenomenon. Initially Raman spectroscopy was solely a specialist technique providing a testing ground for quantum theories when applied to molecules, as seen by the first reported image plate of Hydrogen by Rasetti in 1929 [Rasetti 29] 2.3B experimentally confirming calculated frequencies characteristic of the hydrogen molecule [Hill 29]. Although a significant experimental challenge at the time, discussed in the next chapter, Raman spectroscopy has since become a prolific routine tool in condensed matter science and an essential pioneering diagnostic for the H_2 system in extended P-T regimes.

In this chapter we will provide some theoretical mechanics of the Raman process. Firstly in a semi-classical framework providing a more intuitive explanation and concluding with the limits of this approach, where instead a simple quantum mechanical picture can be employed.

We start our description from the most applicable and also perhaps the simplest model, a homonuclear symmetric molecular system; real world examples being H_2, O_2 and N_2. These molecules possess no permanent dipoles and therefore vibrational spectroscopy using infra-red radiation is forbidden. Raman spectroscopy therefore is the only viable method to determine their vibrational structures, however this may not always be the case in extended pressure regimes.

Initially we consider a molecular system not undergoing any vibrations or rotations in an applied quickly alternating electric, ie. visible light. In this situation there is a negligible nuclear response to the alternating electric field due to the large inertia of the nuclei. The electric orbtials however can undergo modification and hence the induced polarisation given by.

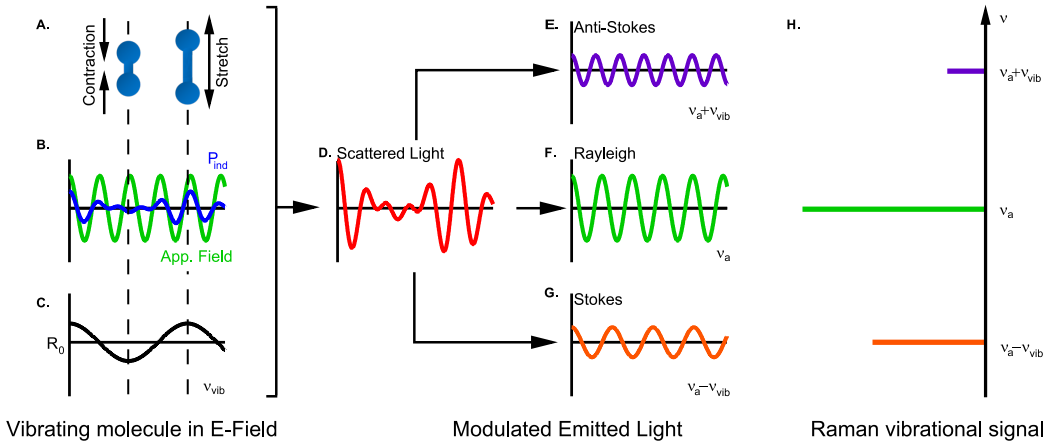

Figure 2.2: A representative cartoon illustrating the vibrational mode of the H_2 molecule **(A)** with the change in intermolecular spacing **(C)**. The induced polarisation described in equation 2.7 in an applied electric field is shown by **(B)**. **(D)** respresents a scattered signal which itself is composed of the superposition of three characteristic frequencies: **(E)** Anti-Stokes, **(F)** Rayliegh, **(G)** Stokes. **(H)** Is a cartoon of the signal which would be observed using Fourier-Transform (FT) spectroscopic techniques seen in figure 2.3B and C.

$$P_{ind} = \alpha E \tag{2.1}$$

Where α is the polarisation matrix of the molecule and E is the applied electric field. As the applied electric feild is oscillatory the induced dipole will be a function of the applied frequency ν_a seen in figure 2.2 B and 2.2.

$$P_{ind} = \alpha E_0 cos(2\pi\nu_a t) \tag{2.2}$$

So far we have assumed the polarisation to be independent of the bond length in our molecule. To include the dependency on changes in the bond length, ie. molecular vibrations, we must take a Taylor series expansion of α around the equiblibrium position.

$$\alpha(R) = \alpha(R_0) + \frac{d\alpha}{dR}|_{R_0}\Delta R + H.O.T \tag{2.3}$$

Next we want to include the eigenfrequencies of the molecule, primarily the

natural frequency of the molecular motion ν_{vib} represented in figure 2.2 A and C. Which to the first approximation can be calculated as a harmonic oscillator.

$$\Delta R = ACos(2\pi\nu_{vib}t) \tag{2.4}$$

Taking equation 2.4 and 2.3 and subsituting into 2.2 we obtain the time-dependent form of the polarisation which takes into account the change of polarisability from the molecular vibrations 2.5.

$$P_{ind}(t) = \left[\alpha(R_0) + \left.\frac{d\alpha}{dR}\right|_{R_0} (ACos(2\pi\nu_{vib}t)\right] E_0 Cos(2\pi\nu_{vib}t) \tag{2.5}$$

Therefore using the following trigometric identity equation 2.6 on the above expression equation 2.5.

$$Cos(A)Cos(B) = \frac{1}{2}[Cos(A+B) + Cos(A-B)] \tag{2.6}$$

Results in the following equation.

$$P_{ind}(t) = \alpha(R_0)E_0Cos(2\pi\nu_{vib}t) + \left.\frac{d\alpha}{dR}\right|_{R_0} AE_0[Cos(2\pi(\nu_a - \nu_{vib}t) + Cos(2\pi(\nu_a + \nu_{vib}t)] \tag{2.7}$$

From the above expression, it can be seen that the modulated scattered signal 2.2 D, which is a response to the induced polarisation $P_{ind}(t)$, is composed of three characteristic frequencies. Firstly, the unperturbed Rayleigh component resulting in a frequency corresponding the applied electric field ν_a, seen in 2.2 F and H, expressed below as:

$$P_{Ray} = \alpha(R_0)E_0Cos(2\pi\nu_{vib}t) \tag{2.8}$$

Secondly, two sidebands: P_{Stokes} - equation 2.9 and $P_{Anti-Stokes}$ - equation 2.10 oscillating at frequencies known as the Raman shift $\nu_{Anti-Stokes/Stokes} = \nu_a \pm \nu_{vib}$ (figure 2.2 E and G).

$$P_{Stokes} = \left.\frac{d\alpha}{dR}\right|_{R_0} AE_0[Cos(2\pi(\nu_a - \nu_{vib}t)] \tag{2.9}$$

$$P_{Anti-Stokes} = \left.\frac{d\alpha}{dR}\right|_{R_0} AE_0[Cos(2\pi(\nu_a + \nu_{vib}t)] \tag{2.10}$$

These simple arguments really demonstrate the power of the Raman process as an experimental diagnostic, that via these mechanisms natural properties of the system (such as vibrational characteristics) can be encoded into the scattered light. The overall modulated signal (figure 2.2D) is therefore decomposed using Fourier-Transform (FT) spectrometry techniques, discussed in chapter 2.4, resulting in a signal represented in figure 2.2H with peaks corresponding to the frequency of the applied electric field as well as the vibrational characteristics of the molecule.

2.3 A Simple Quantum Mechanical Interpretation of Raman Spectra

Although the classical description presented in the previous chapter describes a lot of the observations in the Raman scattering process, it does however fail to correctly determine the intensities of the excitations or the quantum nature of the rotational excitations.

A pictorial description of the quantum nature of the Raman scattering process is shown in figure 2.1A and 2.3A(iii). The description is of a two photon process, where an initial photon is absorbed and elevates the system to an intermediate virtual state. Then a secondary photon is emitted and the system relaxes. As a result the emitted photon is shifted in energy relative to the incident by an amount corresponding to the net change in energy of the system. This process results in three scattering mechanisms described previously classically: Rayleigh, Anti-Stokes and Stokes scattering (figure 2.2H).

- **Rayleigh:** An elastic scattering mechanism in which the vibrational state of the system remains unchanged through the scattering process (V_1 ->V_1),

and therefore the energy of the scattered photon remains the same as the incident ie. $\nu_{Ray} = \nu_a$

- **Anti-Stokes:** An inelastic scattering mechanism in which the system is returned to a lower vibrational state (V_1 ->V_0) resulting in a more energetic scattered photon (Fig. 2.3 Aiii). $\nu_{Anti-Stokes} = \nu_a + \nu_{vib}$
- **Stokes:** The reverse mechanism to the Anti-Stokes in which the system is returned to a higher vibrational state (V_1 ->V_2) emitting a lower energy scattered photon. $\nu_{Stokes} = \nu_a - \nu_{vib}$

The relative intensities of the anti-Stokes to Stokes scattering are dependent upon the occupation of the vibrational states and dictated by a Boltzman distribution. Using equation 2.11 [Herzberg 60, Haken 95] and using $\nu_{vib} = \nu_{H_2} = 4100\text{cm}^{-1} = 1.32\text{x}10^{14}$ Hz at room temperature the relative intensity of anti-Stokes to Stokes is $\sim 7\text{x}10^{-10}$ (e^{-21}). The contribution of anti-Stokes scattering is therefore negligible at room temperature compared to the Stokes contribution for H_2 and will further diminish at lower temperatures as more molecules relax into the lower energy vibrational states. Therefore all spectrometers during the contributing experiments were configured to purely collect spectra from the Stokes mechanism (negative Raman shifts) as seen in figure 2.3C and 2.2H.

$$\frac{I_{Anti-Stokes}}{I_{Stokes}} = \frac{n(V_1)}{n(V_0)} = e^{-\frac{h\nu_{vib}}{KT}} \tag{2.11}$$

2.3.1 Rotational Structure and the Influence of Nuclear Spins

If again we refer to the spectra obtained experimentally figure 2.3 B and C it is evident that we have not accounted for all the Raman active excitations observed. We're missing the multitude of evenly spaced excitations seen at lower frequencies (<1300 rel. cm^{-1}), which are H_2's rotational modes. Typically these modes are an order of magnitude less energetic than the molecule's vibrational mode and as such, if the molecule possesses a permanent dipole their rotational structure can be observed directly through the use of longer wavelength microwave radiation seen in figure 2.1.

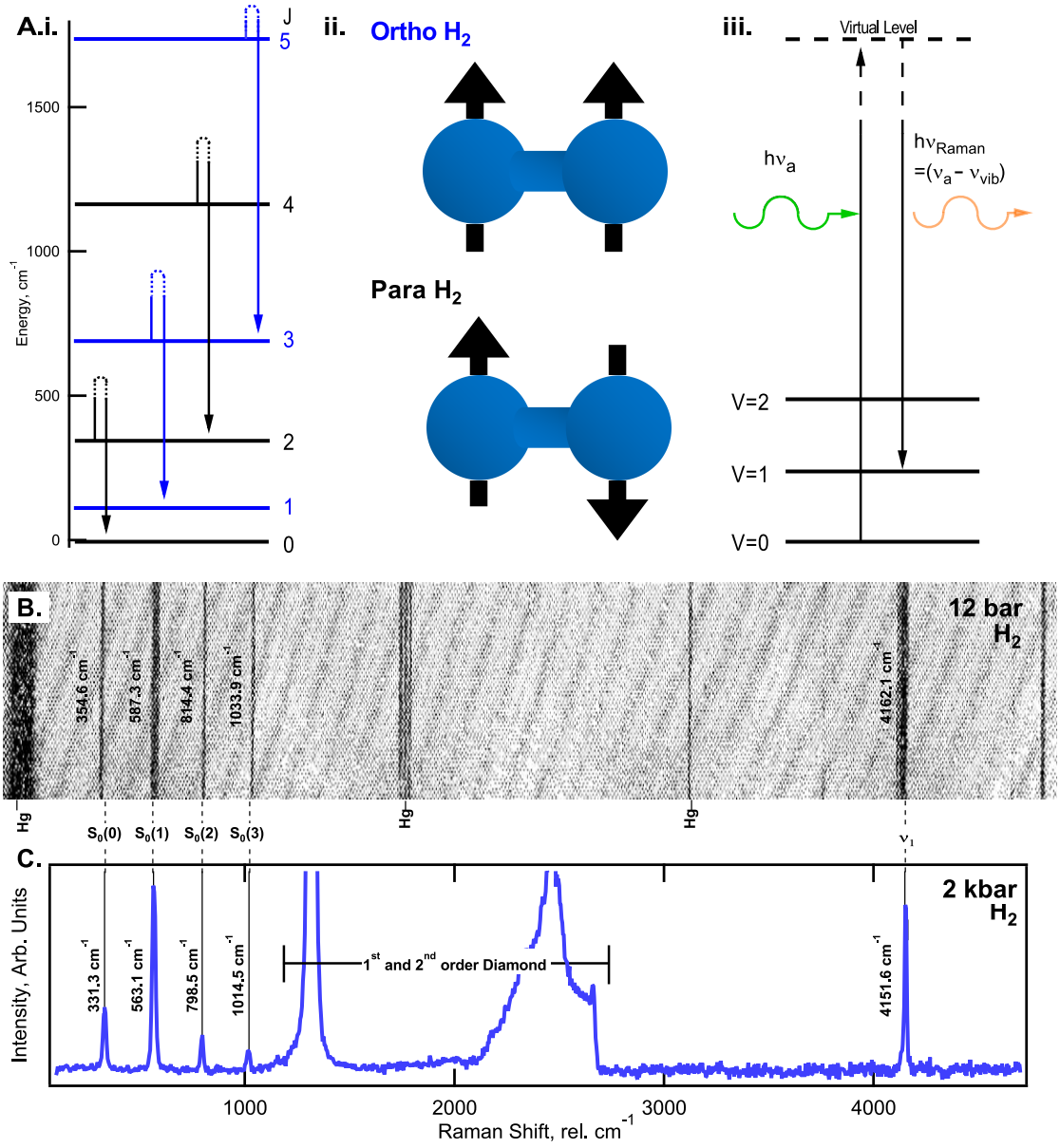

Figure 2.3: **(A)** (i)The allowed rotational transitions for a Hydrogen molecule, blue represent the allowed states for o-H_2 and black for p-H_2 [Mao 94]. (ii) A representative cartoon of the nuclear spin states of a hydrogen molecule. (iii) A representative schematic depicting the quantum picture of the anti-stokes component of the Raman scattering process. **(B)** The first reported image plate taken of the Raman spectra of H_2 [Rasetti 29]. **(C)** A contemporary representative Raman spectrum taken of H_2 in a DAC, with the setup described in chapter 2.4.

Similar to the vibrational spectrum, described in the previous chapter, H_2s molecular rotation also leads to a periodic modulation in the scattered light seen in 2.2. As the induced polarisibility returns to its original value twice in one molecular rotation, the values for the frequencies observed in the spectra 2.3 are then in fact frequency doubled and this is analogous to the quantum selection rules for a rigid rotor being ΔJ=$\pm$2 shown in figure 2.3A(i). These changes in rotational quantum therefore lead to several branches, which have since been used to define the H_2 excitations seen in figure 2.3A(i), B and C and are described below.

- ΔJ = 2 (**S Branch**) $\quad \nu_a - 2\nu_{rot}$
- ΔJ = 0 (**Q Branch**) $\quad \nu_a \pm \nu_{vib}$
- ΔJ =-2 (**O Branch**) $\quad \nu_a + 2\nu_{rot}$ (not shown in figure 2.3C)

The respective intensity landscapes for these rotational modes are also very intriguing and reflect the coupling of rotational eigenstate, nuclear spin and complete symmetry of the molecule.

Firstly, considering the nuclear spins the H_2 molecule it can come in two flavours, ortho-hydrogen (o-H_2) or para-hydrogen (p-H_2) with the nuclear spins aligned or anti-aligned respectively (a pictorial example of this can be seen in figure 2.3 A(iii)). A physical manifestation of these nuclear spins can be readily seen by thermally equilibrated normal-H_2 (n-H_2) used in the contributing experiments having a mixture of o-H_2 to p-H_2 of 3:1 due to possible triplet and singlet states respectively.

The symmetry of the hydrogen molecule also has to be taken into account. As we have previously discussed the molecule can exhibit a rich array of quantised behaviour (ψ_{Rot},ψ_{vib},ψ_{ns} - nuclear spins) which all have a contribution to the overall wavefunction (Ψ_{H_2}) given by the following equation, where ψ_e is the electronic contribution.

$$\Psi_{H_2} = \psi_{Rot}\psi_{vib}\psi_{ns}\psi_e \tag{2.12}$$

We can now consider selection rules are allowed/forbidden to be in agreement with the Pauli exclusion principle which states:

"The total wavefunction of two identical fermions must be antisymmetric with respect to exchange of the particles."

As protons are fermionic therefore the total wavefunction for H_2 (Ψ_{H_2}) must be antisymmetric under exchange of nucleii. The ground state of the electronic (ψ_e) and vibrational (ψ_{vib}) contributions are symmetric under exchange, resulting in the parity of the molecule to be dictated by a combination of its nuclear spins and its rotational mode. It can be readily seen that an inversion of the nuclei (x, y, z = -x, -y, -z) is simply shown by a rotation of the molecule by 180 degrees. It is therefore evident that o-H_2 is symmetric under rotation and p-H_2 is antisymmetric. The parity of rotational eigenstates are found to change in successive values of **J** ie. anti-symmetric under the exchange operation for odd **J** and symmetric for even **J**. Combining the rotational component and the nuclear spin component we can derive two statements to be in agreement with the previously mentioned Pauli exclusion principle, the allowed transitions in figure 2.3A(i), B and C:

- **o-H_2**: Even **J** states are forbidden, **J** = 1, 3, 5 ... with statistical weight 3.
- **p-H_2**: Odd **J** states are forbidden, **J** = 0, 2, 4 ... with statistical weight 1.

From these simple arguments we have now introduced all the excitations and their relative intensity landscape seen in the low spectra pressure spectra of n-H_2 presented in figure 2.3B and C.

2.4 High Pressure Raman Setup

Through advacements in technology, namely the advent of charged coupled devices (CCDs) and lasers, the versatility of Raman scattering as a diagnostic has been vastly increased over the course of the last 80 years. This is emphasised by the comparison between a novel (figure 2.3 B) and a contemporary measurement using a DAC (figure 2.3 C) of H_2. The novel measurement was taken on a volume of $\sim$ 250 ml and over an exposure time of up to 40 hours. On the other hand the contemporary measurement represented in figure 2.3C was a sample a

trillionth of the volume ($\sim$ 0.25 pl) and had an exposure time of a few seconds. Clarifying that Raman spectroscopy techniques have come of age and providing the user with quick, accurate and easily interpretable information. It has since been found useful in a wide range of applications from extraterrestial planetary rovers [Pérez 06] to drug/explosive detection at transportation hubs [Vestel 12].

This chapter serves to provide explanation to the experimental Raman Set-up used in the contributing study, and how the signal is optimised when interfaced with high-pressure equipment, namely the DAC (see chapter 3). The components in the experimental setup will be introduced following the path of the laser from its creation to terminus seen in 2.4.

The advent of the laser has since made Raman spectroscopy prolific as a versatile non-destructive probe, the intense monochromatic source replaced mercury arc light sources used in the early generation Raman setups. Lasers are found to be far superior, as the original arc light sources produced a complicated signal which consisted of several excitation lines and require much longer exposure times (figure 2.3B) [Rasetti 29]. The lasers used in the contributing work were Argon-ion and Krypton-ion lasers of wavelength 514 nm and 647 nm respectively and typically operated at a power of $\sim$20 mW.

The first component in the laser's path is a holographic Band Pass Filter (BPF), first integrated into Raman spectroscopy setups in the late 80s. The function of the BPF is to filter undesired wavelengths from the laser line. Via a process of hololithography the BPF is engineered to reflect solely the laser line at an angle of 90 degrees to the incidence. This process is highly efficient typically losing only $\sim$ 2% of the incident laser intensity.

After the beam is filtered the laser then arrives at a "Z" configuration consisting of two permanent mirrors and a Holographic Notch Filter (HNF) [Yang 91]. The HNF here serves two functions one in reflection and one in transmission, in the current stage of the laser's progress were concerned with the properties of the former. In reflection the HNF acts similar in function to the BPF previously described and reflects solely the laser line however at a significantly reduced angle, thus requiring the two mirrors for the complete setup to have a functional geometry. Unlike previous Raman setups [Goncharov 12, Howie 13b], this configuration has forgone using a 50:50 beam cube to reflect the laser, a

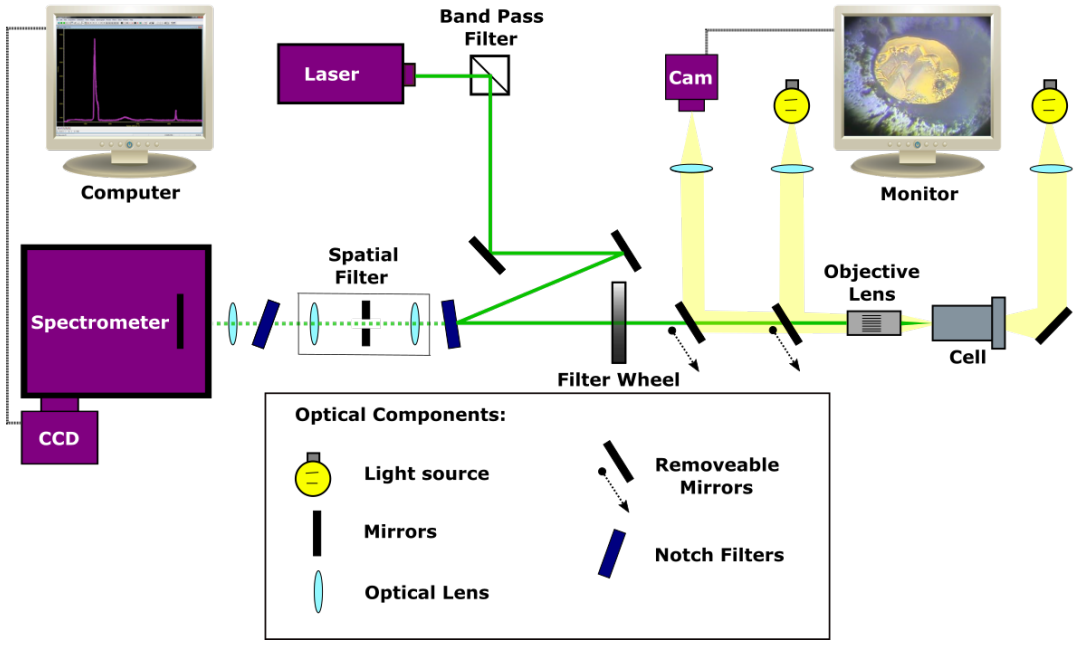

Figure 2.4: Diagram of the micro-focussed high-pressure Raman setup

modification resulting in greater efficiency by minimising the intensity losses in transmission from the laser.

The laser is then focused onto the sample using a Mitutoyo objective, this component is interchangeable depending on demands dictated by the sample size and can vary from x10-x50 magnification. All objectives used have long working distances to accommodate the high pressure cell as well as high temperature equipment (see chapter 3). Sample observation is also provided in reflected and transmitted light using a configuration of removable mirrors, the mitutoyo objective lens and closed circuit television (CCTV), seen in figure 2.4. This arrangement can allow visible observation of the sample for phase transitions, first approximation optical transmission measurements and also to assess the evolution of the mechanical stability of the sample under load.

The 180 degree backscattered light is then collected and collimated by the same mitutoyo objective lens that focused the laser onto the sample. The modulated laser signal then travels down the same path originally taken toward the sample back towards the HNF. Here again the HNF scatters the laser line at an obtuse angle creating a high laser attenuation in the transmitted light but not modifying the intensities of the frequency shifted signal, seen in figure 2.4 as the dashed

green line. The HNF is tuned such that there is an optimum trade-off between attenuating the intensity of the laser line and conserving the spectral range of the anti-stokes scattering, the smallest shifts we can detect using this method can be of the order of $\sim$200 cm^{-1}.

The frequency-shifted signal is then passed through a spatial filter which is an essential component when interfacing conventional micro-focussed Raman spectroscopy with the DAC [Goncharov 12]. First used in confocal microscopy [Minsky 57] its function here is to heavily reduce the depth of focus when probing the sample. This is desirable when dealing with very small sample sizes as it can further diminish spurious signals that can come from other sources, such as the scattered light from the diamond anvils. The spatial filter used here is composed of two optical lenses that focus the light to a focal point where a pinhole is located. All components in this filter can be tailored in three dimensions to optimise signal to background ratio ensuring the best quality data is acquired during the experiments.

The signal is then passed through a Super Notch Filter (SNF) which further attenuates the laser line before being focused into the spectrometer and finally imaged by a Princeton Instrument's array CCD. The measurement outputs to a computer running WinSpec software so qualitative analysis of the spectra can be done *in-situ*. When possible the 514nm (green) laser is used as the CCD drops in quantum efficiency at longer wavelengths. At higher pressures however to avoid the enhanced floresence from the diamond anvils a 647 nm excitation wavelength is used. Finally, data is exported and analysed using Igor pro and fityk software packages.

Chapter 3

High Pressure and Temperature Techniques

Melting characteristics, which at high pressures often require high-temperature techniques, are an essential diagnostic in studying the properties of the interactions within a material as well as differences between the solid and liquid states. Hydrogen despite being a simple system displays immense complexity and rich physics when under extreme pressures and temperatures (discussed in chapter 4). Recent experimental advances, discussed in this chapter, have allowed us to probe these phenomena in a regime of pressure-temperature space which was previously inaccessible.

3.1 Diamond Anvil Cell

The understanding of pressure on a material has always played an essential role throughout history. For example breathing life into the machines that powered the industrial revolution, from pressurised steam inside the Flying Scotsman to the hydraulics that lifted the large bascules of Tower Bridge. In the modern age where quantum mechanics plays an essential role in cutting edge technology the understanding of pressure on matter today is no less important. The staple in most extreme static pressure experiments is the Diamond Anvil Cell (DAC) [Weir 63], which is compact and simple in design as it is powerful. The concept

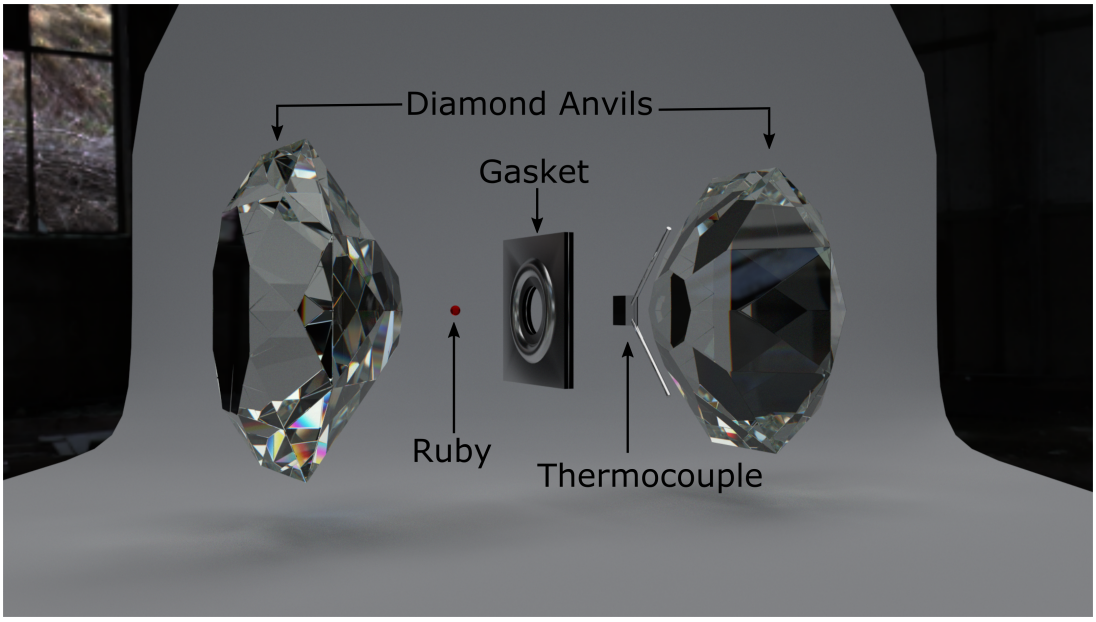

Figure 3.1: Basic opposed diamond anvil cell (DAC) setup. The sample is contained within a sample chamber in the gasket and the two opposing diamond culets. Additionally a ruby chip/sphere can be placed in the sample chamber as a pressure diagnostic (see section 3.3) and a thermocouple attached to one (or both) of the diamonds to determine the temperature (see section 3.2).

is simple; a sample is placed between two opposing diamonds, see figure 3.1, with a force applied generating a pressure. When coupled with the lovingly known Stiletto effect, a trivial consequence of the $P = \frac{F}{A}$ equation, probing pressures comparable to planetary interiors are accessible with a device that can fit into the palm of your hand.

The introduction of diamond anvils revolutionised high-pressure technology resulting in an order of magnitude increase in pressure compared to the several gigapascal presses pioneered by the bastion of high-pressure Percy Bridgman. The modern day DACs are essentially the same as the presses used by Bridgman, the dramatic increase in the pressures generated was in fact a direct consequence of replacing tungsten carbide with diamond for the anvil material. The large bulk modulus of diamond ($\sim$ 440 GPa) means it can withstand much higher strains before mechanical failure, another useful property is that it is transparent to vast regions of electromagnetic radiation, therefore *in-situ* optical diagnostics (discussed in chapter 2) such as Raman, infrared spectroscopy and X-Ray diffraction can be employed.

Since the invention of the DAC by Weir in 1959 [Weir 59], they now come in an array of designs and are tailored to the requirements of the experiments. The DACs used in the contributing experiments are a modification of the Mao-Bell design [Mao 76], which were the first to probe pressures in excess of 100 GPa. Figure 3.2 represents an exploded diagram of a typical cell which was used. It consists of a piston-cylinder configuration with a tight fit to ensure stability of alignment of the small diamond culets, an integral aspect for obtaining the highest pressures at high temperatures.

To optimise the pressures achieved, the diamond's geometry can be modified, this is often a trade-off of cost and functionality for the type of experiments. The basic geometry for the diamond anvils has largely remained unchanged since their introduction. Interesting research however is currently being carried out on achieving higher pressures, which include diamond anvil shaping as well as introducing an internal secondary anvil. The latter having reported astounding static pressures in excess of 600 GPa [Dubrovinsky 12]. In the work conducted for this thesis, the diamonds varied from low-pressure relatively large volume experiments using Almax type IIa flat 250 μm culet geometry to the highest

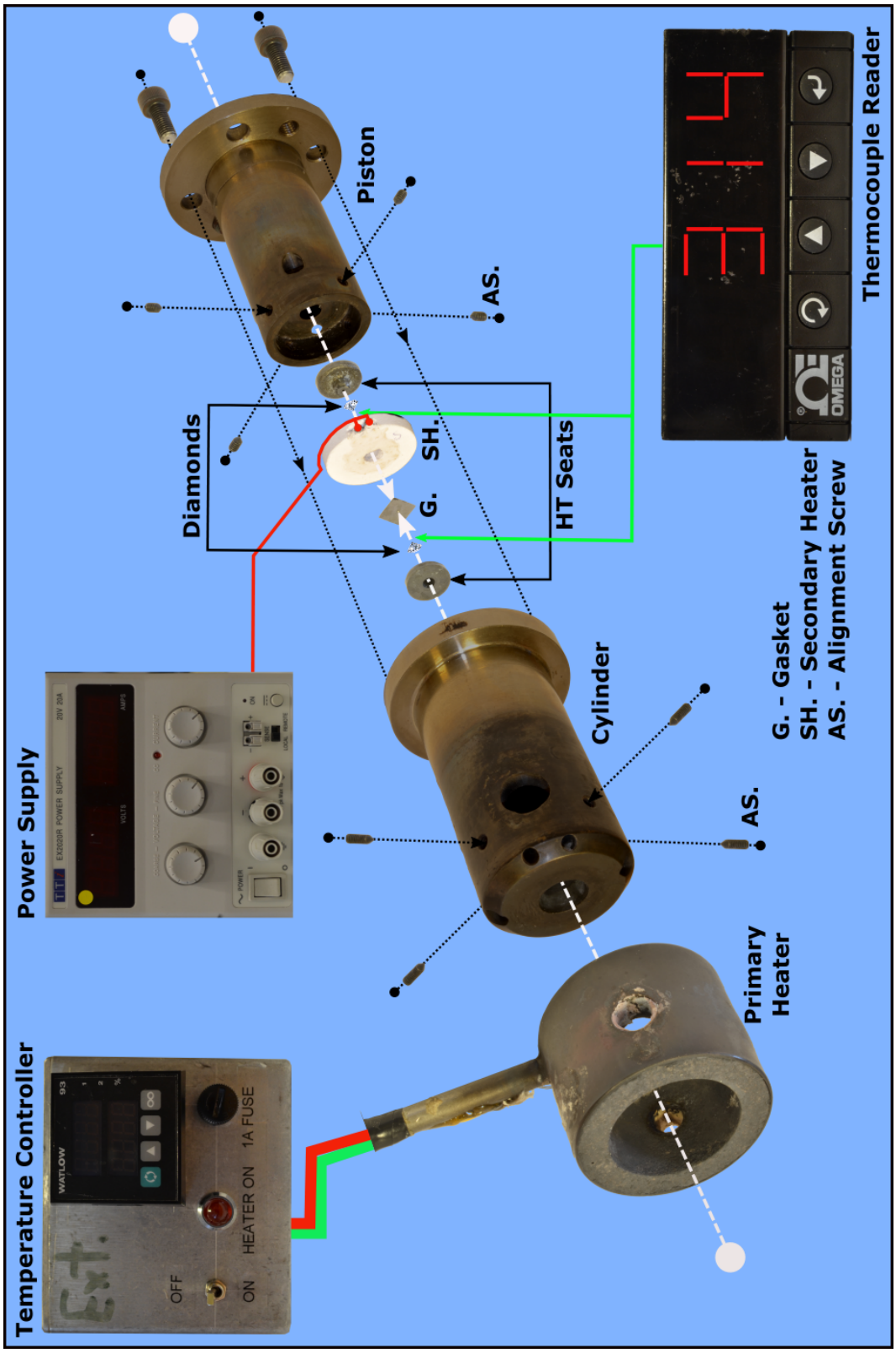

Figure 3.2: Exploded diagram of a typical piston-cylinder Diamond Anvil Cell (DAC) used in high-temperature high-pressure studies.

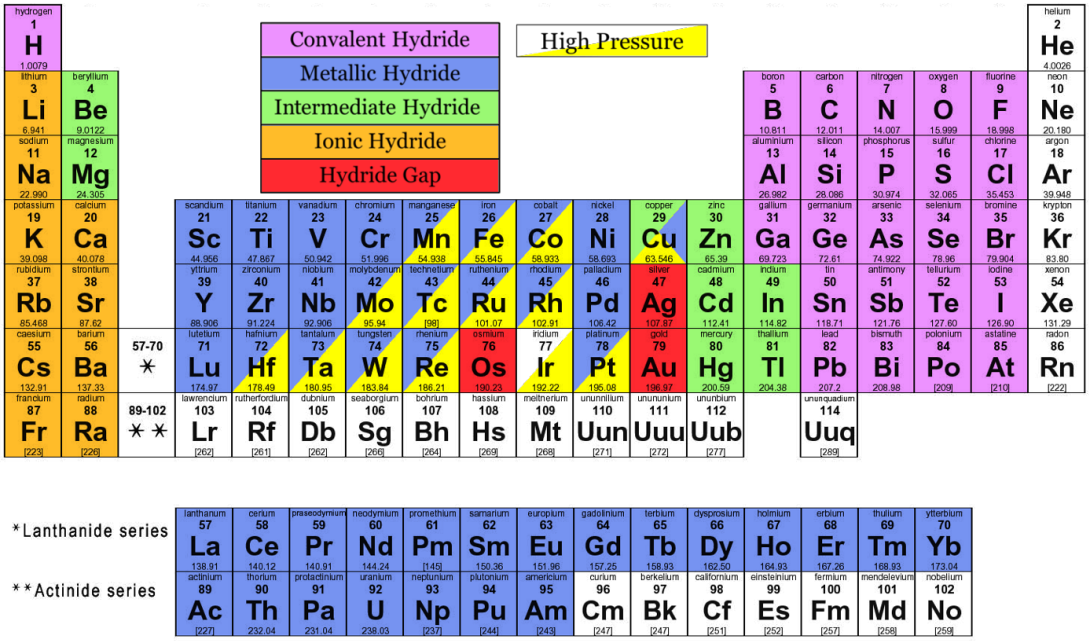

Figure 3.3: The periodic table summarising binary hydrogen-bearing systems at ambient conditions and at high pressures.

pressures using 8 μm type IIac Boehler-Almax [Boehler 04] double bevelled geometry.

Due to hydrogen's exceptional reactivity, demonstrated by the ready formation of binary hydrides at ambient conditions, its interaction with the gasket material needs to be taken into consideration. A review of the binary systems is seen in figure 3.3 and in its own right an important area of research. Hydrides currently boast the T_c record for superconductvity (H_2S - 203 K [Drozdov 15]) as well as find application as candidates for commercial space-efficient energy-storage materials. The gaskets used in these studies were rhenium foils varying in thickness from 150-250 μm and are of dimensions such that they fitted inside the internal diameter of the secondary heater, seen in figure 3.2, if it was required. The hydrogen-rhenium system is well studied and hydrogen is found to be soluble in the metal host. Given time, above 15 GPa, hydrogen and rhenium will form the compound with stoichiometry ReH_2 [Scheler 11], observed visually in all experiments as a blackening of the gasket material around the sample chamber. Above 420 K and 23 GPa, rhenium undergoes isomorphous phase transition and hydrogen solubility is further increased until a stoichiometry of ReH is reached

[Scheler 11], the formation of these hydrides have to be considered and pressure fluctuations monitored (see chapter 3.3.2) during heating cycles in case of loss of sample.

To prepare the sample chamber the gasket is dusted with ruby powder and indented to a pressure of ∼30 GPa by measuring the shift of the ruby fluorescence (see chapter 3.3). A hole half the diameter of the culet is then milled using a pulsed IR laser, which ablates the gasket material. For the smallest chambers a x50 IR mitutoyo objective was used and found it could adequately mill a symmetric centred hole with minimal IR damage to the surrounding rhenium. IR drilling proved to be far more time efficient compared with previous Focussed Ion Beam (FIB) milling approaches [Howie 12a, Howie 13b, Orloff 00]. The thickness of the chamber is then measured using interferometry and tailored for the experiment, typically a third of the diamond culet diameter [Dunstan 89]. After the initial milling, if the sample chamber is too thick iterations of collapsing and milling are completed to achieve the desired sample chamber parameters, for the highest pressures this can be of the order of several microns. The samples are gas loaded by clamping the hydrogen between the diamonds in a 1750-2000 bar environment and then pressurised at room-temperature using a watercooled leverarm.

3.2 Resistive Heating Techniques

The application of heating techniques, another thermodynamic variable other than pressure, can be used cocomitantly to assess the stability field of various condensed matter phases, one of the main objectives in the contributing work. A range of heating techniques have already been interfaced with high pressure studies and are already well established, such as: Compression heating (a consequence of using shock techniques) [Smith 14], Laser heating [Sanloup 13], internal-resistive heating [Zha 03] and external-resistive heating [Gregoryanz 03].

External resistive heating was the technique employed in the contributing work as it's an efficient simple in-house technique with an accuracy of the order of $\sim \pm 20$ K. Using this technique temperatures in excess of 1000 K can be obtained, which is within the temperatures the maximum desired for this study ie. below

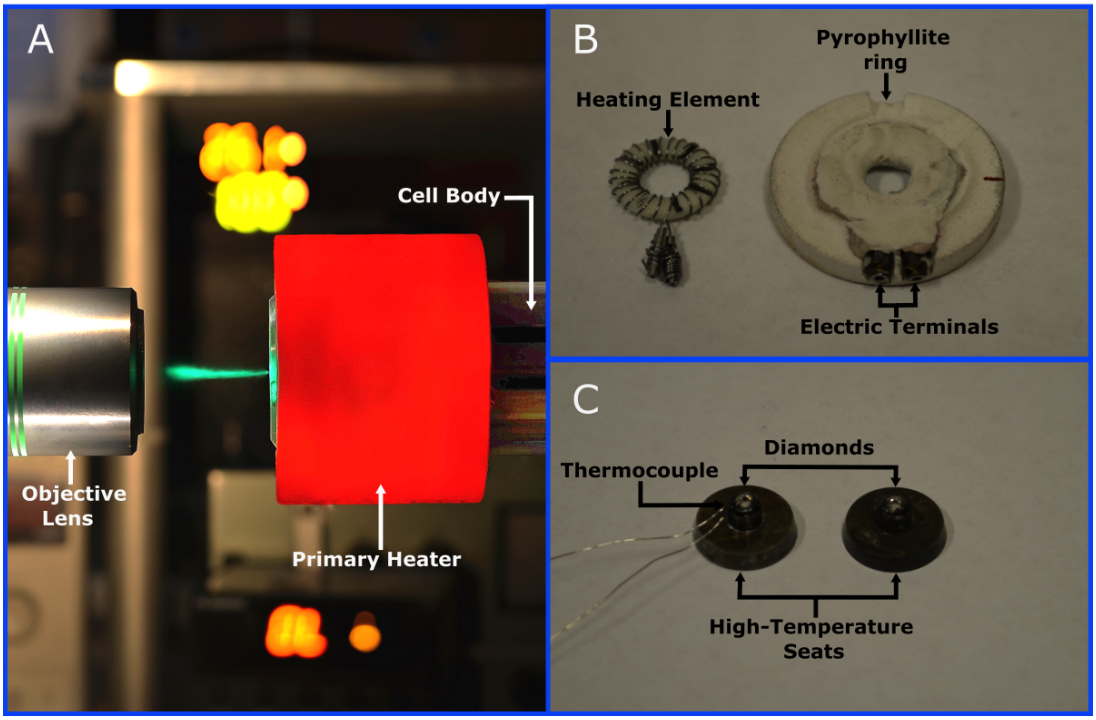

Figure 3.4: **(A)** A picture of a microfocussed Raman experiment of a H_2 sample at 600 K and 150 GPa. **(B)** A picture of the secondary internal heater, the left component is bare to reveal the metallic heating element and internal wiring. **(C)** A picture demonstrating how the diamonds and thermocouple are attached to the high-temperature seats

the melting curve for hydrogen (∼875 K and 90 GPa [Bonev 04] - see chapter 4.2 for futher discussion). Therefore, this is a very applicable technique when assessing the stability of solid hydrogens.

The contributing work used a combination of two heaters, named the primary and secondary heater for convenience, a procedure similar to previous high-temperature studies on hydrogen where temperatures of ∼800 K and pressures of 45 GPa were reached [Gregoryanz 03]. The entire cell body is initially heated using the primary heater, which is external to the cell assembly and managed by a temperature controller shown in figures 3.4A and 3.2. The primary heater allows us temperatures of up to ∼ 500 K, although the maxiumum operation temperature of this heater is much higher, a limit is imposed so as to not affect

the mechanical stability of the lever arm and to also reduce possible damage to the objective lens 3.4. At pressures exceeding 200 GPa only the use of the primary heater is necessary.

At pressures below ∼200 GPa, higher temperatures are required and an addtional small secondary heater, which fits around the diamonds within the cell assembly, is used. Firstly, to accommodate the heater, specially designed high-temperature tungsten carbide seats are required, see figure 3.4C. These heaters are built in-house and are often disposed after a single use, usually due to failure during the course of an experiment. A construction of the secondary heater can be seen in figure 3.4B. The heater itself is composed of a metallic molybdenum heating element, a material chosen for its desirable high-melting temperature (2620 K) whilst having a workable malleability. The heating element is coiled around a thin alumina ring and tightly wound around molybdenum tubes to provide ports for electrical probes so that it can be driven by an external power supply, seen in figures 3.4B and 3.2. The element is then set in high-temperature cement and a pyrophyllite ring, providing thermal insulation as well as preventing oxidation of the heating element and premature failures. When this secondary heater is used in conjunction with the primary heater temperatures in excess of 1000 K can be explored.

During the course of the experiments the sample temperature is monitored through the use of type-S thermocouples epoxied to one or both of the diamonds (see figure 3.1 for placement) and electrically insulated through the application of high-temperature cement, see figure 3.4C and 3.2. Additional thermocouples are found on the primary heater, used as a feedback to control the operation temperature (see temperature controller in figure 3.2), as well as an additional thermocouple placed on the table of the diamond. These additional thermocouples allow us to guage thermal gradients, and assess the accuracy of the measurements which was typically found to be of the order of ∼20 K.

3.3 Pressure Metrology

As ever higher pressures are recorded through dynamic and static techniques, pressure metrology needs to be continuously developed. Although such research

may not be considered illustrious, if a novel technique/calibration is successfully implemented within the field it can inherit a significant number of citations. For example a calibration of the ruby scale - which will be discussed - [Mao 76] has since acquired over 2200 citations. There exist two definitions of pressure standard:

- **Primary:** Pressure is derived directly from known quantities of mass and area.
- **Secondary:** Pressure derived from a standard calibrated to a primary standard.

Primary gauges offer the greatest accuracy, resulting in an error of $\sim$1% when using dead weight piston-cylinder apparatus, however this is only applicable in very low pressure studies. At higher pressures where tight fitting cells are required to ensure perfect diamond alignment (see chapter 3.1), an unquantifiable friction is introduced ruling out the use of any primary pressure standard. Therefore, in the field of extreme high-pressures research, secondary pressure standards are implemented, such as: the pressure dependence of ruby florescence, the shift of diamonds T2g Raman mode and using the equation of state (EoS) of noble metals. Only the former two techniques were employed in the contributing work and discussed in this chapter. The latter diagnostic is unfavourable due to limitations of the dimensions of the sample cavity, the noble metal's chemistry with the sample and the dependency on external synchrotron facilities.

3.3.1 Ruby Scale

Within the extreme static pressure regime, 1-100 GPa, the ruby scale as a pressure diagnostic is arguably the most prolific. The measurement requires essentially the same equipment to that of the Raman diagnostic, discussed in chapter 2.4, the only requirements are slight modifications to the spectrometer. The resultant technique is therefore extremely powerful, allowing a quick an easy *in-situ* measurement of pressure in conjunction with Raman measurements. As an example of the prolific nature of this calibration scale, most high-pressure x-ray user facilities have integrated online ruby pressures measurement systems. For a critical and in-depth review of the ruby scale, the reader is referred to the

reference [Syassen2008].

The technique is simple; ruby powder or a small chip of ruby, corundum (α-Al_2O_3) doped with Cr^{3+}, is placed within the sample chamber (see figure 3.1). The scale then harnesses the shift of the R_1 ruby line $\Delta\lambda_{R1}$ under applied hydrostatic pressure. The pressure dependence of R_1 was originally proposed as a scale by Forman *et al.* [Forman 72] and was later calibrated by Piermarini *et al.* in 1975, who reported a linear shift ($\Delta\lambda_{R1} = 2.74\ \frac{nm}{GPa}$) up to ∼20 GPa. This scale was then further extended to by Mao *et al.* and revised by the same group in 1986 up to 80 GPa [Xu 86].

At high pressures,> 200 GPa, the enhanced pressure-induced florescence from the diamond anvils and broadening of the R_1 line determination of pressure by this method becomes increasingly difficult. Also, as sample chambers become exceedingly small at higher pressures, they can no longer accommodate a ruby chip or powder. Therefore, in these pressure regimes an alternative method for pressure determination, namely the diamond edge scale, is used and is discussed in the following chapter.

3.3.2 Diamond Edge Scale

Diamond has two atoms per primitive unit cell and as such exhibits an optical phonon at a frequency of 1332 cm^{-1} under ambient conditions, which has been known for over 85 years and originally measured by Ramaswamy [Ramaswamy 30]. The pressure dependence of diamond's optical phonon, originally observed by Mitra *et al.* [Mitra 69] by Raman spectroscopy, has since found great application in determining pressure and has become known as the Diamond Edge Scale (DES). The DES technique was used extensively in the contributing work, being the sole pressure determination technique employed at elevated temperatures and pressures exceeding 100 GPa.

The power in the DES technique lies in its ability to simultaneously conduct a Raman and pressure measurement in a single exposure without requiring any additional components, such as a grain of a noble metal or a chip of ruby. This is particularly important under extended pressure regimes where sample sizes and longevity of the experiments are heavily limited. For a representative example of

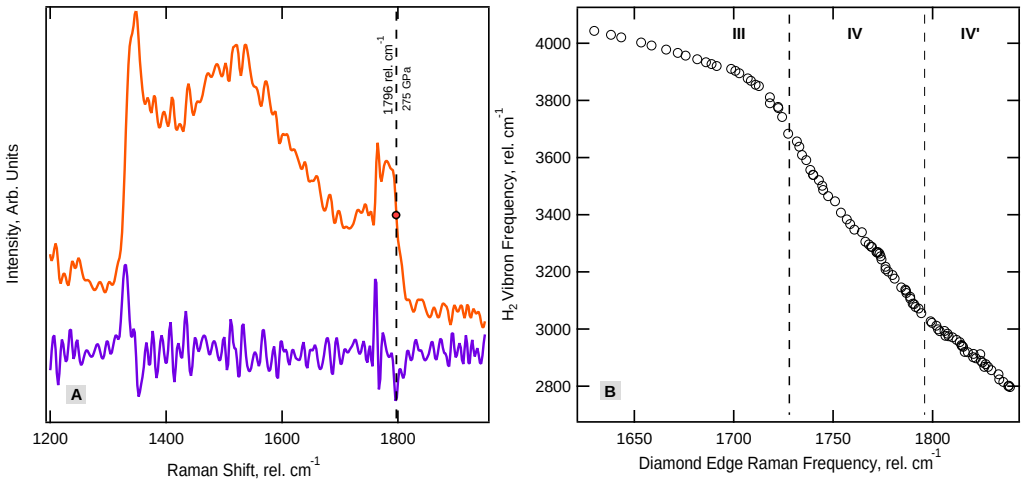

Figure 3.5: **(A)** A typical example of the spectra taken from the first order Raman band of diamond when probing the sample (orange). The frequency of the stressed edge is given by the veritcal dashed line at 1796 rel. cm^{-1} corresponding to a pressure of 275 GPa [Akahama 04]. This frequency was determined by the frequency that minimises the differential $\frac{dI}{d\omega}$ (purple) (I-Intensity, ω-frequency). **(B)** H_2 vibron frequency (ν_1) plotted as a function of the stressed diamond edge frequencies.

the pressure evolution of the optical mode from the diamond anvils with Raman spectroscopy compare figure 2.3C (unstressed) with figure 3.5 (stressed). It's seen that under stress the Raman profile from the anvils becomes quite complex, reflecting the inherent strain profile within the anvil and the spatial filtering of the Raman set-up. The feature of importance is the peak located at the highest frequencies, which stems from the stressed culet and has been calibrated as a function of pressure [Hanfland 85, Akahama 04, Akahama 06, Akahama 10b]. In the contributing work to provide consistency, the scale by Akahama *et al.* in 2004 is used throughout and the stressed edge frequency is chosen such that it minimises the differential $\frac{dI}{d\omega}$ of the signal. A technique proposed in the initial calibrations [Akahama 04], and represented by the purple curve in figure 3.5.

It is important to comment on the inaccuracies of this technique, which are perhaps most evident by the large disagreement between different research groups in the literature. An example is given in figure 3.6A, where a pressure difference as large as ~25 GPa corresponds to the same H_2 ν_1 vibron frequency. There could be a multitude of reasons for these discrepancies, for example different pressure

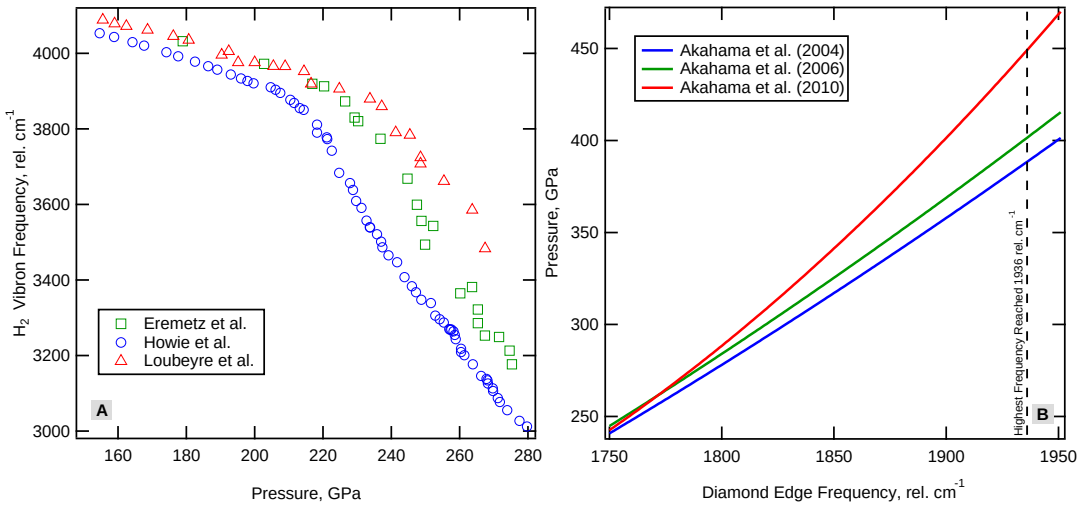

Figure 3.6: **(A)** H_2 vibron frequencies (ν_1) plotted as a function of pressure from three different studies: Eremets *et al.* (green squares) [Eremets 11], Howie *et al.* (blue circles) [Howie 12a] and Loubeyre *et al.* (red triangles) [Loubeyre 13]. **(B)** Three pressure guages plotted as a function of pressure: blue [Akahama 04], green [Akahama 06] and red [Akahama 10b], the dashed line corresponds to the highest frequency of the stressed diamond recorded in the contributing work, 1936 rel. cm^{-1}.

scales could have been used. Seen in figure 3.6B the most contemporary scale significantly diverges at higher pressures compared to its predecessors. Another reason could be the diamond/sample geometry, already observed to have an effect at lower pressures [Baer 08]. Therefore care has to be taken when interpreting results that the observations aren't a manifestation of the choice of pressure scale and is a property of the sample.

Due to the weak temperature dependence of diamonds optical mode, $\Delta\omega$=10 cm^{-1} over 800 K at ambient pressures [Liu 00], it can also be implemented as a pressure gauge whilst traversing P-T space, assuming it there is a continued weak temperature dependence under load. In the contributing work this was done via two approaches:

- **Spanning PT Space:** Shown in figure 3.7A throughout the course of a heating and cooling cycle pressure is allowed to fluctuate, which is typically found to increase. Pressure is then determined from changes in the frequencies from the stressed diamond edge during the heating and comparing principle vibrational frequencies before and after the heating

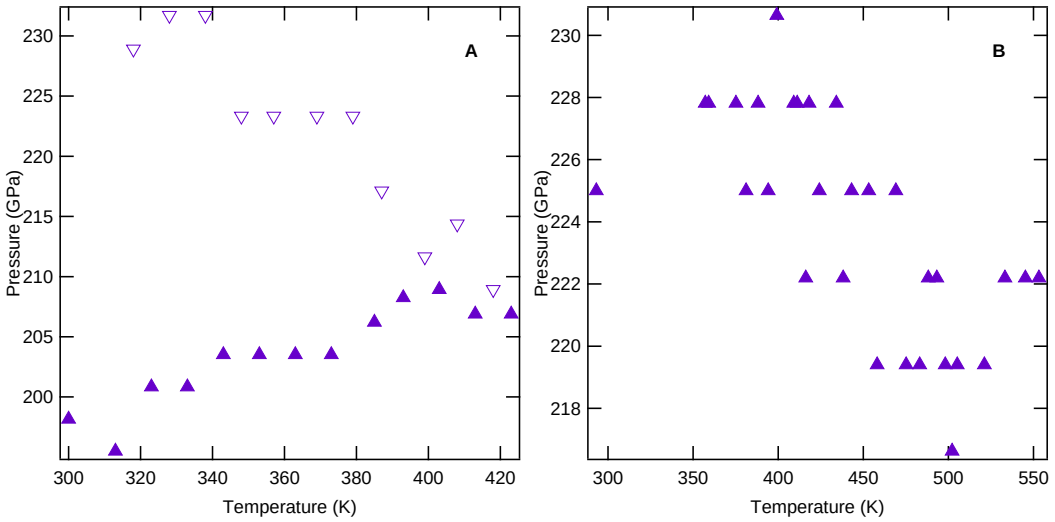

Figure 3.7: Representative data showing the evolution of pressure during heating, pressures have been calculated using from the stressed diamond edge and assumed to be largely temperature independent. **(A)** The pressure increase of a heating run starting at 198 GPa up to 423 K. Pressure was measured on heating (solid triangles) and cooling (empty upside-down triangles), pressure was found to increase by $\sim$ 30 GPa over the complete cycle. **(B)** Pressure fluctuations in an isobaric run on heating to 555 K, isobar was maintained to within $\sim$ 5 GPa of 225 GPa.

cycle.

- **Quasi-Isobaric:** The stressed diamond edge can also serve as a diagnostic for negative feedback allowing us to track a "Quasi-Isobaric" path in P-T space. For example, during a heating run when the stressed diamond edge drifts to higher frequencies (indicating an increase in pressure) the load is reduced on the lever arm and vice versa if the stressed diamond edge drifts to lower frequencies. Using this technique it is possible to heat along an isobar to within ± 5 GPa of the initial pressure at room-temperature, an example is shown in figure 3.7B.

Chapter 4

Review of the Hydrogen Phase Diagram

This chapter serves as a review for the reader of the current understanding of the Hydrogen phase diagram over the region probed in the contributing work. As seen in figure 4.1 there are currently three experimentally observed solid molecular phases, a recently discovered solid "mixed" molecular and atomic phase [Howie 12a, Eremets 11]. There exists some experimental constraint on the melting line, a disorder transition from phase I, and also some predicted and evidenced dissociation phenomena within the liquid phase [Scandolo 03, Tamblyn 10, Morales 10, Knudson 15].

4.1 Solid Hydrogens

Seen in figure 4.1, Phase I is found to cover a broad area of PT space, currently the only known phase bounded by a transition to complete disorder at high temperatures. Phase I has been found to be stable up to pressures of ∼180 GPa at room temperature [Baer 07] and been observed via laser heated Raman measurements up to 1050 K at 125 GPa [Eremets 09], making it hydrogen's most thermodynamically extensive phase. The structure has been determined as a quantum solid with freely rotating molecules arranged on a hexagonal close packed lattice [Hazen 87]. Interestingly, the pressure dependence of vibron

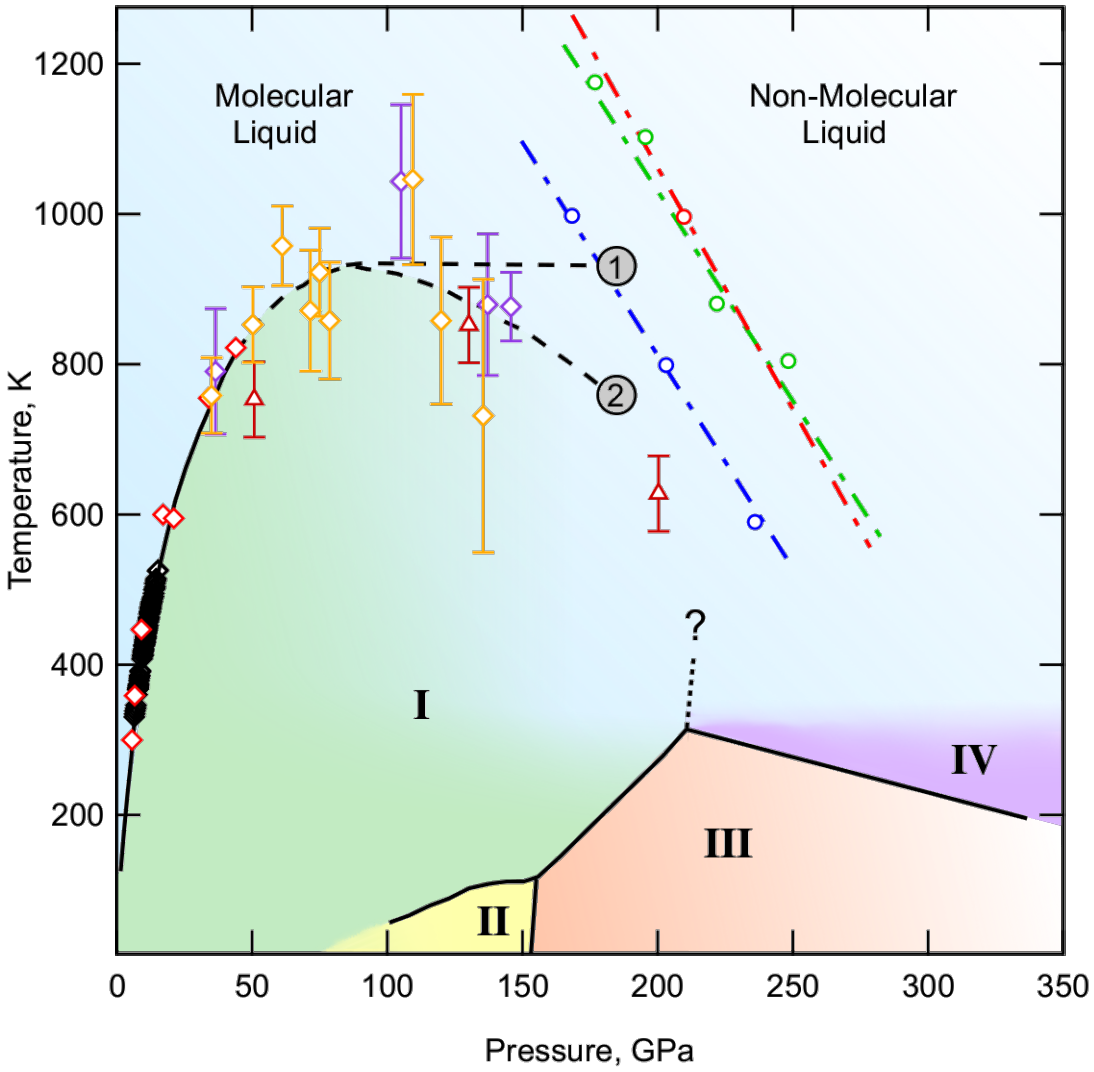

Figure 4.1: Hydrogen Phase Diagram up to 325 GPa. The different colours correspond to the different known phases of hydrogen: liquid (blue), phase I (green), phase II (yellow), phase III (orange) and phase IV (purple). The experimental data on the melting curve is given by the black [Datchi 00], red [Gregoryanz 03], yellow [Subramanian 11] and purple [Eremets 09] hollow diamonds. The thoerical melting points by hollow red triangles [Bonev 04]. The melting line accurately determined up to 45 GPa (solid line) is extraplated to higher pressures using both a Kechin fit (1-dashed) and a Kraut-Kennedy fit (2-dashed). Predicted theoretical points on the first order liquid-liquid transition [Scandolo 03] are also shown by hollow blue [Morales 10], green [Morales 10] and red circles [Tamblyn 10] and correspondingly coloured dashed line extrapolations.

at higher pressures was found to turnover becoming negative above $\sim$ 60 GPa, a manifestation of increased intermolecular interactions, which soften the intramolecular mode [Mao 78], the first experimental evidence that the molecule might dissociate under sufficient compression.

At low temperatures below 135 K and 150 GPa, a region out of the scope of the contributing work, is the existence of phase II, found via vibrational spectroscopic measurements [Mao 94]. The I-II transition is regarded to be a transformation to a lower symmetry phase as the hydrogen molecules become orientationally ordered, a large isotopic effect in this transition is suggestive that this could be transition to a quantum ordered state. At higher pressures, above $\sim$ 150 GPa and below 135 K phase II is superseded by phase III [Mao 94], the small isotopic change in this phase transition is indicative of classical ordering. The experimental difficulties of conducting X-ray measurements of hydrogen under these conditions have resulted in these low-temperature lower-symmetry phases being structurally undetermined. However, with the development of ever brighter X-ray sources and X-ray free electron lasers, structural solutions may soon be realised. Currently, our best understanding of hydrogen's structural phase diagram comes from theoretical insight. Hydrogen's Density Functional Theory (DFT) phase diagram has been extensively explored using structure searching methods, such as *ab-initio* random structure searching (ARSS) developed by Pickard *et al.* [Pickard 07]. These techniques, which determine the most favourable groundstate structures at a given pressure, have suggested: $P6_3/m$-*24* structure for phase I [Pickard 07]; $P2_1/c$-*24* structure for phase II [Drummond 15]; $C2_1/c$-*24* structure for phase III [Drummond 15].

Recent room-temperatures investigations have reinvigorated hydrogen research in the solid state, which had been limited up to 180 GPa at room-temperature for over 20 years. Probing into a far extensive pressure regime, up to $\sim$310 GPa at room temperature, these new studies revealed a novel solid phase of hydrogen, phase IV, above 220 GPa [Howie 12a, Eremets 11]. The transition evidenced by the unique and rich Raman spectra, seen in figure 4.4 allows the assessment of suitable structural candidates. The *Pc* structure, a modified version of a structure previously proposed for phase III [Pickard 11], was attributed to phase IV [Pickard 12], seen in figure 4.2B. The *Pc* structure in itself is very intriguing being a layered structure consisting of partially dissociated molecules found

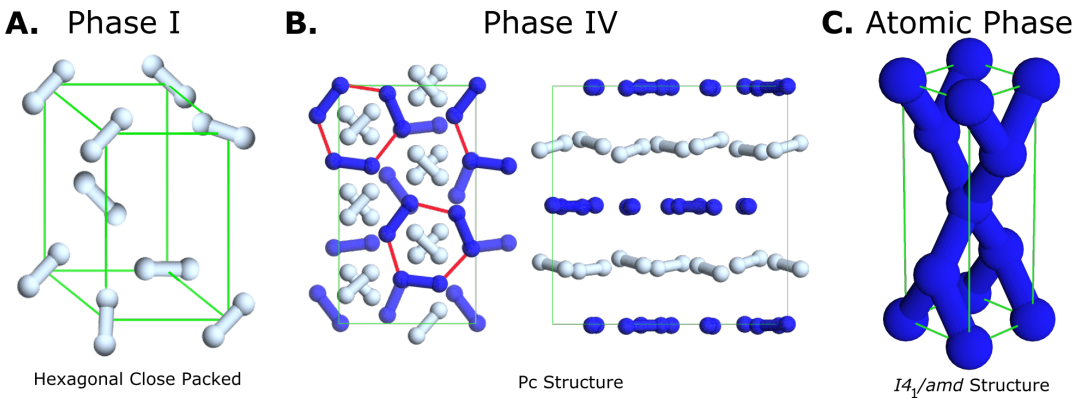

Figure 4.2: Known and predicted hydrogen structures in different pressure regimes.**(A)** Hexagonal close packed (HCP) structure of freely rotating molecules of the low pressure phase I [Mao 94, Loubeyre 96].**(B)** Mixed *Pc* structure consisting of layers of 6 atom rings (G-layer), the red lines illustrate the next nearest neighbour, interspersed with unbound molecules - a reasonable structural cadidate for phase IV [Howie 12a, Howie 13b, Pickard 07, Pickard 12].**(C)** Atomic $I4_1/amd$ structure predicted to be the stable hydrogen phase above 380 GPa [Azadi 14, McMahon 11].

in a graphene like arrangement (G-layer) interspersed by layers of unbounded molecules, which explains the characteristic two vibrational modes ν_1 and ν_2 seen in figure 4.4A. The large discrepancy between the vibrational mode ν_1 and the frequency from the *Pc* structure has since been reconciled with molecular dynamic (MD) calculations [Magdău 13].

The evolution to a layered structure isn't entirely unexpected and is discussed in the concluding statements of the seminal paper by Wigner and Huntington [Wigner 35], as well as already being observed in nature, such as the allotropes of carbon and tin. The "mixed" atomic and molecular arrangement however is rather beautiful and rewrites the narrative of how hydrogen will further dissociate into the atomic presumably metallic state. If the evolution into phase IV (*Pc* structure) marks an intermediatry process of dissociation, the pressure evolution will be of much interest and a is key motivator for the contributing work. One possibility is the gradual symmetrisation of the distorted hexagonal rings in the G-layer of the *Pc* structure transforming it ultimately to the *Ibam* structure, a tendency already observed in DFT calculations [Pickard 12]. This arrangement will be a truly "mixed" molecular and atomic phase and is believed to have delocalisation of the electrons within the G-layer. However, under

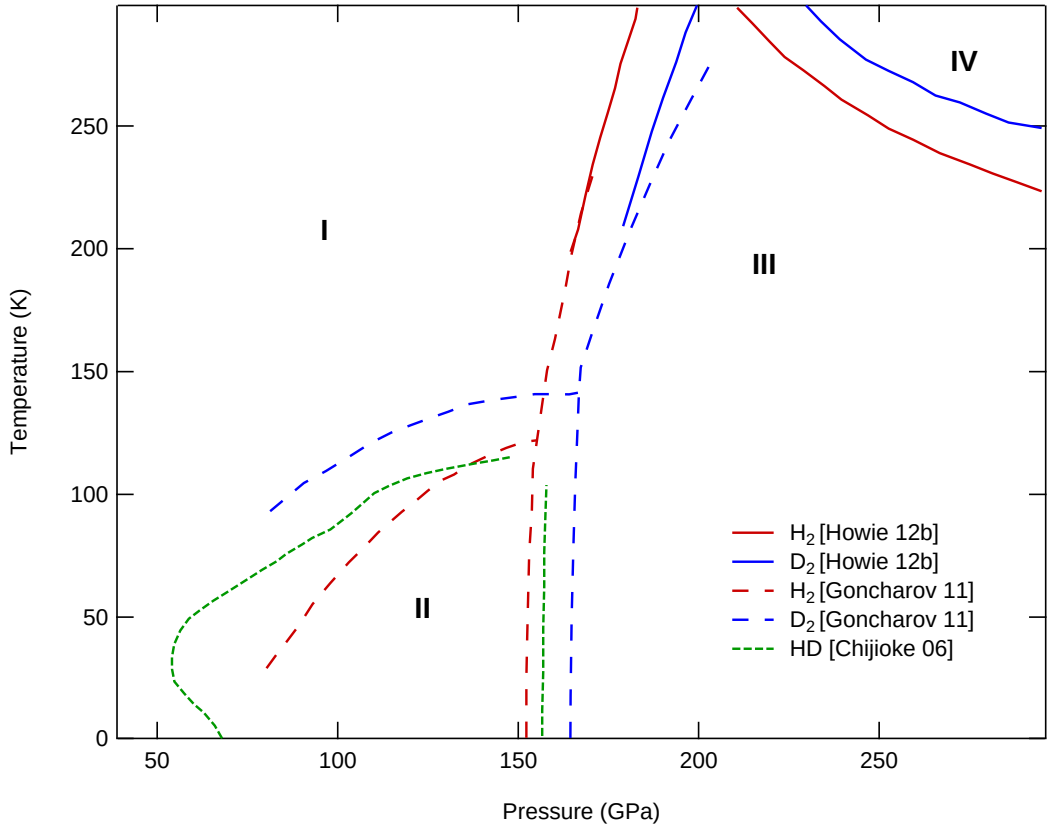

Figure 4.3: A review of the high-pressure and low-temperature phase diagram of H_2 (red), D_2 (blue) and HD (green).

sufficient compression hydrogen is still believed to undergo a complete pressure-induced dissociation and adopt a purely atomic metallic state. Recent theoretical investigations conducted at 0 K, suggest that this dissociation could happen at 380 GPa where the atomic $I4_1/amd$ (seen in figure 4.2C) and $R3m$ structures are found to be the most competitive.

As the contributing work is concerned with different isotopes, it is of importance to review their respective impacts to the phase behaviour. Qualitatively, all isotopes of the hydrogens (H_2, HD and D_2) exhibit the current well known molecular phases I, II and III. As briefly discussed earlier the phase lines between phases I, II and III are isotopically sensitive and a review of the phase diagram can be seen in figure 4.3 [Goncharov 11]. Interestingly, at very low temperatures, pure hydrogen deuteride exhibits re-entrant phase behaviour between phases I and II [Chijioke 06], seen in figure 4.3. However, above $\sim$

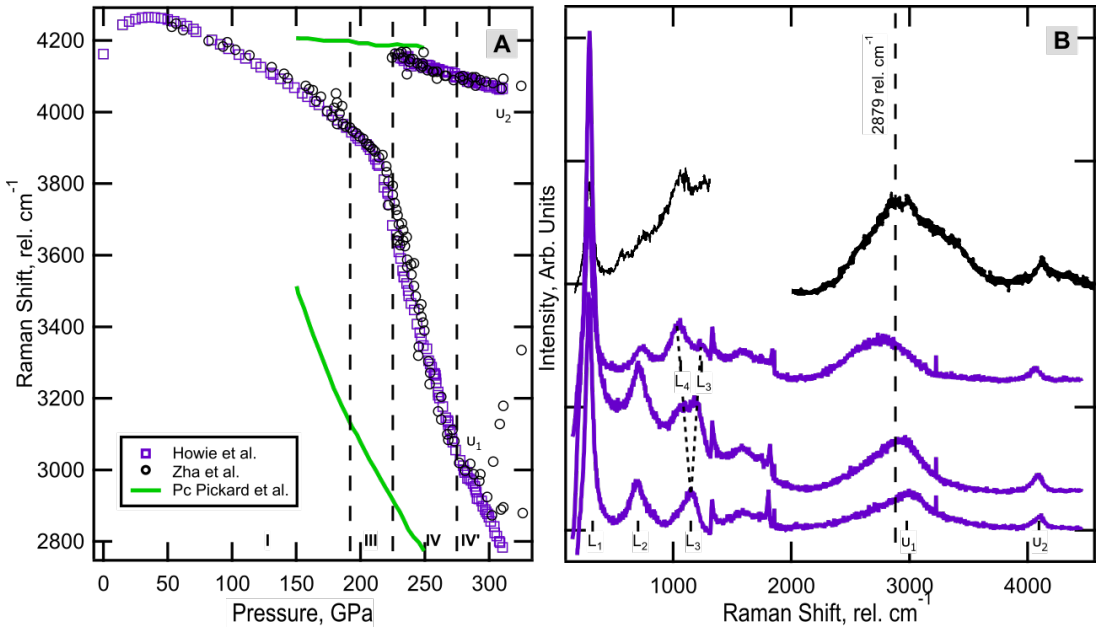

Figure 4.4: **(A)** Comparison of vibron frequencies from previous Raman experiments (purple) [Howie 12a] compared with the highest-pressure spectra taken from the recent Zha *et al.* publication [Zha 14] (black) the vertical dashed lines corresponds to the tranistion pressure for the relative phases. Additionally the theoretically predicted vibrational frequencies of the *Pc* structure [Pickard 07] (figure 4.2) are also given for reference. **(B)** Representative raman spectra from previous experiments (purple) [Howie 12a] compared with the highest-pressure spectra taken from the recent Zha *et al.* publication [Zha 14] (black) the vertical dashed line corresponds the lowest vibron frequency claimed by Zha *et al.* [Zha 14].

120 K the phase behaviour of HD is not known. On the other hand, the phase behaviour of H_2 and D_2 have been well resolved up to room-temperature and 300 GPa[Goncharov 11, Howie 12b], observing that the I-III and III-IV phase lines possess a large isotopic dependency similar to what is observed in the II-III transition at lower temperatures. Currently, the stability of the solid phases above 300 K and their isotopic dependency is not well understood and its clarification was one of the key motivators for the contributing work.

Currently, the limitation of compression at room temperature hydrogen studies is ∼310 GPa evidenced by Howie *et al.* Recent investigations by Zha *et al.* have claimed higher pressures and the appearance of new phases denoted by *"phase V, VI, VII"* over a 275-325 GPa range [Zha 14]. These claims however, conflict with

the earlier study by Howie *et al.*, which at lower vibron frequencies, an absolute indication for higher compression, observe no characteristics after the appearance of phase IV′ which could constitute a novel phase transition.

4.2 The Melting Curve

Conventionally a materials melting temperature is found to increase in response to increasing pressure, first experimentally realised by Perkins in 1826 observing the crystallisation of acetic acid (the main component of vinegar) around 1 kbar at room temperature. [Perkins 26]. Two prominent scientists of the 19th Century, Kelvin and Faraday, proved this wasn't consistent for all systems demonstrating that water's melting temperature falls under applied pressure [Thomson 50, Faraday 59]. The group I elements are found to exhibit the same nature, evolving through a maximum in the melting curve and then possessing a negative melting curve [Guillaume 11, Gregoryanz 05, Narygina 11]. Hydrogen, also being a group I element albeit molecular in nature, is also believed to exhibit a turnover in the melting curve.

An applicable mechanism for a negative melting curve was proposed by Abrikosov in 1960, suggesting that pressure enhanced zero-point energies could be sufficient in destabilising a crystalline lattice. It was later argued that hydrogen could exhibit this phenomenon, attributed to its light mass, and could possibly even transition into a liquid at 0 K [Brovman 72]). A contemporary first principles investigation by Bonev *et al.* has indicated that a maximum in hydrogen's melting curve may exist at 82 GPa and $\sim$ 900 K [Bonev 04]. The author's extrapolations of the meltline to higher pressures suggest that a solid-liquid transition exists at 300 GPa at 300 K and for a solid-ground state liquid transformation to exist at 400 GPa, both experimentally obtainable pressures. Interestingly, the proposed groundstate liquid has since been predicted to be a completely novel state of matter, exhibiting superconductivity or superfluidity depending on the magnetic fields applied [Babaev 04, Babaev 05].

Hydrogen was the last of Faraday's "permanent gases," categorised due to their reluctance to change state using the techniques of the time, to be liquified. Liquified hydrogen was finally achieved by James Dewar and was shortly after

solidified providing the first melting point on the hydrogen phase diagram, 13.8 K at ambient pressure [Dewar 01]. It took a further 80 years for the second melting point when Mao *et al.* solidified hydrogen at 5.7 GPa at 300 K using DAC technology [Mao 78].

The first systematic study of the melting curve was subsequently carried out by Diatschenko *et al.* mapping the melting curve from a melting temperature (T_m) 25 K at 0.04 GPa up to 368 K at 7.7 GPa [Diatschenko 85]. Datchi *et al.* further extended the melting line up to 15.2 GPa and 526 K (seen as the black diamonds in figure 4.1) [Datchi 00]. In this study, melting was determined by visual observation of the sample, it was found that the melting law proposed by Kechin best described the melting line [Kechin 01]. Interestingly, this empirical melting law features a maximum, after a bold extrapolation the authors suggested that a maximum could feature in the hydrogen phase diagram at 128 GPa and 1100 K [Datchi 00].

Gregoryanz *et al.* further extended the melting curve measuring subtle shifts in the vibron frequency using Raman spectroscopic techniques. The containment issues, suffered by the previous experimentalists [Datchi 00, Diatschenko 85], were circumvented through the use of non-metallic inserts allowing the constraint of the melting curve to 45 GPa and 850 K (seen as the red diamonds on figure 4.1)[Gregoryanz 03]. In agreement with Datchi *et al.* Kechins empirical melting law best described the data [Kechin 01], suggesting again that the melting line might evolve through a maximum at higher temperatures and pressures.

Laser heating techniques were subsequently employed to achieve melting at higher pressures, figure 4.1 provides examples of two studies Eremets *et al.* (Purple diamonds) and Subramanian *et al.* (yellow diamonds). The large temperature gradients, inherent to laser heating techniques, make the criteria for melting vague and the presence of a metallic coupler introduces chemistry that may not be accounted for. Nevertheless, if we take into account all the experimental melting data discussed it is noticed that empirical melting curves that do and don't feature a maximum, can adequately describe the melting line, seen by the extrapolations denoted (1) and (2) in figure 4.1.

The manifestation of a melting curve maximum is a highly unusual phenomenon and usually driven by interesting characteristics between the relative

densities of the solid and liquid states. The melting curve in the celebrated example of water for example, is driven by the solid phase being a large open cage-like crystalline structure resulting in a volume reduction when entering the liquid state. Hydrogen however is even more unusual as phase I is found in an efficiently packed hcp structure. Within the liquid phase of hydrogen, there is evidence for potential first-order phase transitions; the transition from a molecular to a dissociated liquid, which could prove to be the origin of the maximum in the melting curve. The first-order liquid-liquid transition was first theoretically treated by Scandolo, who observed a reduction in volume as low as 125 GPa and 1500 K using first principles calculations [Scandolo 03], which in close vicinity to previously extrapolated melting lines [Gregoryanz 03, Datchi 00]. The liquid-liquid transition has since been observed in theory by other groups in similar pressure-temperature conditions and are shown on figure 4.1 as hollow circles. However, a rather exciting recent ramp shockwave technique has observed an abrupt insulator-to-metal transition at much higher pressures and similar temperatures, which could be the manifestation of this first order phase transition [Knudson 15].

4.3 Summary

Now we have summarised the nature of hydrogen in these conditions, it is interesting to see that we have extrapolated, predicted and recently discovered phenomena, all happening in a region of P-T space where quantum, intermolecular and intramolecular effects come into play. It is clear that the most ambiguous region of hydrogen's phase diagram could prove to be the most informative and is therefore its exploration is of fundamental importance, providing answers for questions such as:

- Will there be any observation of a maximum in the melting curve? Any experimental evidence for a different type of liquid above the maximum, such as evidence for a first order phase transition in the liquid?
- What is the nature of the I-III-IV triple point? How will the phase line continue at higher pressures and temperatures?

- What is the thermodynamic stability of phase IV?
- What will happen at higher compressions: the persistence of phase IV or evolution to a new phase?

Chapter 5

Exploring the Stability of the Known Solid Phases of Hydrogen

5.1 Introduction

Using the aforementioned techniques discussed in the introductory chapters, we have succeeded in confining pure n-H_2 at temperatures in excess of 1000 K long enough to collect Raman spectra of sufficient quality to accurately track the parameter evolution, position and FWHM of the characteristic H_2 excitations in phases I, III, IV and the liquid. The data presented further extend the current understanding of the Hydrogen phase diagram up to 800 K below 200 GPa, up to 500 K between 200-275GPa and up to 325 GPa at 300K. These results will consequently require a significant revision of the H_2 phase diagram and is at odds with previous theoretical understanding [Bonev 04] see figure 4.1 and discussions in chapter 4.2.

5.2 Melting at Low Pressures

The diagnostic widely used within the contributing work was the parameter response of the hydrogen vibron, largely due to the rotational modes broadening with pressure and becoming increasingly difficult to deconvolute at higher

pressures or even be resolved at higher temperatures within phase I, shown in figures 5.3 and 5.2. Figure 5.1 demonstrates the parameter evolution of hydrogen's vibrational mode as a function of pressure.

Within the liquid phase at lower compressions, <2 GPa and 300 K, we observe a rather beautiful Raman structure attributed to rotational-vibrational phenomena [Haken 95]. The structure consists of several side bands, S and O-branches, to a sharp central peak with a width of 2.3 cm^{-1} at 0.2 GPa. Whilst remaining in the liquid phase and increasing pressure, increasing molecular collisions broadening the excitation and the resolution limit of the spectrometer this rotational-vibrational structure is gradually lost. Above 2 GPa only a fully symmetric vibron remains with a width of ∼12 cm^{-1} and remains approximately at this value until solidification at 5.5 GPa, seen in figure 5.1A and C.

The solid-liquid transition along the room-temperature isotherm was found at 5.5 GPa and is marked by the vertical dashed line in 5.1 B and C. In a previous study this phase transition was characterized by small positive shifts in the raman frequency upon melting, typically by a few cm^{-1} [Gregoryanz 03]. In the results obtained here, this feature is masked in figure 5.1 by the vibron's more significant isothermal pressure dependence ($(\frac{d\nu}{dP})_T$). There is however, a marked reduction in the vibron's width, by a factor of two from 12 cm^{-1} to 6 cm^{-1} upon solidification. A feature noticed in the first experiments to solidfy hydrogen at room temperature [Mao 78]. The reduction in the width of the vibrational mode is attributed to molecular collisions that are inhibited when the molecules form a crystalline lattice.

Along the room-temperature isotherm in phase I (5.5-180 GPa) the vibron persists as a complex function of pressure. $(\frac{d\nu}{dP})_T$ is found to be positive up to 35 GPa and progresses through a maximum, after which it starts to decrease, which is inidicative of an increased intermolecular interaction. After solidification the width of the vibrational mode is found initially to decrease with pressure reaching a shallow minimum ∼19 GPa after which it increases linearly at a rate of 0.5 $\frac{cm^{-1}}{GPa}$ due to pressure induced broadening.

Inverse behaviour to what was observed upon solidification (figure 5.2) is seen upon melting as expected and is represented in figure 5.2. Here, a solid-liquid transition is noted at 8 GPa, 14 GPa and 20 GPa at roughly 400 K, 590 K and

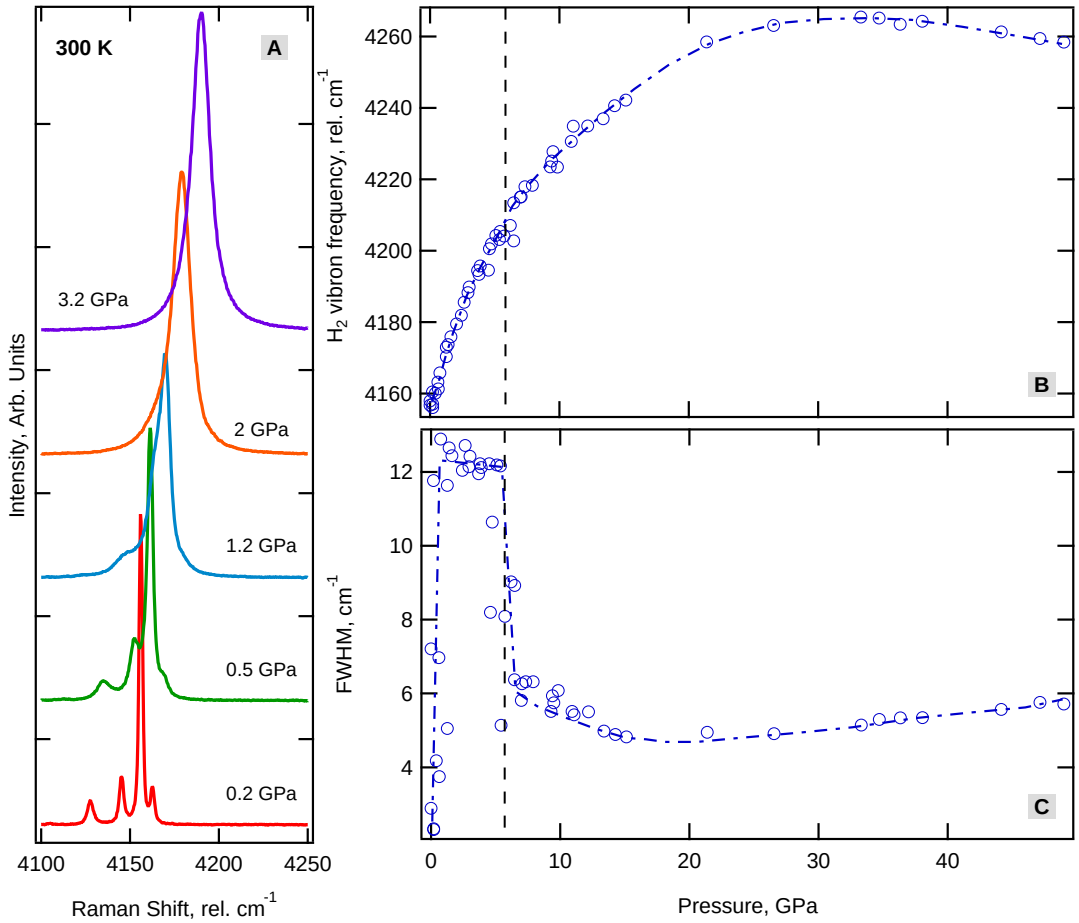

Figure 5.1: (A) Representative Raman spectra taken in the fluid state at 0.2 GPa up to 3.2 GPa, showing the amalgamation of several rotational-vibrational excitations of low density fluid into a single vibron at higher densities. The frequency of the vibrational mode (B) and full width at half maximum (FWHM) (C) as function of pressure along an isotherm at 300 K. The solidification at 5.5 GPa is marked by the black dashed line.

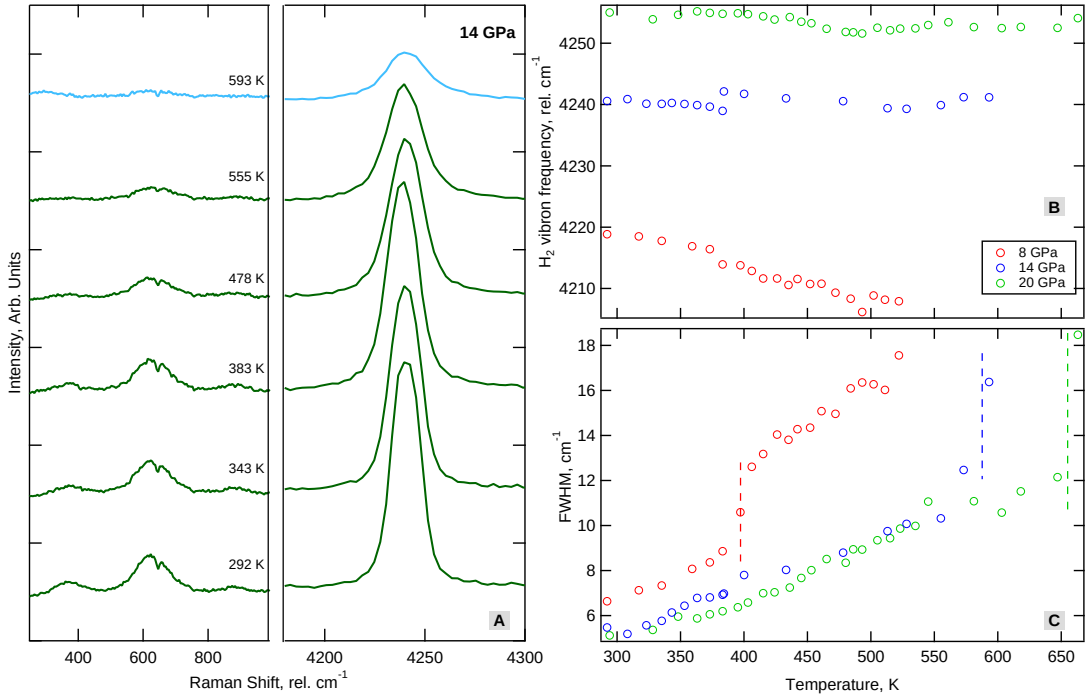

Figure 5.2: **(A)** Representative raman spectra at 14 GPa, melting is indicated by a change in colour from green to blue around 593 K. Panels **(B)** and **(C)** give the vibrational frequency and FWHM of the vibrational mode at 8 GPa (red), 14 GPa (blue) and 20 GPa (green) up to ∼660 K. Melting at each temperature is indicated by a dashed line of corresponding colour.

650 K respectively again by a significant change in the excitation's widths. The previously mentioned small frequency shifts, $\Delta\nu$, characteristic of crossing the solid-fluid phase boundary, which have previously been reported [Gregoryanz 03] are masked. The characteristic is most likely obscured, because of the choice of grating within the spectrometer and also possible pressure fluctuations during heating. It is therefore noted that a more sophisticated approach, measuring both the excitations width and frequency, needs to be taken to accurately track this phase transition in extended regimes. This is crucially important at higher pressures, where the characteristic frequency shift upon melting is significantly reduced [Gregoryanz 03]. Apart from melting, the other consistent features of hydrogen's response to elevated temperatures >300 K at low pressures (<180 GPa) are as follows:

- **Loss of rotational modes:** The low-frequency rotational modes become indistinguishable from the background at higher temperatures, and are not apparent in the fluid phase. This is evidenced by the blue spectra in figure 5.2A.
- **Softening of the vibron:** In all heating runs up to ∼180 GPa the vibron is found to soften, it shifts to lower frequencies. At higher pressures the softening upon heating is more pronounced, indicative of an increased anharmonicity suggesting that higher pressures coupled with high-temperatures could provide another P-T path to dissociation. Assuming isobaricity, ie. directly measure the pressure independent thermal dependency of the vibron $(\frac{d\nu}{dT})_P$, the effect was quantified, shown in figure 5.5. Reassuringly, these measurements are in excellent agreement with a previous study up to pressures of 150 GPa [Gregoryanz 03].
- **Loss of Sample:** We also note that when in the vicinity where melting is expected, extremely rapid sample loss becomes very common, attributed the increased mobility and diffusion of hot liquid hydrogen. Other than mechanical failure of the diamond, this was often found to be the hard limit to the experiments.

Above 130 GPa the vibrational mode's response to melting is quite unusual and doesnt follow the previously discussed criteria observed at lower pressures. In the heating run between 132-155 GPa we clearly observe a phase transformation

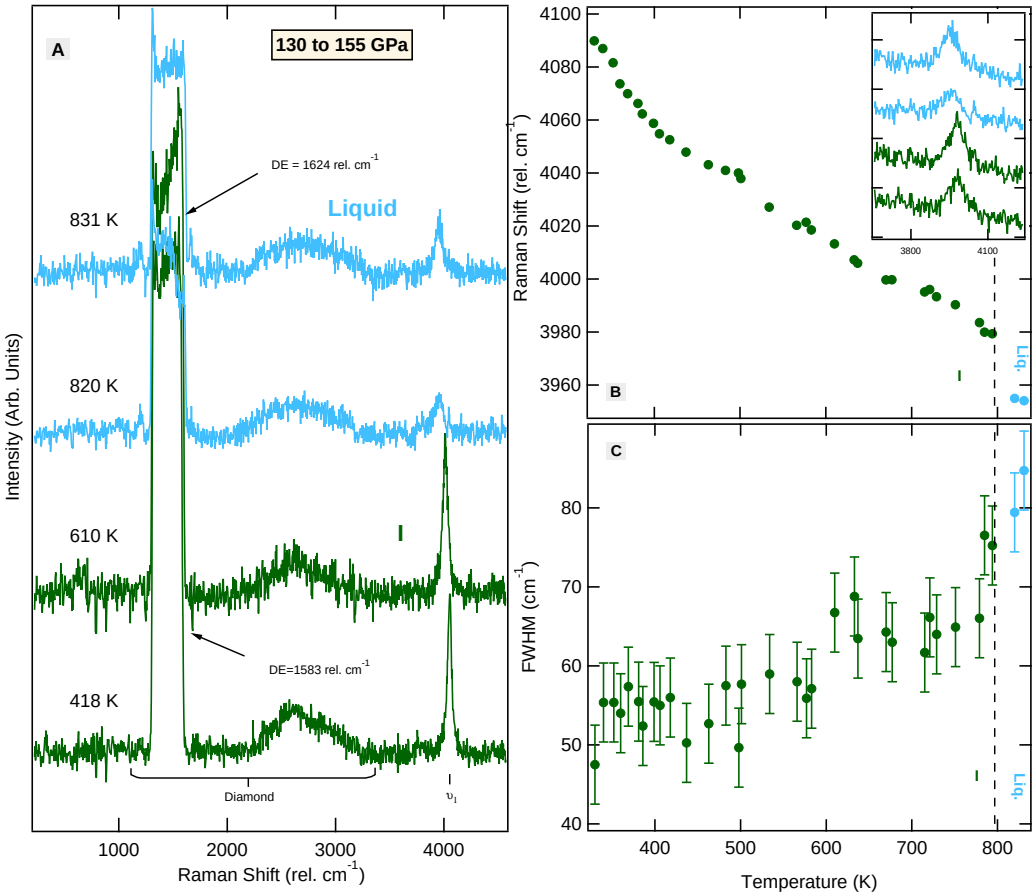

Figure 5.3: **(A)** Representative Raman spectra starting at 130 GPa and drfited up to 155 GPa during the course of the experiment, melting is indicated by a change in colour from green to blue around 800 K. Panels **(B)** and **(C)** give the vibrational frequency and FWHM of the vibrational mode up to $\sim$ 850 K. Melting temperature is indicated by the dashed line. **(B)**-Inset, is the raw Raman spectra of the vibron taken over the last 4 points.

which could be interpreted as melting at around 800 K, seen in 5.3. Both parameters, FWHM and frequency, of the vibrational mode (ν_1) change concomitantly and discontinuously. The FWHM is found to broaden, similar to what was observed at lower pressures seen in figures 5.1 and 5.2, whilst the vibrational mode is seen to significantly downshift by ~ 30 cm^{-1}. The downshift is intriguing and counter to what was observed at lower pressures in the contributing work and that of a previous study [Gregoryanz 03]. The downshift, ie. an increased bondlength, it is most likely a direct consequence of hydrogen's exotic melting characteristics and is probably due to gradual changes in the relative densities between the solid and the liquid phases.

5.3 Solid-Solid Transitions

Above 180 GPa and at room temperature H_2 is found to transform from a randomly orientated hexagonal close packed (hcp) phase I into the structurally elusive phase III. Originally characterised by observing a large discontinuity in the vibrational frequency at 70 K and 150 GPa [Hemley 88]. Here, for the first time, we report a solid-solid phase transition in the hydrogen system above room temperature, shown in figure 5.4. The transition, a continuation of the I-III transition discovered in the aforementioned study, is noted by profound changes in the molecule's vibrational characteristic. The transition is observed at 370 K and 220 GPa as a concomitant hardening, 20 cm^{-1} and a reduction in the width to a third of its original. The knowledge of this additional P-T point provides further constraint on the continuation of the I-III phase line and suggests that its gradient ($\frac{dP}{dT}_{I-III}$) must remain positive up to these pressures and temperaures. In the continuation of this experimental run, represented in figure 5.4, above 550 K we observed a rapid loss of signal, although there was no vibrational information to evidence melting, we do attribute the enhanced diffusion and sample loss to the increased problems with containment of the liquid - a similar trait to what was observed at lower pressures.

The vibron's response to temperature after the III-I transition is quite fascinating and perhaps is evidence for an altered electronic structure or a possible evolution into a different liquid state. As such, the region of P-T space where we observe such characteristics is tentatively denoted as phase I′. Firstly, the previously observed characteristic vibrational mode softening upon heating which was accentuated by the application of pressure, seen in figure 5.3 and the inset to figure 5.5, is now instead hardening, seen in figure 5.4B. This unusual effect is observed in all runs in phase I above 180 GPa and it becomes more pronounced with pressure. It is important to note that this change of temperature dependence can't be explained by the pressure fluctuations during the heating cycle. For example, in figure 5.4 an observed 5 GPa increase should incur a 50 cm^{-1} decrease in the frequency (assuming $\frac{d\nu}{dP}_T$ ∼-10 $\frac{cm^{-1}}{GPa}$ at 300 K), instead a greater than double 120 cm^{-1} in the vibron frequency is recorded. This change coupled with the gradual decrease of the vibrational mode's width (figure 5.4), is suggestive, quite counterintuitively, that the molecules in hydrogen phase I above 180 GPa

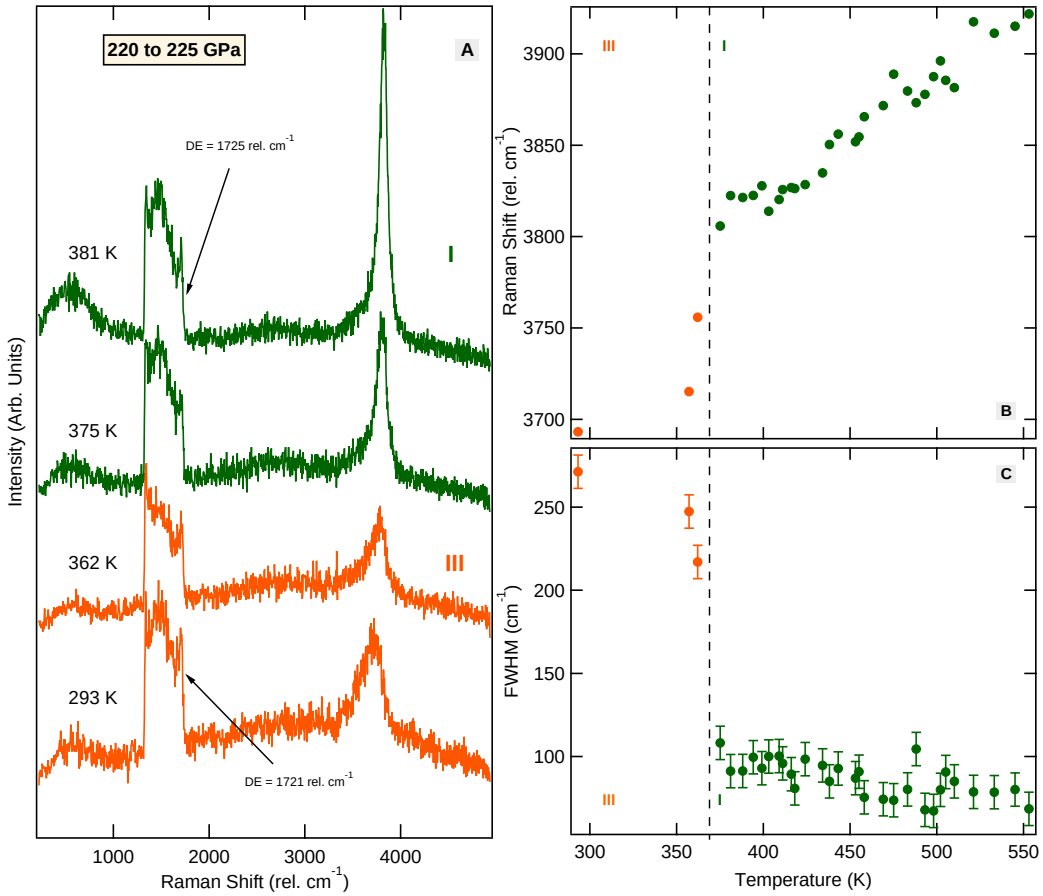

Figure 5.4: **(A)** Representative Raman spectra of hydrogen upon heating in phases III (orange) and I green) at pressures between 220 and 225 GPa. Position **(B)** and FWHM **(C)** of the vibrational mode ν_1 at 220 and 225 GPa as function of temperature through the phase I $\leftrightarrow$ phase III transformation, which is marked by the vertical dashed line.

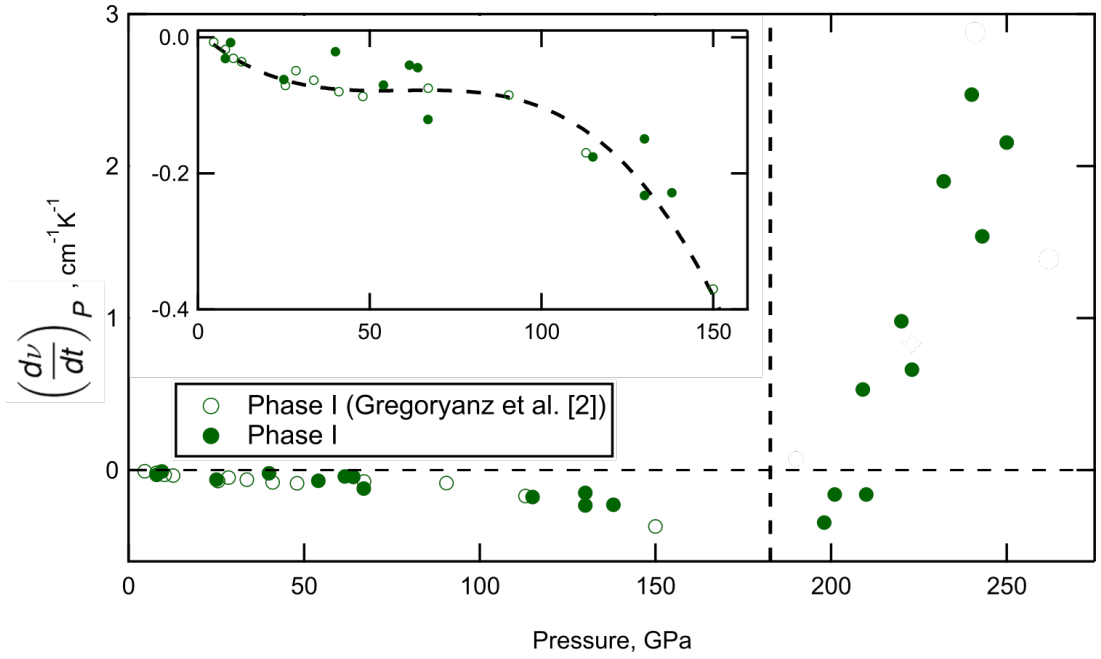

Figure 5.5: $(\frac{d\nu}{dT})_P$ over the investigated pressure range. Filled green circles are points from this study in phase I, while open cirlces are from Gregoryanz *et al.* [Gregoryanz 03]. The dashed line at 180 GPa indicates the pressure at which there might be a possible phase I $\leftrightarrow$ I' transition. The inset shows a "blown up" view of the nature of the vibron anharmonicity below 150 GPa with the symbols and axis corresponding to the host figure, the dashed line serves as a guide to the eye.

are becoming less anharmonic with temperature.

Figure 5.6 is representative of an experimental run where we allowed pressure to fluctuate through several heating and cooling runs during which we observed a net increase of $\sim$ 60 GPa to ultimately 258 GPa. Cycling through pressure and temperature we observed many solid-solid transitions outlined below:

1st Cycle: (Figure 5.6A, B and C) Pressure was found to increase by $\sim$ 30 GPa. On cooling, hydrogen was found to enter into phase III with the vibron characteristically broadening and softening, similar to what was characterised earlier and seen in figure 5.4.

2nd Cycle: (Figure 5.6D, E and F) Pressure again increased throughout the cycle with a net increase of $\sim$ 10 GPa. On heating the phase III to phase I transition is observed. However, on cooling we observe hydrogen

entering into phase IV at around $\sim$ 332 K and 243 GPa characterised by the appearance of an additional vibrational mode. This demonstrates that Phase IV is not stable at elevated temperatures at this pressure and prefers to transform into Phase I at higher temperatures.

3rd Cycle: (Figure 5.6G, H and I) In this heating cycle the previously undetermined IV-I phase line is further experimentally constrained with the transformation observed at 349 K at 245 GPa and 373 K at 253 GPa.

Throughout all these cycles, apart from the initial heating (solid symbols in figure 5.6B), the vibron in phase I was observed to harden with temperatures, a positive $((\frac{d\nu}{dT})_P)$. A phenomena which was noticed in all phase I heating/cooling cycles at these pressure and the almagamated $((\frac{d\nu}{dT})_P)$ data is represented in figure 5.5. We can see not only has the vibron dependence with temperature changed, but there is also an increase in the order of magnitude,$\sim$-0.5 to 2.5 $cm^{-1}K^{-1}$, at higher pressures. As discussed previously, this phenomenon can't be described by pressure fluctuations alone. Ideally, if one could accurately measure the isothermal pressure dependence $(\frac{d\nu}{dP}_T)$, the values in figure 5.5 could be corrected for the changes in pressure during heating/cooling. However, at pressures above 150 GPa, where we observe the onset of a positive $((\frac{d\nu}{dT})_P)$, the measured $(\frac{d\nu}{dP}_{T=300K})$ can not provide an accurate correction as it is a characteristic of a different solid phase (phase III/IV not phase I).

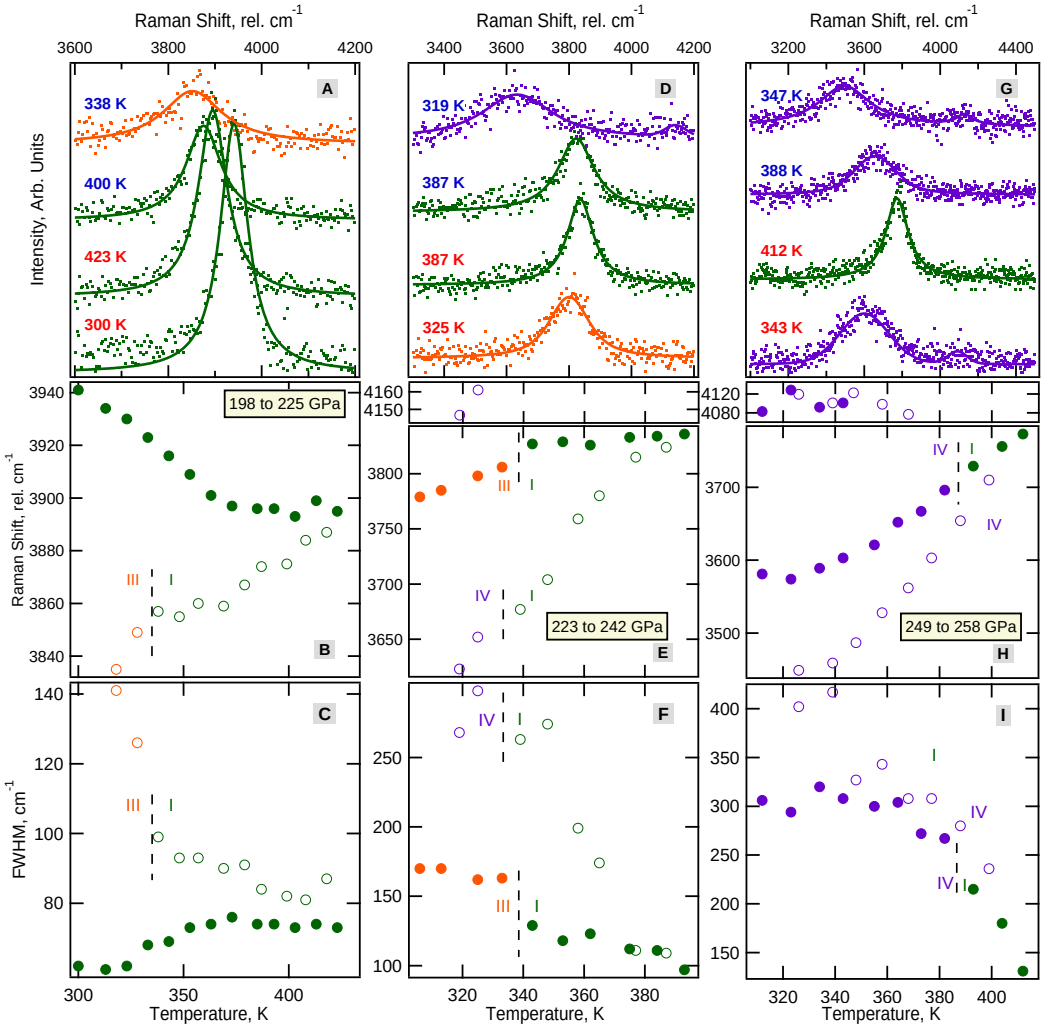

Figure 5.6: Representation of several consecutive heating runs conducted on hydrogen: 1st heating ((**A**),(**B**) and (**C**), 2nd heating ((**D**),(**E**) and (**F**)) and 3rd heating ((**G**), (**H**) and (**I**)). Each set of graphs has representative Raman spectra as well as the frequencies and FWHMs of the vibrational modes. The solid and empty circles represent points taken on heating and cooling respectively. Colours of the circles signify different phases in which the measurement was taken: I (orange), III (green) and IV (purple). During the first heating, the sample was at a nominal pressure of 198 GPa, which increased to 225 GPa. In the second heating cycle the starting pressure was 223 GPa, which increased to 242 GPa and in the third heating, the pressure increased from 249 GPa to 258 GPa.

5.4 Melting above 200 GPa

Above 220 GPa at vibrational frequencies below 3800 cm^{-1} at room tempertature, hydrogen enters into the recently discovered phase IV [Howie 12a, Eremets 11]. This phase is easily identifiable due to its remarkable vibrational structure, containing two vibrational modes and a multitude of excitations at lower frequencies. It is observed at lower pressures in the last chapters that phase III upon heating, transforms into either phase I or phase IV. Within the experimental runs reported in this section, where heating is initiated in phase IV at room temperature, two transformations are observed. The first transformation being a IV-I transition, with identical characteristics shown in 5.6, and the latter into a new phase that could be interpreted as melting (I-Liquid transition).

The initial transformation into phase I is observed by the two consecutive heating and cooling cycles shown in figure 5.7 and 5.8 respectively. The transformation to phase I is in agreement with what we have observed in heating/cooling cycles at lower pressures, seen in figure 5.6 and is again determined by the (dis)appearance of the additional vibrational mode and librational modes. Within these heating/cooling cycles it is observed that the transformation happens at higher temperatures for higher pressures, indicative that the I-IV phase line must continue with a positive gradient in P-T space.

At higher temperatures, a further phase transition is noticed, attributed to melting and is much more abrupt than what has been noticed at lower pressures and temperatures. Shown in the quasi-isobaric heating run (figure 5.7) at 245 GPa and ∼500 K, the vibrational frequency of ν_1 becomes seemingly temperature independent when compared to its nature at lower pressures and temperatures. The vibrational mode also becomes exceedingly narrow with a FWHM of < 200 cm^{-1}, remarkably low for these pressures. Identical behaviour is observed when the load on the sample is increased by 5 GPa and cooled down back to room-temperature, figure 5.8. Upon cooling it is noticed that the Liquid-I transition happens at lower temperatures, whilst the IV-I transition happens at higher pressures. If this trend continues it is suggestive that a new triple point may exist in the hydrogen phase diagram (I-IV-Liquid) and would have profound implications on the continuation of the melting curve.

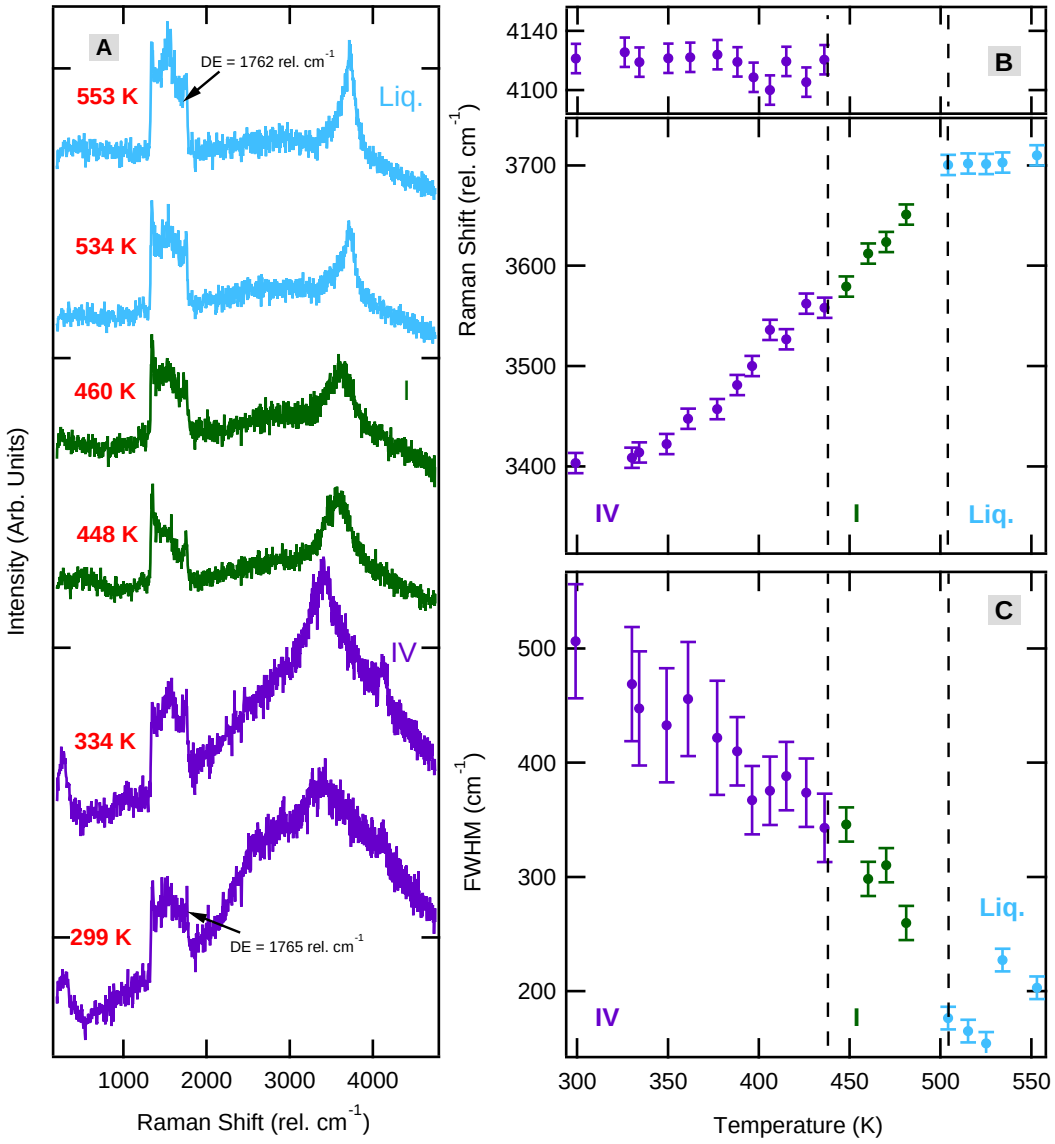

Figure 5.7: **(A)** Representative Raman spectra of hydrogen upon heating in phases IV, I and the liquid phase at 245 GPa. The observed diamond edge frequency is indicated on spectra at room and highest temperature spectra. Positions **(B)** and FWHMs **(C)** of the vibrational modes ν_1 and ν_2 are plotted. The colours correspond to the different phases: IV (purple), I (green) and liquid (blue). The vertical dashed lines indicate the IV $\leftrightarrow$ I $\leftrightarrow$ liquid phase transitions.

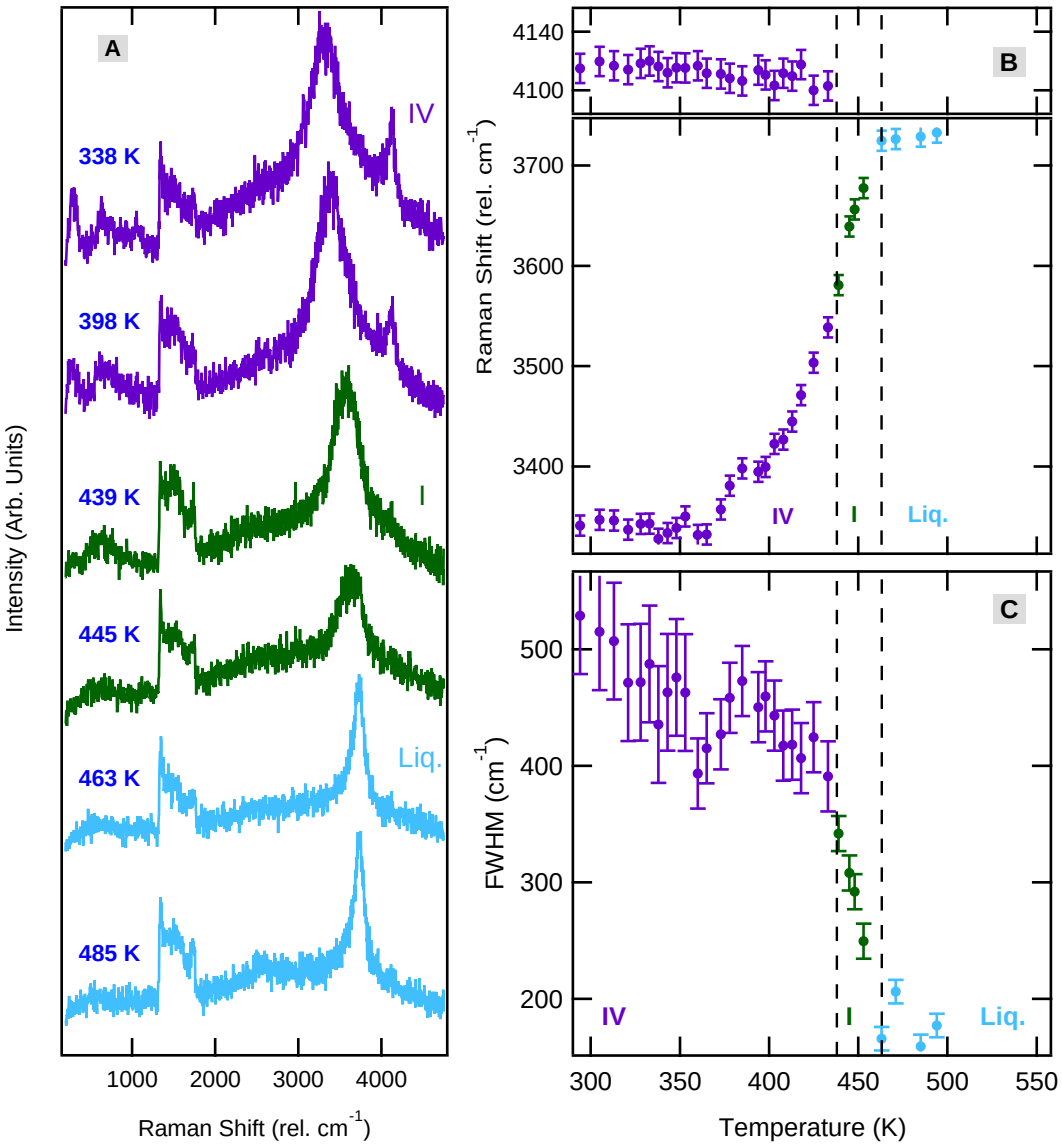

Figure 5.8: **(A)** Representative Raman spectra of hydrogen on subsequent cooling after heating (figure 5.7) in phases IV, I and the liquid phase at 250 GPa. Positions **(B)** and FWHMs **(C)** of the vibrational modes ν_1 and ν_2 are plotted. Again the colours correspond to the different phases: IV (purple), I (green) and liquid (blue). The vertical dashed lines indicate the IV $\leftrightarrow$ I $\leftrightarrow$ liquid phase transitions.

5.5 Discussion

Figure 5.9 is a completed phase diagram and acts as summary of all the P-T points studied during the course of this research project. The melting points from this study and also previous experimental works have been fitted the empirical Kechin melt formula, equation 5.1 where $\Delta P = P - P_0$ [Kechin 01]. Taking P_0 and T_0 to be the solidifaction at room temperature (300 K and 5.5 GPa [Mao 78]), the fitting parameters were found to be: a=6.7(4), b=0.65(7) and c=8.2(2)x10^{-3}. Primarily, it is clearly evident here that the melting curve, which is in astoundingly good agreement with the theoretically calculated points by Bonev et al. [Bonev 04], constrains the maximum in the melting curve at around 80 GPa and 900 K. Perhaps what is more interesting, is the implications for the evolution of the melting curve at higher pressures, which would involve a revision of the predicted pressures of room-temperature melting and a ground state liquid.

$$T_m(P) = T_0(1 + \frac{\Delta P}{a})exp(-c\Delta P) \tag{5.1}$$

Firstly, we turn our attention to the nature behind the turnover in the melting curve. The macroscopic relationship between the solid and liquid states was one of the earliest conjectures in thermodynamics and is dictated by the Clausius-Clapeyron equation, $\frac{dP}{dT} = \frac{\Delta S}{\Delta V}$. Assuming that upon melting there is always an increase of entropy, the melt line's gradient in figure 5.9 will be defined by the relative molar volumes between the solid and liquid phases. It could be argued that the volume reduction in the liquid could be due to a dissociation mechanism. However, due to the prominence of the vibrational mode up to the highest pressures (figure 5.8), a direct observation of a continued molecularly bonded state, we can rule this out as a mechanism for a relative volume reduction between the solid and liquid states. Instead, gradual changes in the liquid phase relative to the solid must be responsible. Interestingly, at pressures above the melting maximum, an abrupt reduction in frequency (30 cm^{-1} - figure 5.3) suggests an increase in the intermolecular interactions. The significant downshift could be explained by the evolution to a denser liquid state, as stated previously a necessity for negative gradient of the melting curve. This experimental result is in agreement with a theoretical study by Bonev *et al.* [Bonev 04] who also attributed

the volume reduction on melting due to a softening of the intermolecular potential.

Phase I is found to be stable in an exceedingly extensive P-T range, which is in contrast to phase IV that has a relatively small stability field (225-275 GPa and 250-450 K). Heating runs in phase I below 200 GPa evolve intuitively, with gradually increased anharmonicity at elevated temperatures and pressures ie. the vibron becomes broader and reduced in frequency. Above 200 GPa however, phase I demonstrates alternative behaviour upon heating, the vibron shifts to higher frequencies and becomes increasingly narrow. The spectral signature still being identical to that of phase I, but alternative behaviour is suggestive of a transition to a structurally similar phase, denoted as phase I$'$ and the dashed line seen in figure 5.9.

Upon heating, phase IV is found to be superseded by phase I and eventually by a further transition to the presumably liquid phase. The provided measurements provide constraints to the previously unknown I-IV phase line and it's seen to be a continuation of the I-III phase line [Hemley 88, Goncharov 11]. The I-IV phase line is found to continue at a constant gradient until it reaches the melt line, constituting a new triple point (I-IV-Liquid). This is the third known triple point in the H_2 system and the first on the melting curve, possibly having implications for the continuation of the melting line which will be discussed later. As discussed previously, measurements in the liquid phase at the highest pressure have no indication of the previously proposed dissociation transition in the liquid. Therefore, much higher temperatures and pressures are required to achieve this state, which is in agreement with a recent experiments that report the transition at $\sim$ 300 GPa and 1000-2000 K [Knudson 15].

The extended understanding of the evolution of the melting curve pose questions about a possible melting minima and the transition to the previously proposed ground liquid state [Brovman 72, Bonev 04]. Heating runs in phase IV and the persistence of solid phase IV up to 350 GPa are suggestive that the extrapolated melting line after the I-IV-Liquid triple point will undergo a deflection. The deflection of the melting line, as seen in figure 5.9, is a reduction in the $\frac{dP}{dT}$ gradient and would rule out the proposed room-temperature melting below 400 GPa [Bonev 04]. Consequently, revising the ground state liquid to much higher pressures [Brovman 72, Bonev 04]. In fact, the most recent results from

numerical laboratories regarding the evolution to the melt line, which includes contributing zero-point energy terms, are in good qualitative agreement with what we have observed in this study. Liu *et al.* have previously observed in their simulations, a revised melt line that flattens at 300 GPa and continues to run quasi-parallel to the pressure axis up to 600 GPa [Liu 13]. In a complimentary study by Chen *et al.* suggest an atomic to ground state liquid transition to above 900 GPa, which would require a modification of the melt line at lower pressures and higher temperatures [Chen 13].

A third possibility of the continuation of the melting curve is that it could evolve though a minimum, the manifestation of this feature would make the hydrogen phase diagram at high density look remarkably similar to the other group I elements, such as: potassium [Narygina 11], sodium [Gregoryanz 05] and lithium [Guillaume 11]. Remarkably the phase digrams for these system all exhibit a melting minimum accompanied by a clustering of rich complex phases. The hydrogen phase diagram could mimic these systems at high densities if with the presence of phase III, IV, IV′ and V (discussed in the following chapter) are accompanied by a speculative melting minimum.

It is important to stress the limitations of Raman spectroscopy as a method to detect melting and therefore, one needs to consider other phenomena which could have led to the changes in the Raman spectra in this study. Speculation that the drastic changes reported here on increasing temperature above 130 GPa could be due to a solid-solid phase transition and not melting. The amalgamated data could probably rule out this speculation for the following reasons: the Raman spectra at the highest temperatures are very simple and characterised by a relatively narrow (at given pressures) single vibrational mode and absence of rotational/librational modes (Figures 5.7, 5.8 and 5.3), mimicking that of the liquid state at lower pressures (figure 5.1 and 5.2). The assumption of a solid-solid phase transition, the alternative to melting, would imply that there is new phase of solid hydrogen existing somewhere between 130 and 270 GPa with very high melting temperatures. The presence of such new high-temperature solid phase (instead of a liquid state) would be an interesting observation in itself and poses several questions that would require a profound revision of our current understanding of hydrogen at these conditions. If it were a new, structurally simple solid phase, then new models of hydrogen are clearly needed to explain

the appearance of new structures and the revision of the melting curve. However, experimental advancements in methods that could directly determine melting of hydrogen at these conditions (*e.g.* Brillouin spectroscopy, x-ray diffraction) would be highly beneficial.

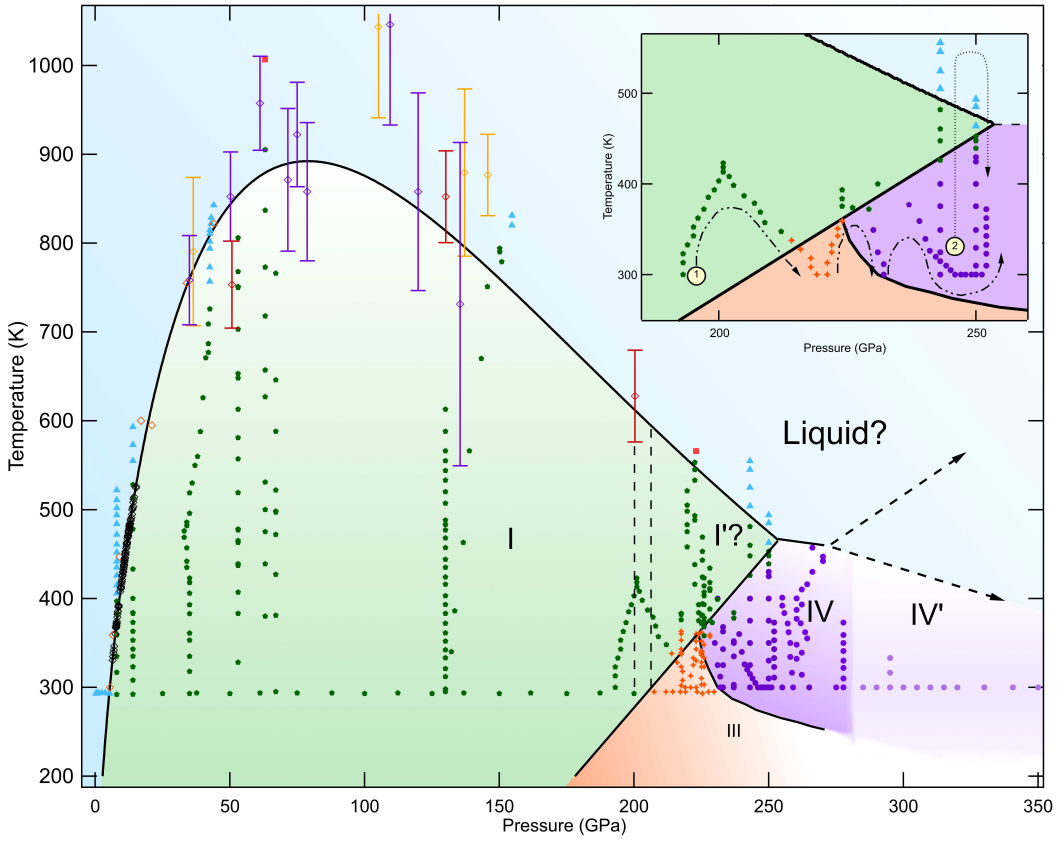

Figure 5.9: Proposed phase diagram of hydrogen up to 400 GPa. The inset shows the P-T paths taken during the temperature cycle as indicated by the arrows: (1) Fig. 5.5 and (2) Fig 5.7 and Fig 5.8. No hysteresis was detected in any of the runs. The melting curve is fitted using the Kechin empirical melting formula [Kechin 01]) to the data points obtained in this and previous studies [Datchi 00, Gregoryanz 03]. Previous experimental and theoretical melting data are overlayed by different colour hollow diamonds: green (Subramanian *et al.* [Subramanian 11]), purple (Eremets *et al.* [Eremets 09]), orange (Gregoryanz *et al.* [Gregoryanz 03]), blue (Bonev *et al.* [Bonev 04]) and black (Datchi *et al.* [Datchi 00]). The phase lines between phases I, III, IV and new solid phase are from this study and Refs.[Howie 12a, Howie 13a] . Some of the P-T paths taken here are shown in solid symbols with different colours corresponding to different phases as in the previous figures 5.6, 5.7 and 5.8. The red squares show where the H_2 rapidly diffused from the sample chamber, resulting in the loss of Raman signal. The vertical dashed lines at around 180 GPa indicates the pressure region at which $(\frac{dv}{dT})_P$ changes sign and magnitude see figure 5.5. The dashed line ending with the question mark is a possible continuation of the melting curve. Phase II and the triple point between I, II and III which are located below 200 K are not shown here, but can be seen on the previous phase diagram 4.1. The lines between the phases have an error bar of about ±15 GPa but are consistent with previous studies [Howie 12a, Howie 13a].

Chapter 6

Room Temperature Compressions up to 400 GPa

6.1 Introduction

The contributing work in this chapter marks a new high pressure achievement as hydrogen and its heavier isotopes hydrogen deuteride and deuterium were compressed to pressures of 384 GPa, 388 GPa and 380 GPa respectively at 300 K. These conservative measurements (using a more contemporary calibration, we record pressures in excess of 450 GPa) are amongst some of the highest static pressures ever recorded in the laboratory and the highest any of the hydrogen systems have ever been subjected to. These experimental data are indicative that above 325 GPa H_2 and HD adopt a new solid phase (phase V). Analysis of the spectra over the IV-V transition is suggestive that under compression, the molecular bonding in the G-layers of the *Pc* structure lengthen and symmetrise, evolving into the *Ibam* structure. It is also speculated that this phase could be a precursor to the elusive, purely atomic $I4_11/amd$ structure which is predicted to be stable at higher pressures (>400 GPa). The transformation to phase IV′ is found to occur above 310 GPa in D_2, resulting in the largest pressure difference between the species and delaying the onset to D_2-phase V to at least 380 GPa.

6.2 The IV-IV′ Transition in Deuterium

Deuterium has already been found to possess the same spectroscopic characteristics of phase IV, analogous to that observed in hydrogen, albeit with isotopically shifted frequencies. Under further compression, phase IV in hydrogen was found to undergo relatively subtle spectral modifications suggestive of a transition to a configuration structurally similar, tentatively denoted in the literature as phase IV′. Here we report spectral changes analogous to the hydrogen phase IV-IV′ transition in deuterium.

Figure 6.1 is representative of the amalgamated data collected in all the experimental runs on deuterium up to 380 GPa and 300 K. This is the highest pressure deuterium has been exposed to experimentally in a static regime and stands amongst the highest pressures ever recorded within a conventional DAC. Up to pressures of 310 GPa, the vibrational response is found to be in agreement with previously reported measurements found in the literature ie. the following transitions at room temperature: I-III at 185 GPa and III-IV at 235 GPa (the latter denoted by the dashed line on figure 6.1).

Above pressures of 310 GPa, marked by the dashed line in figure 6.1A and B, we observe spectral modifications analogous to that of the previously reported IV′ transition in hydrogen (seen in figure 6.9 and figure 6.8 for a direct comparison between the isotopes). The L_3 mode broadens and splits to produce the new L_4 branch, meanwhile the soft vibronic mode ν_1 becomes less pressure dependent, $\left(\frac{d\nu_1}{dP}\right)_T$ changes from -7.5 to -2 $\frac{cm^{-1}}{GPa}$. Concomitantly with these changes there is also an overall enhanced Raman response from the sample; for example compare the spectra at 300 GPa with 380 GPa in the waterfall presented in figure 6.1B, a feature previously reported for the pure hydrogen species. Above 350 GPa all the librational modes appear to be weakly pressure dependent, reflecting a similar gradient to that of the hard vibronic mode (ν_2) emanating from the strongly bonded molecular layer. Upon further compression, above pressures of 310 GPa, there was no spectral evidence indicative of a futher phase tranisition of modification of IV′ up to 380 GPa.

A wealth of information can be derived from the low-frequency modes, which themselves are a consequence of rotational and translational movements within

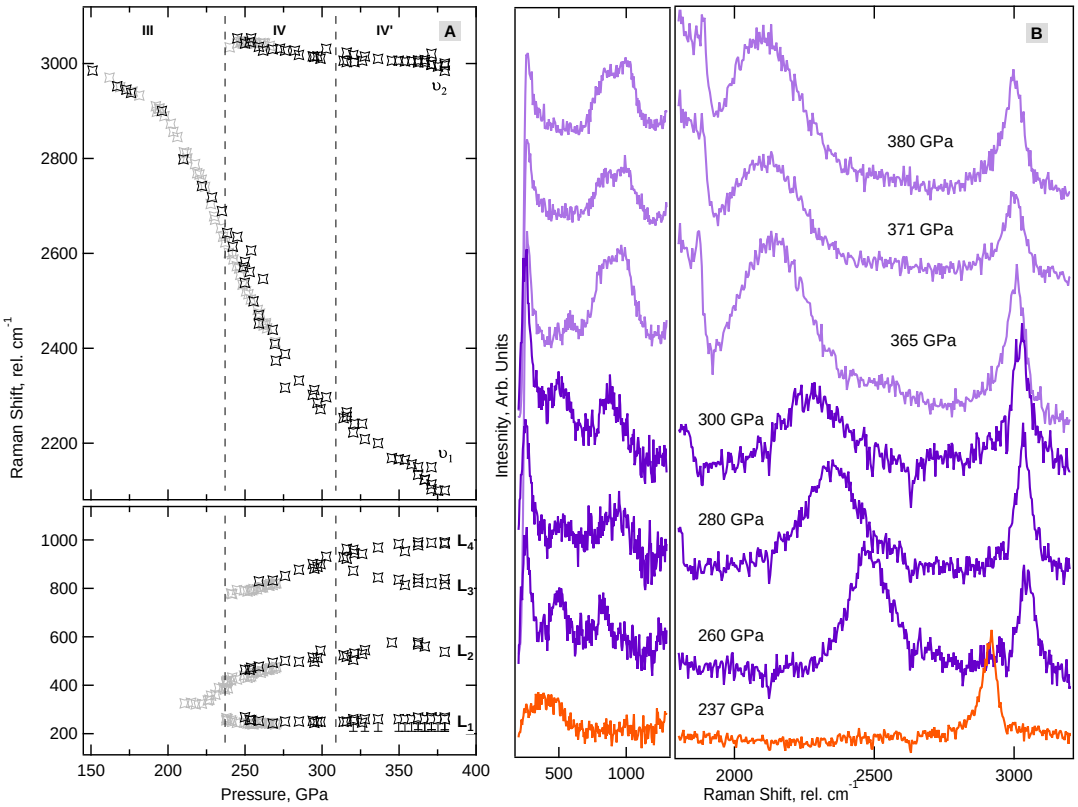

Figure 6.1: **(A)** Experimentally measured frequencies of the vibrational and low energy modes as a function of pressure, data collected from this study (empty black stars) are overlayed with previously reported results (empty grey stars). **(B)** Representative Raman spectra of deuterium up to 380 GPa all at 300 K, different colours correspond to different phases: phase I (green), phase III (orange), phase IV (dark purple) and phase IV' (light purple).

the structure. Unfortunately due to the experimental configuration, the L_1 mode is partially cut by the notch filter, clearly seen in the spectra in figure 6.1. Despite this upon its emergence, originally in phase IV, it seemingly remains the most intense librational mode and persists up to the highest pressures diplaying a weak pressure dependence. The other librational modes characteristic of phase IV′ (L_2, L_3 and L_4) are all clearly resolved in the spectra, seen in figure 6.1. There are interesting differences in the intensity landscape of the librational modes when comparing deuterium with the lighter isotope, hydrogen. Most noticeably, L_2 in deuterium becomes hard to distinguish from the background whilst being clearly visible in all pure hydrogen IV′ spectra [Howie 12a]. Additionally, the observed redistribution of intensity after the splitting of the L_3 appears to be enhancing the L_3 and not the L_4 mode, which was observed previously in hydrogen spectra.

Finally, we report the lowest ever vibrational frequency ever reported for any of the hydrogens of 2100 cm^{-1}, resulting in a rather spectacular Raman signature where the vibrational hydrogen band ν_1 overlaps with an optical phonon from the stressed diamond anvil.

6.3 Evidence for Phase V

In this section we report the first optical studies on Hydrogen and Hydrogen Deuteride (present in a hydrogen (75%) deuterium (25%) mixture) just below 400 GPa and ambient temperatures. Up to 325 GPa our data is in agreement with previous Raman studies, observing the evolution from solidification up to phase IV′, characterized by the presence of 6 excitations - two of which are vibrational modes. Above 325 GPa by profound concomitant changes in intensities, the soft vibrational modes (ν_1), pressure dependency and the loss/modification of librational modes, we infer a transition to a novel structural configuration of hydrogen, phase V.

Calculating the relative Raman intensities in the diamond anvil cell is a difficult task especially when with a low signal-to-noise ratio (seen in figure 6.2). Therefore, the intensity analyses presented in this chapter (figure 6.6) are only from spectra with the highest signal-to-noise ratio and from the same experimental run. Firstly, the background generated by the pressure-induced fluorescence of the diamond anvils is subtracted. The residual data is then fitted with Voigt profiles, producing the values for the integrated intensity of each excitation. Often the Voigt profiles tend to provide an accurate fit, however results need to be taken with caution when dealing with complex excitation shapes, such as the broad 2^{nd} order Raman diamond band. The cumulative area under the fit is then calculated and a percentage of total Raman activity is deduced. It's important to note that due to the extremely small sample volume, the 2^{nd} order Raman band of diamond becomes comparable in intensity to the vibrational excitations (see inset to figure 6.2). Consequently, at higher pressures where the ν_1 excitation overlaps with the 2^{nd} order Raman diamond band extra care has to be taken. To solve this issue, the evolution of the spectra with pressure (using fits from a previous pressure step as an initial guess) and the observed relative intensities between the 1^{st} and 2^{nd} order diamond are used to determine the integrated intensity of ν_1.

Above 325 GPa, upon reaching phase V, there is a rapid loss in intensity of the vibrational modes ν_1 and ν_2. In the case of HD, the vibrational modes become indistinguishable from the background above 350 GPa, seen in figure 6.3. With hydrogen however the vibrational modes, although with a heavily

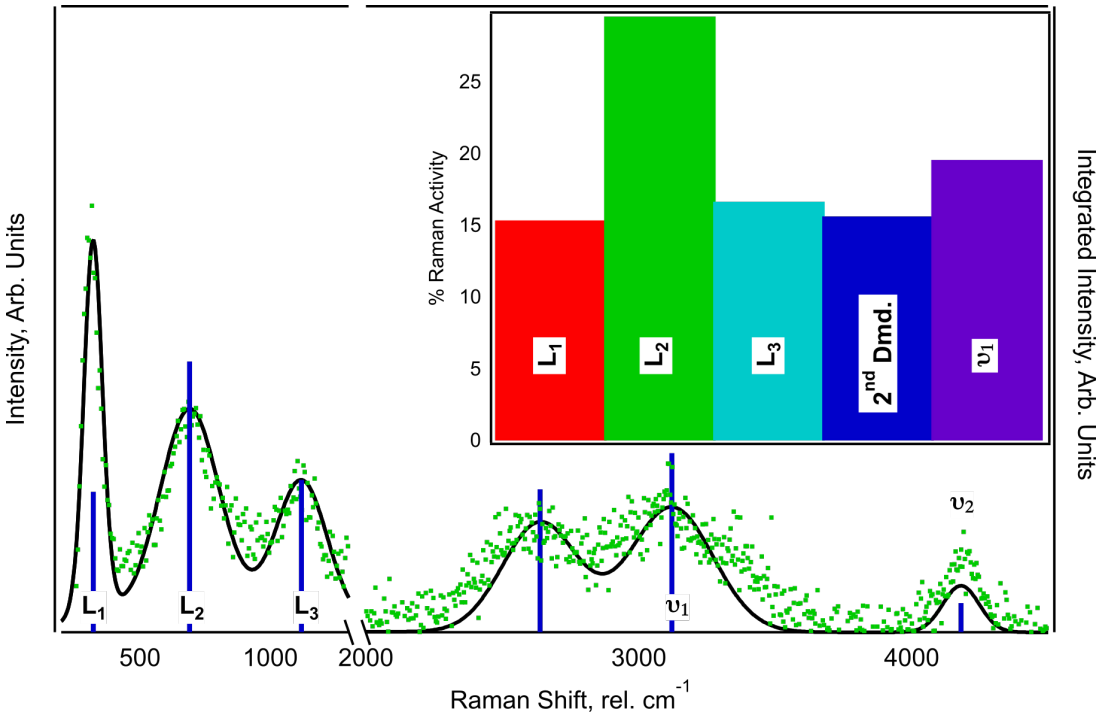

Figure 6.2: Representative Raman spectra demonstrating how intensities were calculated for a particular spectra. The best fit (black curve) to the experimental data (green points) is shown along with the integrated intensities for each excitation (blue bars). The insert demonstrates the raw value of the integrated insenties of the excitations divided by the integrated intensity over the 1^{st} order diamond.

diminished intensity, were observable up to the highest pressures in the study, seen in figure 6.4. Analysis of the relative intensities of these experimental runs are shown in figure 6.6, calculated by the method proposed above. The quantitative analysis, although quite imprecise, shows a radical decrease of the vibrational modes intensity and a comparitive enhancement of the low-frequency modes L_1 and L_4. For example, the vibrational mode which was previously found to dominate the spectra, now only constitutes ∼10% of the total Raman activity.

Perhaps the most pronounced effect of this transition is the abrupt pressure dependency change of the vibrational mode ν_1, $\left(\frac{d\nu_1}{dP}\right)_T$. Above 325 GPa, when the soft vibronic frequency (ν_1) in hydrogen evolves below a value of 2700 cm^{-1}, a 37 % reduction of the maximal value found at 40 GPa at 300 K, $\left(\frac{d\nu_1}{dP}\right)_T$ changes from -7 to -1.37 $\frac{cm^{-1}}{GPa}$. The abrupt change is indicative of highly modified bonding characteristics and quite interestingly, these new values of $\left(\frac{d\nu_1}{dP}\right)_T$ in phase V reflect that of the hard vibrational mode, $\left(\frac{d\nu_2}{dP}\right)_T$=-1.01 GPa/$cm^{-1}$, which itself is found to be unchanged through the transition.

Concomitantly with the vibrational changes reported above, there are also significant modifications in the lower energy excitations (<1300 cm^{-1}). In H_2 and HD after the splitting of the L_3 mode producing the new L_4 mode, characteristic of the IV-IV′ transition, there is a gradual redistribution of intensity from the L_3 mode into the L_4 mode (seen in figure 6.9) [Howie 12a]. Upon reaching phase V, the L_3 mode completely disappears along with the L_2 mode, and the integrated intensity of L_4 becomes comparable to the previously dominant L_1 mode, seen in figure 6.6. On the disappearance of the L_2 and L_3 modes, the L_1 excitation is observed to undergo a significant change. Above 330 GPa and up to the highest pressures reached in this study, the FWHM of the L_1 is increased dramatically, reaching more than 2-fold of its original value (90 cm^{-1} at 325 GPa to 180 cm^{-1} at 380 GPa). Although this broadening is very significant, it still remains the most dominant feature of the spectra up to the highest pressures, contributing over 40% of the overall Raman activity (figure 6.6).

Above pressures of 325 GPa, there is also a dramatic change in the appearance of the sample in transmitted and reflected light; an example of HD is given in figure 6.5, an identical effect was noticed during H_2 experiments in similar P-T conditions. The change from a transparent sample at 50 GPa to its dark

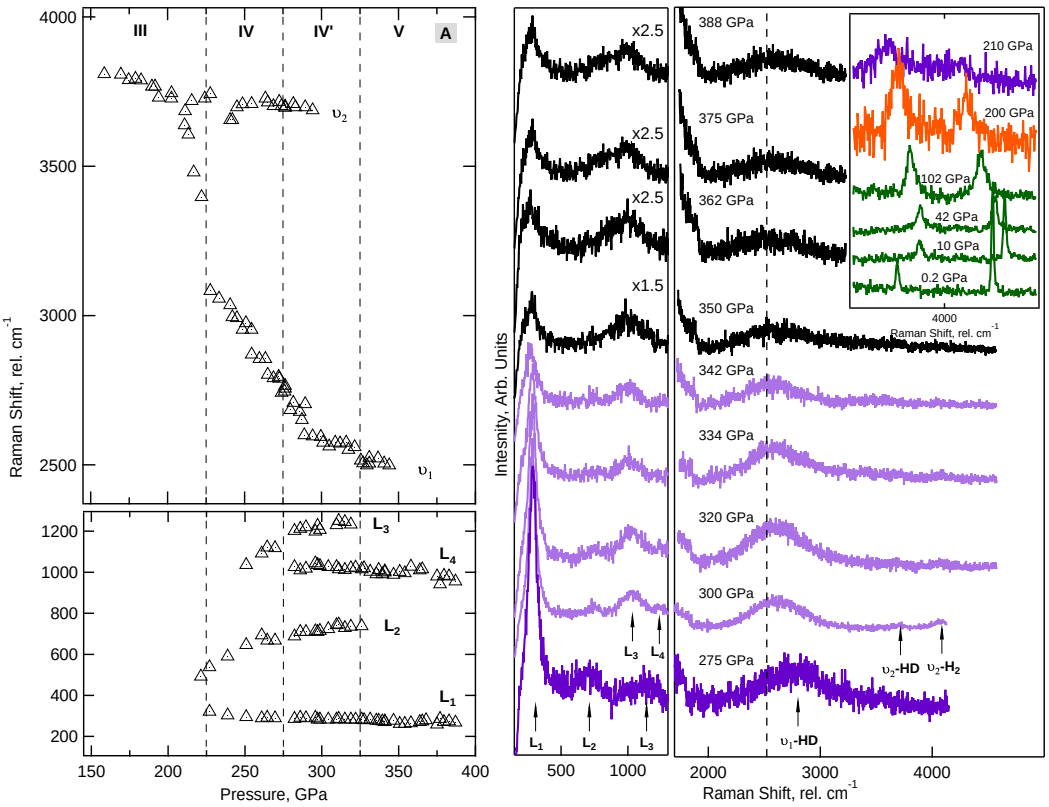

Figure 6.3: **(A)** Experimentally measured frequencies from a hydrogen (75%) and deuterium (25%) mixture, of the vibrational and low energy modes as a function of pressure, data collected from this study (empty black traingles). **(B)** Corresponding representative Raman spectra as function of pressure up to 388 GPa at 300 K. Different colours correspond to different phases: phase I (green), phase III (orange), phase IV (dark purple), phase IV' (light purple) and phase V (black). The inset shows the evolution of the vibrational modes of HD-ν_1 and H_2-ν_1 from loading at 0.2 GPa to 210 GPa. Above 47 GPa there is an observed transfer of integrated intensity from the H_2-ν_1 band to the HD-ν_1 band, the latter vibrational mode superseding the former at 150 GPa and becoming the only resolvable ν_1 band above pressures of 218 GPa.

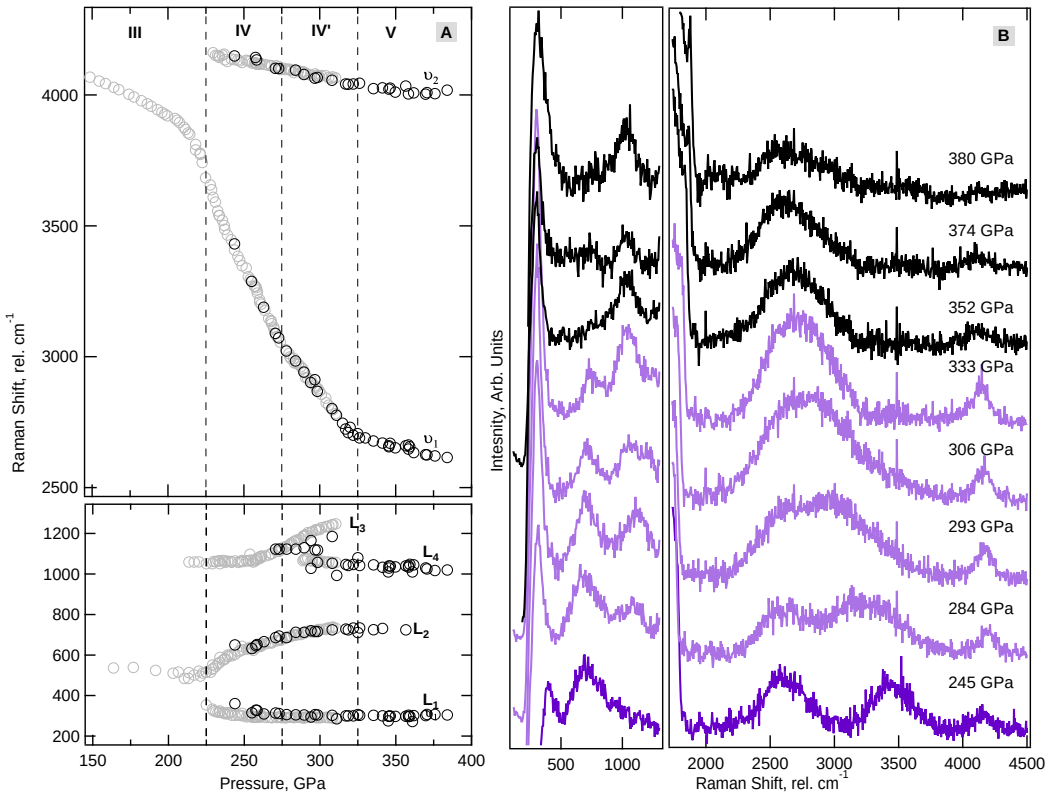

Figure 6.4: **(A)** Experimentally measured frequencies of the vibrational and low energy modes as a function of pressure, data collected from this study (black circles) are overlayed with previously reported results (empty grey circles). **(B)** Representative Raman spectra of hydrogen up to 380 GPa, different colours correspond to different phases: phase IV (dark purple), phase IV' (light purple) and phase V (black).

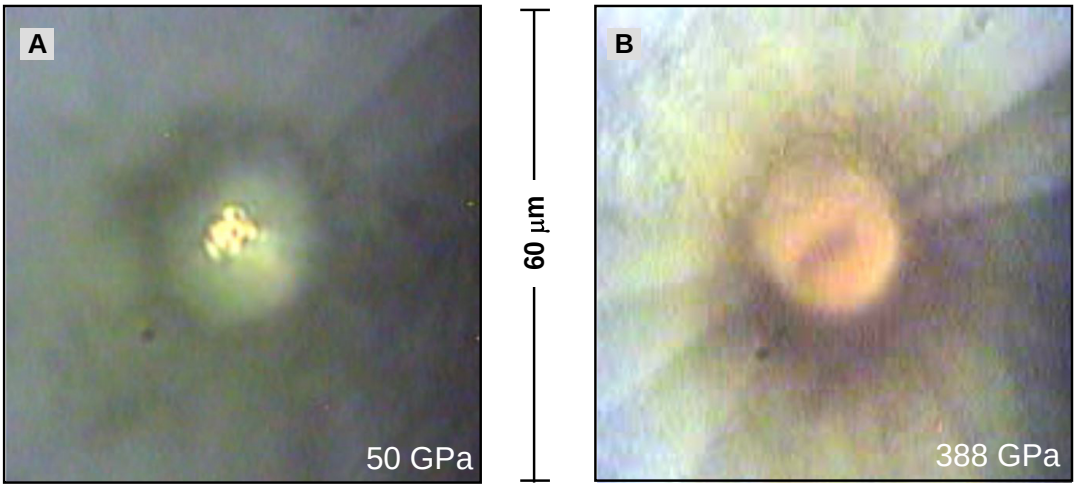

Figure 6.5: **(A)** and **(B)** are pictures taken of the sample at 50 GPa and 388 GPa respectively, the bounding box is 60x60 μm.

appearance is intriguing and to a first approximation, it is indicative of some sort of band gap closure. It is important to stress however, that caution must be taken when interepreting these measurements, even qualitatively, as chamber deformation is unfavourable and poorly understood under these pressures.

We also investigated extended P-T regimes to ascertain the stability of phase V. Figure 6.7 shows representative Raman spectra of a heating run conducted at 350 GPa, the highest pressure heating run ever conducted on hydrogen, and did not observe any transformation up to pressures of 465 K. Combined with results at slightly lower pressures, but still above the I-IV-liquid, we heated phase IV$'$ and observed no transformation to phase V. Therefore the amalgamated P-T points suggest that the transition line between phase IV(IV$'$) must lie somewhat parallel to the temperature axis.

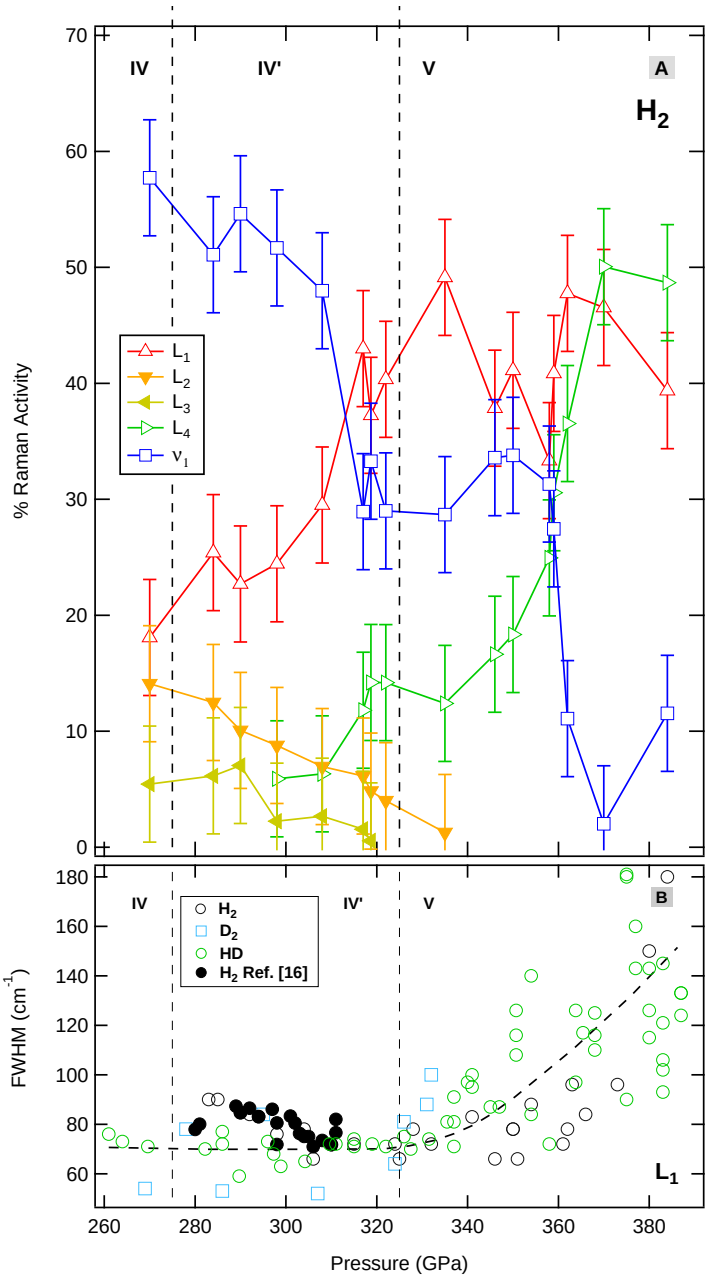

Figure 6.6: **(A)** Relative intensities of the 4 low frequency modes (L_1, L_2, L_3 and L_4) as well as the vibrational mode ν_1 of pure H_2 as a function of pressure up to 384 GPa and 300 K. The dashed lines correspond to the IV $\leftrightarrow$ IV' and IV'$\leftrightarrow$ V phase tranistions. **(B)** The full width at half maximum (FWHM) of the L_1 mode as a function of pressure of H_2, D_2 and HD up to 380 GPa and 300K, the dashed curve serves as a guide to the eye.

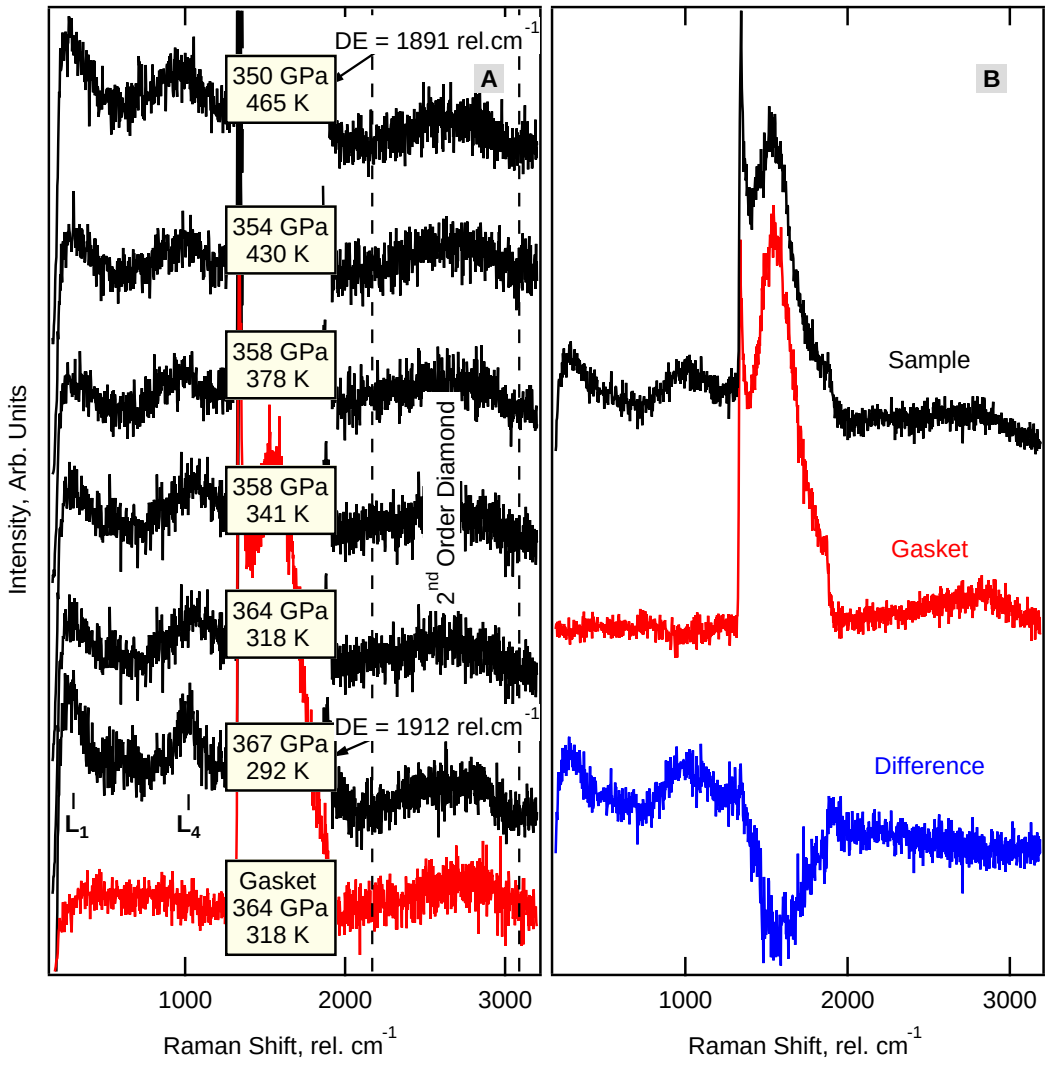

Figure 6.7: **(A)** Raman spectra taken using a probe laser of 647 nm on a pure hydrogen sample as function of temperature between 367 and 350 GPa (black). The Raman spectrum collected 2 μm away on the rhenium gasket is shown in red. The vertical dashed lines indicate the frequency space occupied by the 2^{nd} order diamond. **(B)** Example of the spectra collected at 361 GPa of the sample (black), 2 μm away on the gasket (red) and difference between them (blue).

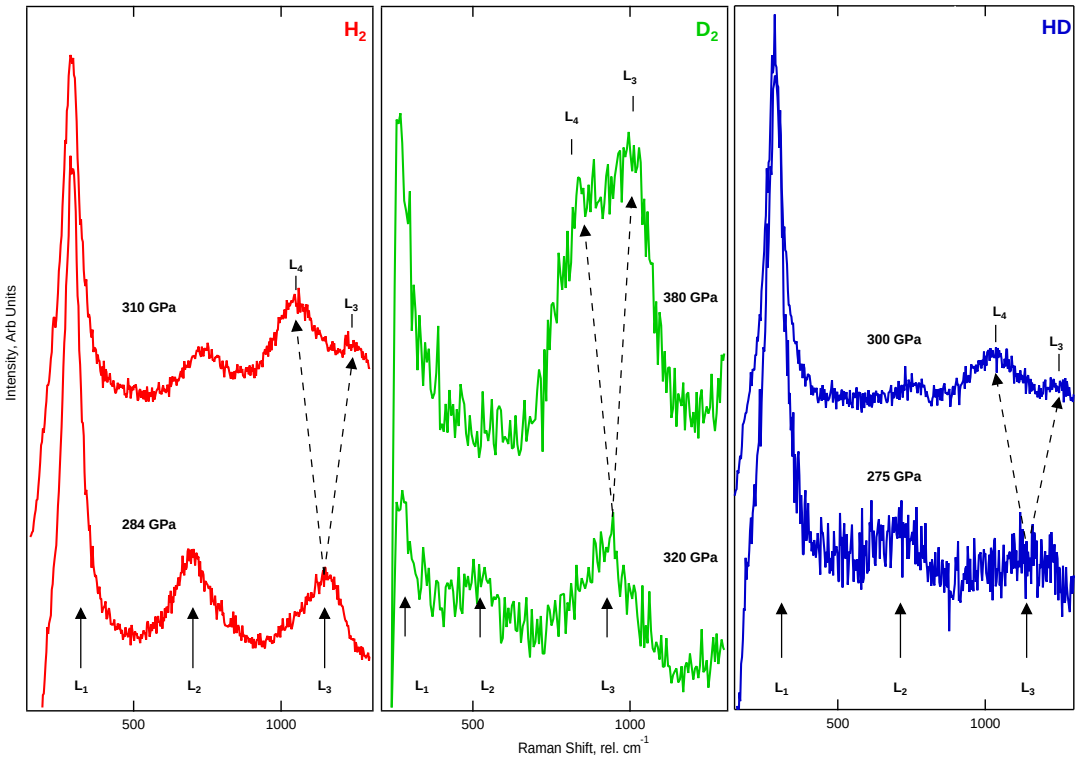

Figure 6.8: Representative Raman spectra of the low frequency excitations of 3 isotopes (left H_2, centre D_2 and right HD) as function of pressure during the phase IV to IV' transition. The low frequency mode L_3 splits to produce mode L_4.

6.4 Discussion

6.4.1 Comparison with other Vibrational Studies

Recent experimental investigations by Zha *et al.* conducted in a similar P-T range, suggest an alternative vibrational evolution for the hydrogen family with compression. Within a range of 50 GPa (275 to 325 GPa) through changes in the vibrational Raman spectra, they propose an evolution of 3 structural modifications of phase IV, denoted as phases "IV′, IV″, IV′..." or completely novel structural configurations phases "IV, V, VI..." The data collected in the previous chapter however, is contrary to the spectral evolution reported by Zha *et al.*.

The evolution from phase IV to IV′ in deuterium constitutes an early part

to this chapter, identified by the splitting of the L_3 mode to produce L_4 and a concomitant change of the pressure dependency of ν_1, a feature already reported in pure hydrogen samples (figure 6.8). Although the report of IV′ in deuterium was novel at the time of the experiment, identical spectral changes have since been published Zha *et al.* [Zha 14]. In support of this publication, the characteristics of the IV-IV′ transition are evident in their presented spectra and shown to happen at 310 GPa, the exact same pressures found within the contributing work. However, the interpretation of the data from the study by Zha *et al.* is conflicting, claiming the IV-IV′ at 285 GPa, a similar pressure to H_2. They claim this transition with the emergence of a new low-energy mode at 850 cm^{-1} with a complex pressure dependency, which appears to not be related to any of the low-frequency modes (L_1, L_2, L_3 and L_4) reported in this and previous studies [Howie 12a]

Above 300 GPa and ambient temperature, the domain where we observe novel characteristics in H_2 and HD, the recent publication by Zha *et al.* [Zha 14] report the emergence of a new soft vibrational mode in close proximity to the main vibrational mode (ν_1). The authors report the appearance of the new vibrational mode at ∼3000 cm^{-1} at 280 GPa and ∼2400 cm^{-1} at 300 GPa for hydrogen and deuterium respectively and is found to rapidly harden with pressure. This feature can be seen in their data represented in figure 6.9, as a “shoulder” to the ν_1 vibrational mode. It was interpreted that a structural modification, phase IV″, or a novel configuration, phase VI, could be attributed to its emergence. Within the contributing work, we observed none of the reported criteria for Zha *et al.*'s phase VI(IV″). Instead within our study at lower ν_1 frequencies (an absolute diagnostic for higher compression at room temperature), where the new excitation reported by Zha *et al.* would be more pronounced, H_2 and D_2 still report a highly symmetric ν_1 and with no appearance of additional vibrational modes. Something that is clearly evident when directly comparing the spectra recorded in the contributing work with the published literature [Zha 14], seen in figure 6.9.

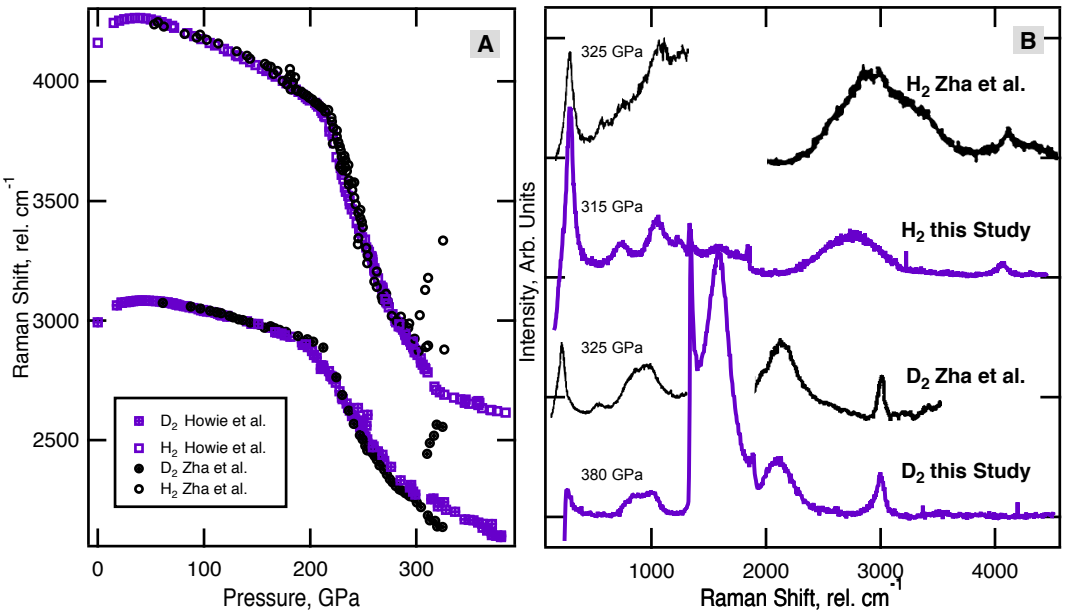

Figure 6.9: **(A)** Comparison of vibron frequencies of D_2 and H_2 from this and a previous Raman experiments (purple) [Howie 12a], compared with the highest-pressure spectra taken from the recent Zha *et al.* publication [Zha 14] (black). **(B)** Representative Raman spectra from the contributing chapter (purple) [Howie 12a], compared with the highest-pressure spectra taken from the recent Zha *et al.* publication [Zha 14] (black).

6.4.2 Determining Structure and Pressure Evolution

Firstly, it must be pointed out that the decrease in intensities above 325 GPa could indicate the loss of sample, particularly in the case of hydrogen. The combined observations, as described earlier in this chapter, rule this out and instead indicate a IV-V phase transition. Evidence that the sample is still present include: The observation of the low frequency mode(s) and a continuous evolution (*i.e* broadening and frequency change) with pressure and only modest drop in the intensity of L_1 mode, the profound change of slope of the vibrational mode frequency with pressure at 325 GPa at 300 K and no loss of sample and/or transformations are detected upon heating above 320 GPa (figure 6.7), contrary to sample loss, which has been readily observed in heating experiments discussed in chapter 5. For example, the result of sample loss is the complete disappearance of *all* Raman activity, therefore resembling a spectra taken on the gasket, seen by the red spectra in figure 6.7.

Therefore, the evolution from phase IV to the proposed phase V is intriguing, although direct structure determination is currently an experimental impossibility, one can propose some speculation from the aquired vibrational spectra and recent DFT calculations. The transition is perhaps best described by the evolution from the *Pc* structure, already attributed to phase IV, to an *Ibam* to describe phase V. Both configurations belong to a family of "mixed structures, containing layers of alternating strongly and weakly bonded molecules, resulting in the appearance of a hard (ν_2) and soft (ν_1) vibrational mode which is observed in both phases IV and V.

The evolution from *Pc* to *Ibam* structures would involve equalisation of the nearest proton-proton distances and next nearest proton-proton distances within the G-layer of phase IV. Essentially this is the elongation and symmetrisation of the hydrogen trimers, $(H_2)_3$, until each hydrogen atom becomes regular and 3-coordinated, forming a honeycomb motif seen in figure 6.10. The transition to *Ibam* from the *Pc* structure has been previously suggested by Howie *et al.* [Howie 12a] and reported in theoretical investigations by Pickard *et al.* [Pickard 12]. To make a quantitative comparison and build an argument for the proposed pressure evolution, measured experimental frequencies can be compared to theoretical frequencies calculated for the predictied phases. The vibrational

modes present in the *Ibam* structure are $2B_1g$, $2B_2g$, $4B_3g$ and 3Ag which are denoted in dark (Ag) and light (B_xg) blue squares in figure 6.10, obtained in private correspondence with Bartomeu *et al.* [Monserrat 15]. As was previously observed with the *Pc* structure, it is only the Ag modes which are believed to be of significant measurable intensity and similar behaviour is expected for the *Ibam* structure.

Firstly, it is evident that both the vibrational properties of phase V and *Ibam* structure share remarkably similar characteristics. Both the calculated vibrational characteristics and experimental measurement report a reduced low-energy Raman activity (< 1300 cm^{-1}) through the IV(*Pc*)-V(*Ibam*) transition. The abrupt loss of low-frequency excitations is intriguing and indicative of a degree of "freezing" in the librational and translational motion within the phase IV(IV′) to phase V transition. The *Pc* structure reports 5 low-energy excitations, 4 of which could be seen experimentally, whilst the *Ibam* structure only has one vibrational mode of significant intensity over the same range of frequencies. A feature highly analogous to what was observed experimentally, as the modes denoted L_2 and L_3 present in phase IV(IV′), the low-energy modes which harden with pressure, disappear upon compression into phase V.

The characteristics of the vibrational modes of both experimentally reported phase V and the *Ibam* structure share similarities. As with what was previously reported and seen in figure 6.10, both the *Pc* and *Ibam* structures accurately describe the pressure evolution of the hard vibronic ν_2. The second most energetic Ag in the *Ibam* structure, 1800 cm^{-1} at 325 GPa, is attributed to the ν_1 vibrational mode experimentally measured in phase V. The Ag mode is very similar to what is observed experimentally for ν_1, as both appear to be weakly pressure dependent, drastically different behavior to the rapid softening seen in phase IV and the theoretical frequencies of the candidate *Pc* structure. However, there is a large discrepancy in the absolute value of the frequency proposed by the *Ibam* structure and ν_1 above 325 GPa of ($\sim$900 cm^{-1}). A large discrepancy was previously observed in the *Pc* description of phase IV (black lines in figure 6.10), however this was later reconciled with molecular dynamic simulations [Magdău 13] and therefore a similar treatment could reconcile the differences with regards to phase V and the *Ibam* structure.

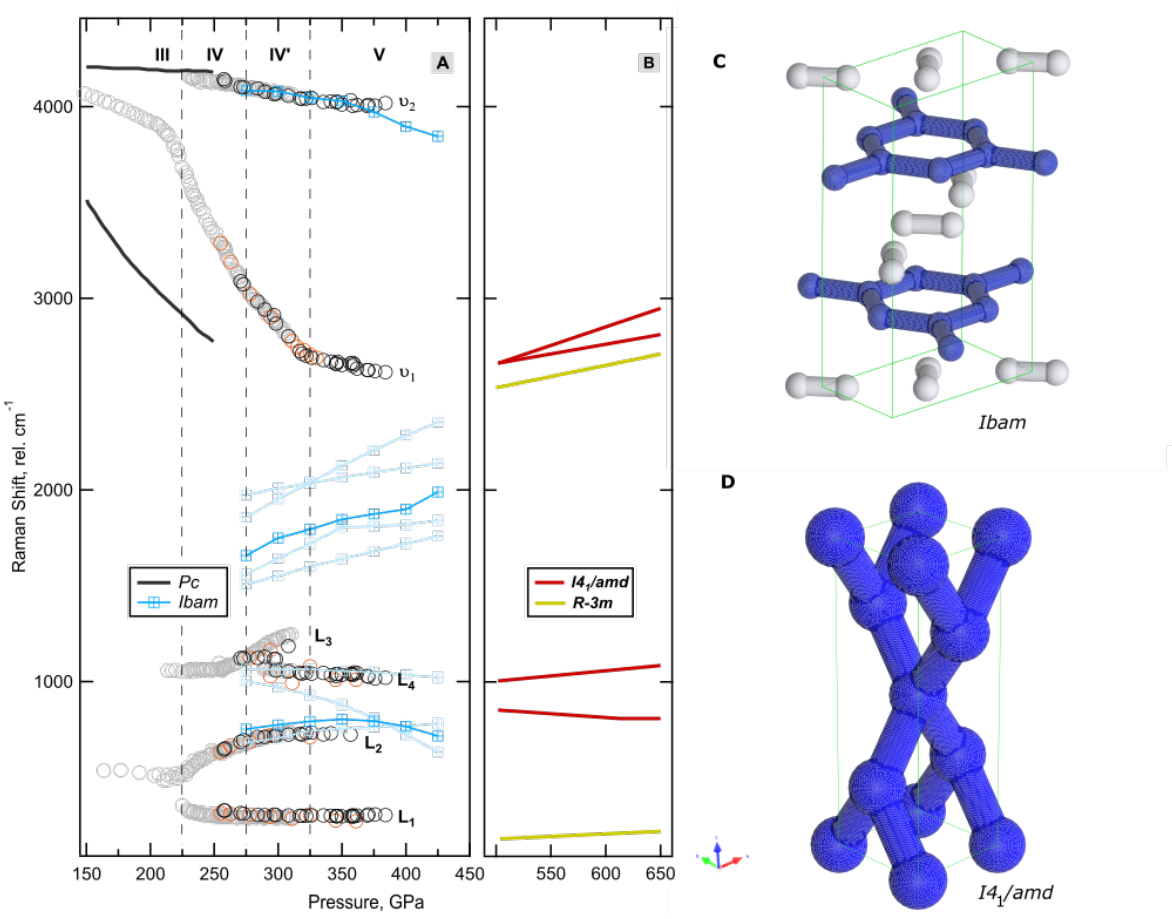

Figure 6.10: **(A)** Experimentally measured frequencies of the vibrational and low energy modes of H_2 as function of pressure. Data collected in this study are shown with empty black circles (H_2) , the data from previous studies [Howie 12a, Howie 12b] is overlayed with empty grey circles, the respective phase transitions are denoted by the vertical dashed lines. Theoretically calculated frequencies of the *Pc* structure a candidate for phase IV is given by the solid black line [Pickard 12]. The theoretical frequencies for the *Ibam* structure are also given by the dark blue and light blue square markers which correspond to the Ag and Bg vibrational modes respectively. **(B)** Theoretically calculated frequencies for the metallic and non-molecular (atomic) structures $I4_1/amd$ (red) in and $R\bar{3}m$ (yellow) from McMahon *et al.* [McMahon 11]. **(C)** and **(D)** are representations of the predicted *Ibam* and $I4_1/amd$ structures respectively.

If the speculative *Ibam* interpretation of phase V, is correct we truly have a mixed molecular and atomic structure, which could perhaps exhibit interesting transport properties. It is observed that the structural evolution to the *Ibam* structure, results in the weakly bound molecules in the *Pc* structure to dissociate; the molecular hydrogen trimers, $(H_2)_3$, in the G-layer of the *Pc* dissociate, forming an atomic honeycomb lattice. Dissociation in the layers could exhibit a degree of electronic delocalisation of the valence electrons, allowing conduction within the layers. This could provide an explanation of the dark appearance of our samples above 325 GPa, where the abrupt change of the vibrational characteristics is observed, and also the marked reduction of intensity of the soft vibrational mode ν_1.

It is interesting, but highly speculative at this point, to discuss phase V (*Ibam*) to be a precursor and superseded by a completely molecularly dissociated phase. The vibrational frequencies for the favoured monatomic structures above 380 GPa [Azadi 14, McMahon 11], $I4_1/amd$ and $R\bar{3}m$, are plotted in figure 6.10. It is interesting that these structures both have a frequency around 2500 cm^{-1}, approximately the same frequency we observe from ν_1 at the highest pressures. It could be interpreted that the apparent weak pressure dependence of the ν_1 vibrational mode above 325 GPa could in fact come to represent a minimum and eventually harden, reflecting the nature of the phonons in the $I4_1/amd$ and $R\bar{3}m$ structures. This pressure evolution of the ν_1 vibron could therefore represent the gradual evolution from a vibrational mode into a monatomic phonon. However, it is important to stress that we still observe the hard molecular vibrational mode up to the highest pressures and neither of the $I4_1/amd$ and $R\bar{3}m$ provide an adequate description of the lower energy modes.

6.4.3 Extended Phase Diagram

Our amalgamated data from this chapter and the previous ("Exploring the Stability of Solid Phases of Hydrogen") provide further insight in the hydrogen phase diagram. A "blown up" phase diagram is represented in figure 6.11, focusing on the region of P-T space, explored by the measurements taken in this chapter.

Investigating the stability regions of phase IV(IV′) and phase V by conducting heating measurements, allow us to ascertain the nature of the phase line between the two phases. In figure 6.11, above ∼300 GPa, heating runs initiated in phase IV(IV′) above the previously discussed I-IV-Liquid triple point, no phase transformations to either phase V or the liquid phase were observed. Similarly, a heating run initited phase V at 350 GPa and up to 465 K didn't observe either a transition to the liquid phase or phase IV(IV′) (figure 6.7). These P-T points suggest that the IV(IV′)-V phase line must have a steep gradient, probably somewhat close to the vertical, tentatively represented by the dashed line in figure 6.11. Extrapolation of the proposed IV(IV′)-V phase line to higher temperatures suggests it meets the melt line, forming a new triple point (IV-V-Liquid). These measurements therefore agree and further support the claims made in the previous chapter, indicating that there is a "flattening" in the melt line and consequently room-temperature melting and the ground state liquid have to be revised to much higher pressures. In agreement with the nature of phase IV(IV′), phase V is not a groundstate structure of hydrogen and is stabilised at these pressures by the elevated temperatures. A phenomenon clearly evident, as phase V is bounded by the presence phase III at lower temperatures (not shown in figure 6.11), which has previously been found to be stable to ∼350 at 200 K [Zha 12].

The inset to figure 6.11 illustrates the phases and transitions observed along deuterium's room-temperature isotherm. Although some P-T points are shown, an extensive study of the solid phases of deuterium were not carried out and is presumed to be analogous to the behaviour of the lighter isotope, hydrogen. Heating runs were carried out at ∼25 GPa and ∼200 GPa observing melting and the I-III transition respectively. Interestingly, we observe that the splitting of the librational modes, characteristic of phase IV′, is isotopically shifted to 35 GPa higher in pressure for deuterium compared with hydrogen. The IV-IV′ transition's large pressure dependency on the isotope, the largest for any phase when comparing the isotopes, is highly suggestive that it is largely driven by quantum effects. The large offset for the transition, coupled with the data presented in the inset to figure 6.11, suggests that pressures in excess of 380 GPa will be required for the appearance of phase V in deuterium.

Finally, an interesting question arises; if phase V is indeed the precursor to the metallic non-molecular states, such as $I4_1/amd$ and $R3m$, under what P-T

conditions would this dissociation occur? Recent shockwave experiments have revealed the presence of an abrupt insulator-to-metal transition at $\sim$ 350 GPa and relatively 900 K in deuterium [Knudson 15] (seen on the inset to figure 6.11) attributed to dissociation. Although highly speculative, a rough extrapolation of this phase transition to lower temperatures is shown in figure 6.11 where presumably it ultimately interfaces with the melting curve above 400 GPa. It could be argued that at this point, dissociation in the solid phase could occur, mimicking the reported two dissimilar liquids, which are all found in very similar P-T conditions.

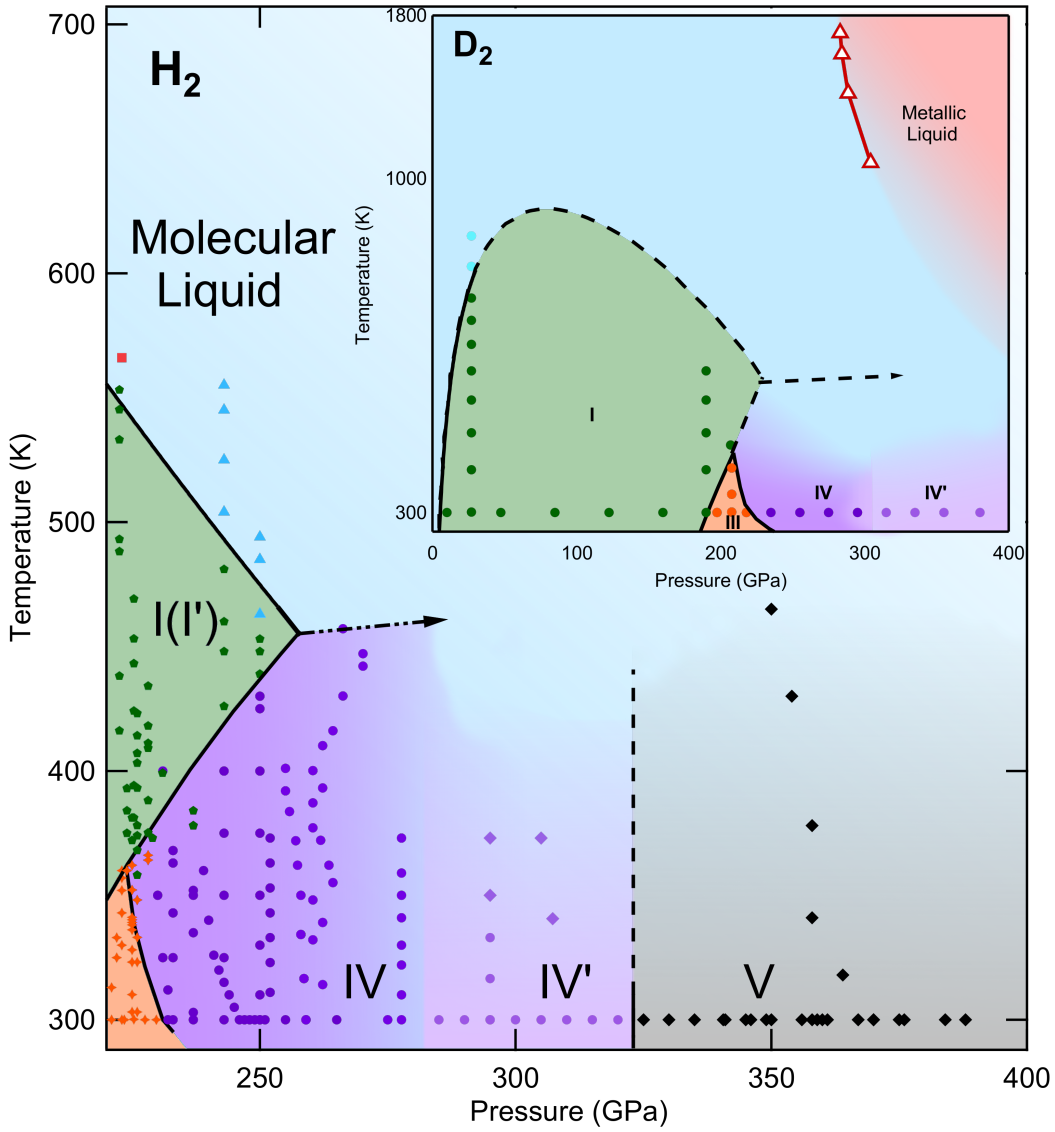

Figure 6.11: A "blown up" phase diagram (see figure 5.9), the coloured filled symbols and solid phase lines below 300 GPa are discussed in the previous chapter and show phases I(I′) (green), III (orange), IV (dark purple) and IV′ (light purple). The solid black diamonds (phase V) are from data presented in this chaper and the dashed-dotted line is the proposed continuation of the melting curve. Inset: Sketch of the phase diagram of D_2. The dashed lines are the proposed melting curve, which has not been experimentally constrained, but is assumed to follow the same trend as the one of hydrogen. The red open triangles are from Knudson *et el.* [Knudson 15] separating the metallic and insulating liquids.

Chapter 7

Conclusion

The motivation of this thesis was to understand hydrogen's response to extended pressure and temperature regimes. Surpassing the P-T conditions already experimentally achieved on hydrogen, we have provided further evidence by implementing microfocused Raman spectroscopy for the turnover in its melting curve, suggesting that it could go through a flattening. We also observe that hydrogen and its heavier isotope, hydrogen deuteride, adopt a novel structure above 325 GPa, phase V.

We first conducted high-temperature studies on the known solid phases of hydrogen, to study their respective stability fields. By doing so, we have constrained the I-III phase line at temperatures above room temperature and find it to be in agreement with previously extrapolated findings. Above 200 GPa upon heating phase IV, we constrained the previously unidentified I-IV phase line, finding it to be a linear continuation of the I-III phase line up to higher pressures and temperatures. At these pressures and at higher temperatures we observed a further transformation to a new phase which could be attributed to melting.

These high-temperature studies are indicative of profound solid stability characteristics, where we have the experimental observation of a previously theorised melting curve maximum in the hydrogen phase diagram. At higher pressures however, we have evidence for a deflection or possible minimum in the melting curve, consequently revising the predicted room-temperature melting

and groundstate liquid transition pressures beyond the scope of this study. Interestingly, the extended hydrogen phase diagram is now found to resemble that of the other group I elements, consisting of a melting maximum, a possible minimum and a clustering of complex phases about the minimum.

By conducting the highest static pressure experiments ever on the hydrogen family, we infer the appearance of a new phase in hydrogen and hydrogen deuteride. This transition manifests itself as marked spectral changes, such as the loss of librational activity, as well as a profound change in the vibrational mode's ν_1 response to pressure. Deuterium was studied to a record pressure of 380 GPa and the transition to phase IV$'$ was found to be 310 GPa at 300 K, 35 GPa higher than that of the pure hydrogen species. This study doesn't provide any evidence of phase V in deuterium and therefore the onset to this phase must be above 380 GPa.

Through vibrational analysis, we propose the structure of this phase to be the *Ibam* structure, suggesting that with pressure the *Pc* structure symmetrises. Interestingly, this structure is believed to be electrically conductive through the atomic layers. We also suggest that this phase could be the precursor to the purely atomic (metallic) structures predicted by McMahon *et al.* [McMahon 11], which are believed to be stable above 400 GPa [Azadi 14]. A recent study by Knudson *et al.* is indicative that the dissociation in the liquid happens at much higher pressure ($\sim$300 GPa) [Knudson 15]. If we assume that dissociation in the liquid and solid phases happen in closely related P-T regimes, this agrees with our contributed deuterium study, in which we don't observe a dissociation or its suggested precursor, phase V, up to pressures of $\sim$400 GPa.

The contributing works suggest that the long awaited atomic (metallic) phase of hydrogen, predicted by Huntington and Wigner over 80 years ago [Wigner 35], could be tantalisingly close to being realised. However, currently we are reaching the limit of conventional opposed diamond anvil devices. Therefore, alternative approaches need to be developed to answer the pressing question of pressure-induced dissociation in hydrogen. Nevertheless, the quest for obtaining such a holy grail, has revealed rich physics and the application of pressure yet again exemplifies, that dense matter disagrees with Newton's conjecture, "Nature is pleased with simplicity" [Newton 87].

Appendix A

Raman Spectroscopy of Hot Hydrogen above 200 GPa

Ross T. Howie, Philip Dalladay-Simpson, Eugene Gregoryanz*
School of Physics and Centre for Science at Extreme Conditions, University of Edinburgh, Edinburgh EH9 3JZ, UK.

Nature Materials **14**, 495499 (2015).

nature materials

LETTERS

PUBLISHED ONLINE: 23 FEBRUARY 2015 | DOI: 10.1038/NMAT4213

Raman spectroscopy of hot hydrogen above 200 GPa

Ross T. Howie, Philip Dalladay-Simpson and Eugene Gregoryanz*

It has been theorized that at high pressure the increased energy of the zero-point oscillations in hydrogen would destabilize the lattice and form a ground fluid state at 0 K (ref. 1). Theory has also suggested that this fluid state, representing a new state of matter, might have unusual properties governed by quantum effects, such as superfluidity or superconductivity[2,3]. Here, by combining Raman spectroscopy and *in situ* high-temperature, high-pressure techniques, we demonstrate that above 200 GPa a new phase transition occurs as temperature is increased, for example 480 K at 255 GPa. If the transformation is interpreted as melting, it would be the lowest melting temperature of any material at these high pressures. We also find a new triple point between phases I and IV and the new phase, and demonstrate that hydrogen retains its molecular character around this point. These data may require a significant revision of the phase diagram of hydrogen above 200 GPa.

It has been argued that the ground state of hydrogen could be an (atomic) liquid under sufficient compression[1]. It is widely accepted that the melting curve of hydrogen features a maximum, even though there is no convincing experimental evidence to establish this. In the first experiment to gigapascal pressures, melting was visually observed between 5 and 15 GPa and then extrapolated to much higher pressures (>300 GPa; ref. 4). The authors found that the empirical Kechin law (which models the melting curve as going through a maximum[5]) provides the best fit to their data. That work was extended to 45 GPa, where melting was detected using Raman spectroscopy[6]; extrapolation to 200 GPa using the Kechin law suggested that the melting maximum would occur at around 130 GPa and 1,100 K. Subsequent laser heating experiments, combined with Raman spectroscopy, extended the pressure range to 150 GPa (refs 7,8). These two studies did not use extrapolations, but owing to issues inherent to laser heating (for example, large temperature gradients and/or chemical reactions) they did not provide a convincing indication of melting, and the data points obtained did not present conclusive proof of the melting temperature decreasing with pressure (Supplementary Fig. 1). Nevertheless, no data above 150 GPa and above 300 K exist, and the extrapolation of the existing data to higher pressures suggests that dense hydrogen might melt at room temperature above 250–300 GPa (refs 6–8). Theoretical calculations find the molecular to atomic transformation in liquid hydrogen over a wide pressure–temperature (P–T) range[9–11]. These calculations show that the line dividing two very dissimilar liquids joins the melting curve between 200 and 300 GPa and between 500 and 1,000 K (refs 9–11). Recently, hydrogen and deuterium were successfully compressed to above 230 GPa at 300 K, where transformations to mixed atomic and molecular structures, phases IV and IV′, were observed[12–15]. It is fascinating that these many measured, extrapolated and predicted phenomena seem to happen in approximately the same P–T area of hydrogen phase space, which represents a crossover of intramolecular, intermolecular and quantum energy scales.

Using available technology, the detection of hydrogen melting in a diamond anvil cell is a formidable task because of numerous factors. The high reactivity, mobility and diffusion of hydrogen at elevated temperatures (>250 K) lead to the destruction of the diamonds and/or rapid loss of sample, making dense hydrogen notoriously difficult to study. The number of available probing techniques is also limited: X-ray diffraction is not straightforward even in the solid state owing to hydrogen's low Z number, and to the best of our knowledge no X-ray studies of liquid hydrogen at elevated pressures have been carried out. Visual observations are impossible at higher pressures owing to the greatly diminished sample size, thus leaving Raman spectroscopy as the only viable tool to probe transformations at high pressures. The appearances of the Raman spectra above 180 GPa at 300 K in phases III and IV(IV′) are very peculiar and characterized by the presence of very intense and temperature dependent librational and vibrational bands[14]. It could be expected that the temperature driven changes in phases III and/or IV(IV′) would be accompanied by changes detectable with optical spectroscopy.

Here, we have succeeded in confining hydrogen at high temperatures in the diamond anvil cell long enough to collect high quality Raman spectra, tracking the evolution of the Raman modes in phases I, III, IV and a new phase, which we speculate could be a liquid state. The monitoring of the phase transformations is more elaborate than before, not only studying the changes of the position (and appearance/disappearance) of the mode(s), but also their full-width at half-maximum (FWHM). The data presented provide points below 200 GPa up to 800 K, between 200 and 275 GPa up to 500 K, and at 325 GPa at 300 K. Our measurements provide constraints on the phase diagram, demonstrating the existence of a third triple point, which suggests a melting minimum.

We find that the behaviour of hydrogen at elevated temperatures and pressures above 130 GPa is very unusual. In the heating run between 132 and 155 GPa (phase I) we clearly observe the transformation, which could be interpreted as melting above 800 K (Fig. 1a–c and inset to 1b). Both the frequency of the vibron, ν, and its FWHM change discontinuously (for examples and explanations of the experimentally observed discontinuous changes in the position and FWHM of the vibrational band through the phase transitions at lower pressures and further experimental details the reader is referred to Methods, Supplementary Methods and references therein). The FWHM broadens as expected through the solid–liquid transition and the frequency of the vibron significantly downshifts ($\sim$30 cm^{-1}). This softening is opposite to what is observed on melting at lower pressures (Supplementary Figs 3 and 4) and could be explained, as suggested by the negative slope of the melting curve, by the liquid being denser than phase I, thus

School of Physics and Centre for Science at Extreme Conditions, University of Edinburgh, Edinburgh EH9 3JZ, UK. *e-mail: e.gregoryanz@ed.ac.uk

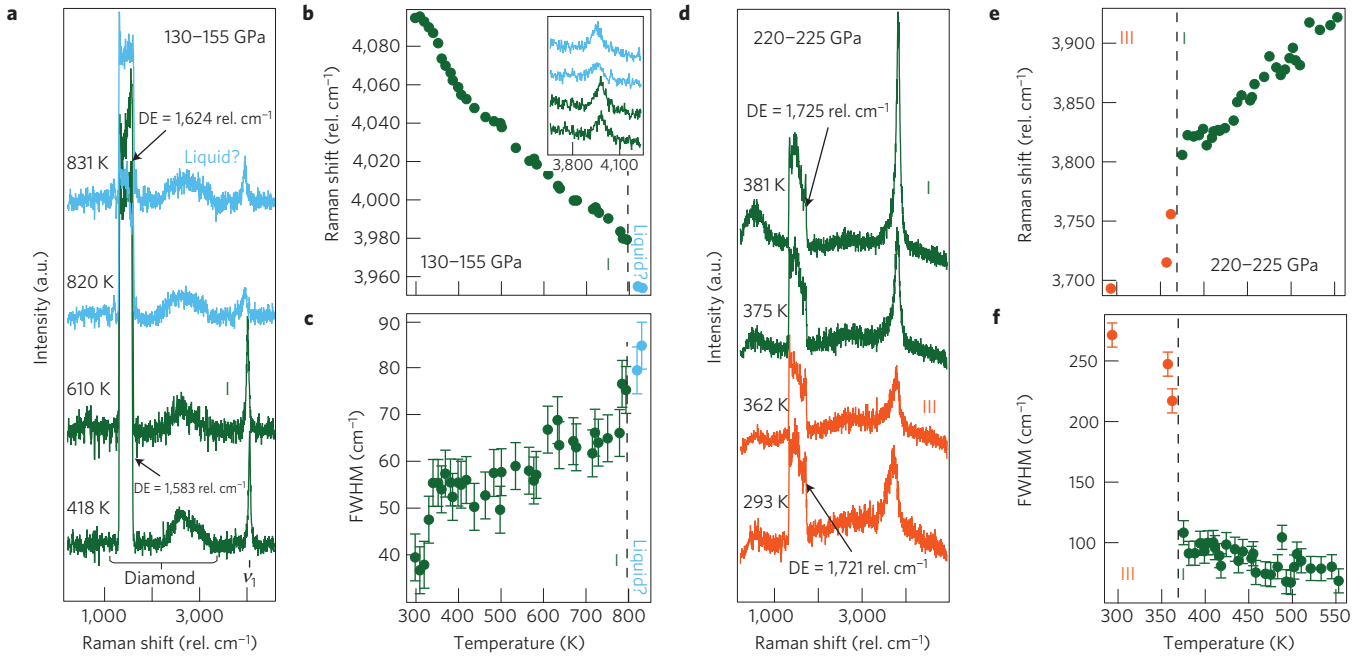

Figure 1 | Representative Raman spectra, position and FWHM of the vibrational band in hydrogen. a, Raman spectra on heating in phase I (dark green) and the HPHT phase (light blue) at pressures between 130 and 155 GPa. **b**,**c**, Position (**b**) and FWHM (**c**) of the vibrational mode ν_1 at 130–155 GPa as a function of temperature through the phase I ↔ HPHT phase transformation, which is marked by the vertical dashed line. The inset to **b** shows a magnified view of the vibrational mode through the transformation. **d**, Representative Raman spectra of hydrogen on heating in phases III (orange) and I (dark green) at pressures between 220 and 225 GPa. **e**,**f**, Position (**e**) and FWHM (**f**) of the vibrational mode ν_1 at 220–225 GPa as a function of temperature through the phase I ↔ phase III transformation, which is marked by the vertical dashed line. The broad peak between 1,333 and ~1,700 cm^{-1} in **a** and **d** is due to the stressed diamond. The observed DE frequency is indicated.

driving the frequency down through melting. Qualitatively similar behaviour is observed up to ~190–200 GPa, which is in agreement with our previous study[6]. However, in the heating runs above 200 GPa, the $(d\nu/dT)_P$ term changes sign, leading to an increase of the vibron frequencies with temperature while the FWHM is very slowly decreasing (Figs 1d–f and 2). For example, in the 225 GPa run, we observe the phase III ↔ I transformation and hardening of the vibron frequencies as temperature is increased in phase I. The effect becomes more pronounced as hydrogen is compressed to above 230 GPa, leading to values of $(d\nu/dT)_P$ of the order of 2–3 $cm^{-1}\,K^{-1}$ (Fig. 2b,d), whereas at 190–200 GPa $(d\nu/dT)_P$ is around $-0.1\,cm^{-1}\,K^{-1}$. We note that, even though at 250 GPa the isothermal pressure-induced vibron softening $(d\nu/dP)_T$ is much larger than that at 150 GPa (ref. 6), the behaviour of the vibron frequency is still mostly driven by thermal effects. In addition to the apparent change of sign of the slopes in the solid, the behaviour of the vibrational mode in the presumed liquid state just above phase I at pressures greater than 200 GPa is different from those at lower compressions (Fig. 2). Figure 2a–d shows that the width and position of the vibrational mode are temperature independent in this state. The absence of a discontinuous jump implies similar molar volumes (densities) on both sides of the transformation line (or melting curve), which in turn would imply a flattening of the melting curve. Interestingly, Fig. 2 shows that the negative slope of the vibron FWHM with temperature is larger than that at lower pressures, leading to an FWHM decrease in phase I by a factor of two to three within 50–75 K.

Two phase transitions are clearly detectable when hydrogen is heated above 200 GPa, III ↔ I ↔ new phase (or liquid), and above 230 GPa the phase sequence is IV ↔ I ↔ new phase (or liquid) (Figs 2a and 3a–d). At these pressures the transformations are characterized by noticeable modifications of the Raman spectra with temperature, such as disappearance of the librational modes, change of slope of the vibrational band, two- to threefold decrease of the FWMH and the disappearance of the second vibrational band ν_2 (IV ↔ I). The combined high-temperature runs (Fig. 3) show that the phase line separating phases I and III does not change its slope at the I–III–IV triple point and continues as the I–IV phase line. Phase IV seems to be stable in a surprisingly narrow range of temperatures above ambient and is superseded by phase I, which occupies a significant portion of the phase diagram up to and above 200 GPa. We traced the I–IV line to 255 GPa and 480 K, where it intersects the extrapolated melting curve forming a triple point, only the third known triple point on the hydrogen phase diagram and what could be the first on its melting curve. The sequence of phases versus temperature at pressures between 225 and 250 GPa is quite instructive. It starts in phase III, and although its structure is unknown it is likely to have some ordering when compared with phase I, for example layered structures with non-rotating molecules[16]. As temperature is increased, phase III transforms to phase IV, more disordered than III, with a big discontinuity in the frequency of the ν_1 vibron and the appearance of ν_2 (ref. 14). If phase IV is heated further, it transforms to phase I, even more orientationally disordered, without any discontinuity in the position of ν_1 (Fig. 2); in fact, the phase transformation is obvious only because of the (dis)appearance of the free-like molecular vibron ν_2. Phase I in this P–T range seems to be quite different from that at lower pressures and temperatures; it is possible that the sign reversal of the position and FWHM slopes described above could be driven by the continuous transformation to a different solid phase that is structurally very similar to phase I, for example, phase I′ (Fig. 3). In turn, phase I(I′) either melts or transforms to a solid state with complete orientational disorder (no observable lattice modes).

If the described changes in Raman spectra are indeed caused by melting, then the P–T paths, as shown in Fig. 3, provide further experimental limits on the phase diagram and pose some

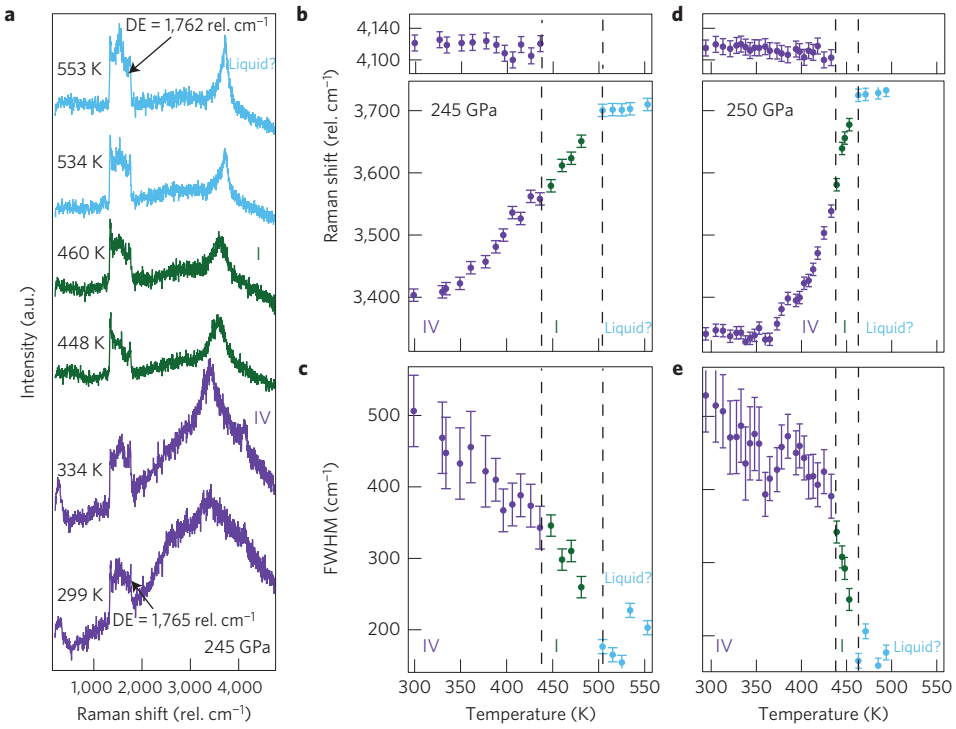

Figure 2 | Representative Raman spectra of hydrogen on heating at different pressures. a, Raman spectra on heating in phases IV and I and HPHT phase at 245 GPa. The observed DE frequency is indicated on room and highest temperature spectra. **b**–**e**, Positions (**b**,**d**) and FWHMs (**c**,**e**) of the vibrational modes ν_1 and ν_2 at 245 (**b**,**c**) and 250 GPa (**d**,**e**) in phase IV. Note that the positions and FWHMs at 250 GPa were measured with temperature decreasing. The error bars are from the fits to the data. The vertical dashed lines indicate the IV ↔ I ↔ HPHT phase transitions.

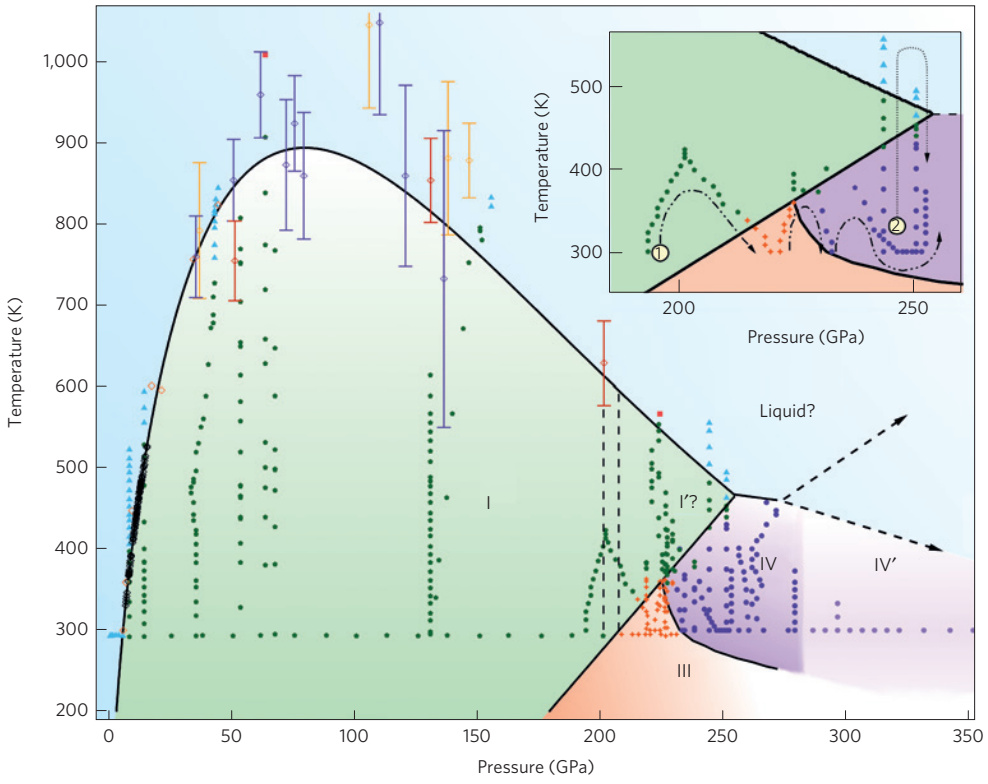

Figure 3 | Proposed phase diagram of hydrogen up to 325 GPa. The inset shows the *P*–*T* paths (1 and 2) taken during temperature cycles. The melting curve is a Kechin fit[5] to the data points obtained here and in our previous study. Previous data are overlaid with different colour hollow diamonds: purple, ref. 8; yellow, ref. 7; orange, ref. 6; red, ref. 9; black, ref. 4. The phase lines between phases I, III and IV and the new phase (liquid) are from this study and refs 13,14. The red squares show where the H_2 rapidly diffused from the sample chamber. The vertical dashed lines at around 190 GPa indicate the pressure region in which $(d\nu/dT)_P$ in phase I changes sign. The dashed lines ending with arrows are possible continuations of the transformation line (or melting curve). The lines between the phases have an error bar of about ±10 GPa but are consistent with our other studies[13,14].

interesting questions about a possible melting minimum and the proposed liquid ground state[1,2]. The P–T paths shown require the extrapolated melting curve to change slope after the I–IV–liquid triple point. The possible continuations of the melting curve (shown with the dashed lines in Fig. 3) effectively rule out the liquid state at temperatures below ~300 K and pressures below 400 GPa. In fact, a very recent theoretical study found that the melting curve remains flat at around 300 K up to 500 GPa, where it regains a positive slope[17], which is in very good qualitative and quantitative agreement with the current study. In principle, the liquid ground state could still exist at much higher pressures (for example, above 500 GPa) and its existence would be determined by such factors as the P–T conditions at which the molecular disassociation of hydrogen occurs, by the zero-point energy terms of the atomic liquid and/or solid versus other energy terms contributing to the Gibbs free energy. The latest theoretical calculations, where some of these effects were taken into account, either do not find the liquid ground state up to 600 GPa (ref. 17) or place it above 900 GPa following the predicted atomic solid phase[18].

It is important to stress the limitations of Raman spectroscopy as a method to detect melting, and therefore we need to consider other phenomena that could have led to the changes in the Raman spectra here and in previous melting studies. We can speculate that the drastic changes observed in the Raman spectra on increasing temperature could be due to a solid–solid phase transformation. The amalgamated data could probably rule out this speculation for the following reasons: the Raman spectra at the highest temperatures are very simple and characterized by a relatively narrow (at given pressures) single vibrational mode and absence of rotational/librational modes (Figs 1a and 2a). Therefore, the overall appearances of the Raman spectra are identical in the liquid state over a broad pressure range (Figs 1a and 2a, 130 and 245 GPa, with Supplementary Fig. 4, 14 GPa). The above assumption would also imply that there is a new solid molecular phase of hydrogen located somewhere between 130 and 270 GPa with very high melting temperatures. The presence of such a new high-temperature solid phase (instead of a liquid state) would be an interesting observation in itself and pose several questions that would require a profound revision of our current theoretical understanding of hydrogen in these conditions. If it were a new, structurally simple solid phase, then new models are clearly needed proposing such a structure and predicting melting temperatures that do not decrease above 120–140 GPa. Several theoretical papers[9–11,17,18] present results on melting, which are in reasonable qualitative agreement with our measurements. However, experimental advancements in methods that could directly determine melting of hydrogen at these conditions (for example, Brillouin spectroscopy, X-ray diffraction) would be highly beneficial. Nevertheless, our presented data further broaden our understanding of a system that was previously found to be highly elusive experimentally at these conditions and is still revealing fascinating physics.

Methods

Loading. We have conducted a total of 50 independent experiments varying in pressures from 3 to 360 GPa. Pressure was generated in long high-temperature piston–cylinder diamond anvil cells of our own design equipped with diamonds of culet dimensions ranging from 250 to 20 μm. The experimental runs mostly followed a procedure similar to the one previously described in ref. 6. However, owing to improved stability of pressures and temperatures in the cells and a refined experimental practice, we have managed to probe a much greater regime of P–T space, for example, 555 K at 223 GPa (Supplementary Methods). Rhenium foils 200–250 μm thick were used as gasket material to form the sample chamber. The hydrogen gas was clamped at ~0.175–0.200 GPa at 300 K and compressed to the target pressure (see 'Pressure and temperature measurements').

Optical measurements. We have used 514.15 and 647.1 nm excitation wavelengths to collect the spectra. Owing to the quantum efficiency of the visible CCD (charge coupled device) used, the high-energy modes, for example hydrogen vibrons above 3,500 cm^{-1}, are much weaker than the low-energy lattice modes if probed with 647.1 nm wavelength (compare the spectra shown in Figs 1a and 2a measured with 514.15 nm and Fig. 2 in ref. 13 measured with 647.1 nm). However, in most of the cases when 514.15 nm excitation is used, the pressure-induced fluorescence from the stressed diamonds obscures the Raman signal, leaving 647.1 nm excitation as the only available source.

Pressure and temperature measurements. After clamping hydrogen gas at 0.2 GPa, pressure was increased at 300 K until it reached its required value. The pressures were determined using both the frequency of the diamond edge (DE) with the calibration proposed in refs 19,20 and the vibrational mode of the hydrogen sample[21], to be consistent with our previous work[13,14]. When the desired pressure according to the vibron frequency was reached, the frequency of the stressed DE was noted as a reference point (Supplementary Fig. 2); in most of the runs the agreement between the two was within 10–15 GPa, as shown in ref. 21. During the heating run the pressure was either adjusted by keeping the frequency of the DE constant or determined later on the assumption that the frequency of the DE is temperature independent. In cases when the sample was brought back to room temperature, the frequency of the hydrogen vibron provided further information on the pressure change during the heating–cooling cycle. Typical examples are provided in Supplementary Methods; for example, Supplementary Fig. 2 shows that a net pressure increase of ~30 GPa was observed when pressure was not adjusted during the experiment. However, when pressure was adjusted, a quasi-isobar could be reliably tracked to within ±5 GPa on heating.

For heating we used two custom built resistive heaters placed around the diamonds and body of the cell. Temperature was determined using one or two thermocouples attached to one of the diamonds and/or gasket.

Received 7 August 2014; accepted 9 January 2015; published online 23 February 2015

References

1. Brovman, E., Kagan, Y. & Kholas, A. Properties of metallic hydrogen under pressure. *Sov. Phys. JETP* **35,** 783–787 (1972).
2. Babaev, E., Sudbø, A. & Ashcroft, N. W. A superconductor to superfluid phase transition in liquid metallic hydrogen. *Nature* **431,** 666–668 (2004).
3. Babaev, E., Sudbø, A. & Ashcroft, N. W. Observability of a projected new state of matter: A metallic superfluid. *Phys. Rev. Lett.* **95,** 105301 (2005).
4. Datchi, F., Loubeyre, P. & LeToullec, R. Extended and accurate determination of the melting curves of argon, helium, ice and hydrogen. *Phys. Rev. B* **61,** 6535–6546 (2000).
5. Kechin, V. Melting curve equations at high pressure. *Phys. Rev. B* **65,** 052102 (2001).
6. Gregoryanz, E., Goncharov, A., Matsuishi, K., Mao, H-k. & Hemley, R. Raman spectroscopy of hot dense hydrogen. *Phys. Rev. Lett.* **90,** 175701 (2003).
7. Eremets, M. I. & Troyan, I. Evidence of maximum in the melting curve of hydrogen at megabar pressures. *JETP Lett.* **89,** 174–179 (2009).
8. Subramanian, N., Goncharov, A., Struzkin, V., Somayazulu, M. & Hemley, R. Bonding changes in hot fluid hydrogen at megabar pressures. *Proc. Natl Acad. Sci. USA* **108,** 6014–6019 (2011).
9. Bonev, S. A., Schwegler, E., Ogitsu, T. & Galli, G. A quantum fluid of metallic hydrogen suggested by first-principles calculations. *Nature* **431,** 669–672 (2004).
10. Tamblyn, I. & Bonev, S. Structure and phase boundaries of compressed liquid hydrogen. *Phys. Rev. Lett.* **104,** 065702 (2010).
11. Morales, M., Pierleoni, C., Schwegler, E. & Ceperley, D. Evidence for a first-order liquid–liquid transition in high-pressure hydrogen from *ab initio* simulations. *Proc. Natl Acad. Sci. USA* **107,** 12799–12803 (2010).
12. Eremets, M. & Trojan, I. Conductive dense hydrogen. *Nature Mater.* **10,** 927–931 (2011).
13. Howie, R. T., Guillaume, C. L., Scheler, T., Goncharov, A. F. & Gregoryanz, E. Mixed molecular and atomic phase of dense hydrogen. *Phys. Rev. Lett.* **108,** 125501 (2012).
14. Howie, R. T., Scheler, T., Guillaume, C. L. & Gregoryanz, E. Proton tunneling in phase IV of hydrogen and deuterium. *Phys. Rev. B* **86,** 214104 (2012).
15. Howie, R. T., Magdău, I. B., Goncharov, A. F., Ackland, G. J. & Gregoryanz, E. Phonon localization by mass disorder in dense hydrogen-deuterium binary alloy. *Phys. Rev. Lett.* **113,** 175501 (2014).
16. Pickard, C. & Needs, R. Structure of phase III of solid hydrogen. *Nature Phys.* **3,** 473–476 (2007).
17. Liu, H., Hernandez, E., Yan, J. & Ma, Y. Anomalous melting behavior of solid hydrogen at high pressures. *J. Phys. Chem. C* **117,** 11873 (2013).
18. Chen, J. *et al.* Quantum simulation of low-temperature metallic liquid hydrogen. *Nature Commun.* **4,** 2064 (2013).

19. Akahama, Y. & Kawamura, H. High-pressure Raman spectroscopy of diamond anvils to 250 GPa: Method for pressure determination in the multimegabar pressure range. *J. Appl. Phys.* **96,** 3748–3751 (2004).
20. Akahama, Y. & Kawamura, H. Pressure calibration of diamond anvil Raman gauge to 310 GPa. *J. Appl. Phys.* **100,** 043516 (2006).
21. Howie, R., Gregoryanz, E. & Gonchaov, A. Hydrogen (deuterium) vibron frequency as a pressure comparison gauge at multi-Mbar pressures. *J. Appl. Phys.* **114,** 073505 (2013).

Acknowledgements

The authors are grateful to A. Hermann and G. Ackland for discussions and to C. Guillaume and M. Frost for help with the experiments. This work is supported by a research grant from the UK Engineering and Physical Sciences Research Council.

Author contributions

R.T.H. and P.D-S. carried out the experiments, analysed the data and wrote the paper. E.G. conceived and designed the project, carried out the experiments, analysed the data and wrote the paper.

Additional information

Supplementary information is available in the online version of the paper. Reprints and permissions information is available online at www.nature.com/reprints. Correspondence and requests for materials should be addressed to E.G.

Competing financial interests

The authors declare no competing financial interests.

Appendix B

Evidence for a new phase of dense hydrogen above 325 gigapascals

Philip Dalladay-Simpson, Ross T. Howie & Eugene Gregoryanz*
School of Physics and Centre for Science at Extreme Conditions, University of Edinburgh, Edinburgh EH9 3JZ, UK.
Nature, **529**, 63–67 (2016).

LETTER

doi:10.1038/nature16164

Evidence for a new phase of dense hydrogen above 325 gigapascals

Philip Dalladay-Simpson[1], Ross T. Howie[1]† & Eugene Gregoryanz[1,2]

Almost 80 years ago it was predicted that, under sufficient compression, the H–H bond in molecular hydrogen (H_2) would break, forming a new, atomic, metallic, solid state of hydrogen[1]. Reaching this predicted state experimentally has been one of the principal goals in high-pressure research for the past 30 years. Here, using *in situ* high-pressure Raman spectroscopy, we present evidence that at pressures greater than 325 gigapascals at 300 kelvin, H_2 and hydrogen deuteride (HD) transform to a new phase—phase V. This new phase of hydrogen is characterized by substantial weakening of the vibrational Raman activity, a change in pressure dependence of the fundamental vibrational frequency and partial loss of the low-frequency excitations. We map out the domain in pressure–temperature space of the suggested phase V in H_2 and HD up to 388 gigapascals at 300 kelvin, and up to 465 kelvin at 350 gigapascals; we do not observe phase V in deuterium (D_2). However, we show that the transformation to phase IV′ in D_2 occurs above 310 gigapascals and 300 kelvin. These values represent the largest known isotropic shift in pressure, and hence the largest possible pressure difference between the H_2 and D_2 phases, which implies that the appearance of phase V of D_2 must occur at a pressure of above 380 gigapascals. These experimental data provide a glimpse of the physical properties of dense hydrogen above 325 gigapascals and constrain the pressure and temperature conditions at which the new phase exists. We speculate that phase V may be the precursor to the non-molecular (atomic and metallic) state of hydrogen that was predicted 80 years ago.

The exchange interaction, a purely quantum mechanical effect, forms one of the strongest bonds in chemistry—the H–H bond. Owing to this bond, hydrogen exists in molecular form, with atoms separated by approximately 0.74 Å and a bond dissociation energy of approximately 4.52 eV (refs 2, 3) at ambient conditions. The first experiments to break this bond[4] demonstrated that extreme conditions are needed to do so; for example, the H_2 molecule dissociates only to a minor extent at high temperatures (at 3,000 K, the degree of dissociation is around 10%)[5]. Another mechanism to break the hydrogen bond—pressure—was subsequently proposed[1]; it was theorized that above 250,000 atm (25 GPa), the hydrogen molecules would dissociate, forming solid, atomic, metallic hydrogen, an entirely new state of the first and simplest element.

The proposed high-pressure route to an atomic metallic state has proved to be one of the great experimental challenges in high-pressure physics. Despite the technological advances in high-pressure physics, this theoretical prediction has yet to be experimentally confirmed, even

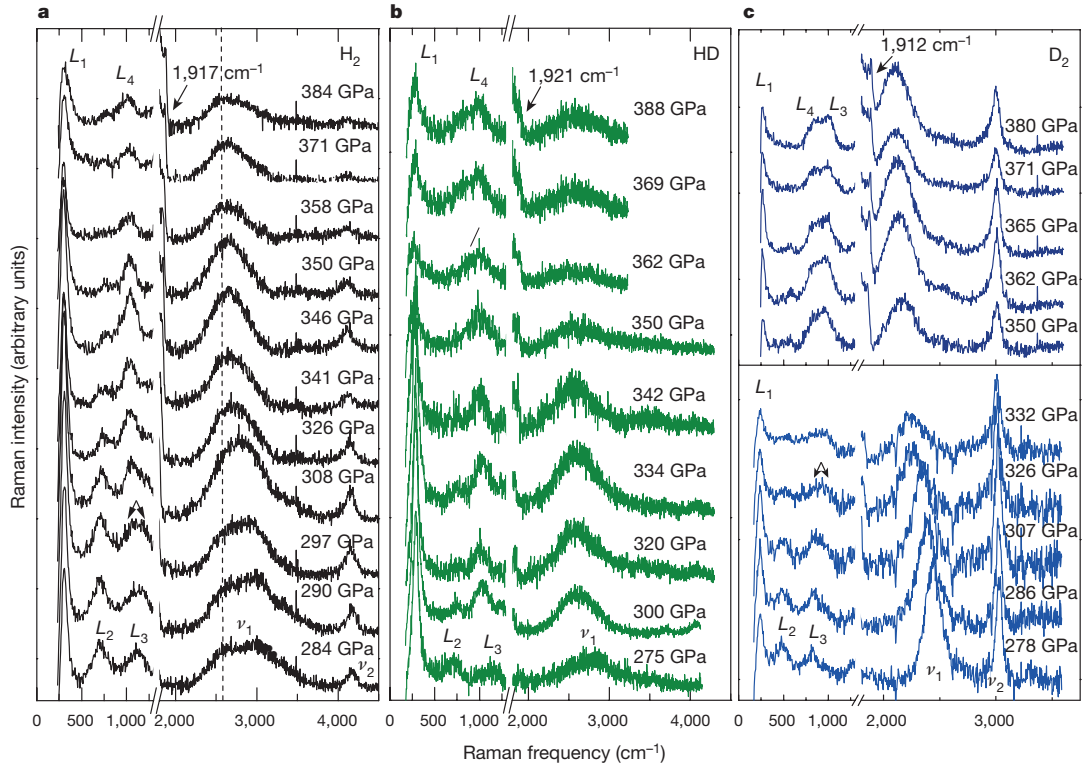

Figure 1 | Representative Raman spectra of three hydrogen isotopes. a–c, Spectra of hydrogen are shown in black (**a**), hydrogen deuteride in green (**b**) and deuterium in blue (**c**). The spectra at different pressures (as labelled) are plotted as a waterfall; the offset is for clarity. The low-frequency modes L_{1-4} and the vibrational modes $\nu_{1,2}$ are labelled. The second-order diamond band spanning 2,300–2,600 cm^{-1} is visible on some spectra; its central position is marked by the dashed vertical line in **a**. The diamond edge for each isotope, which was used to determine the pressure, is labelled on the highest-pressure spectra (1,917 cm^{-1} for H_2, 1,921 cm^{-1} for HD and 1,912 cm^{-1} for D_2). HD was formed from a mixture of H_2 (75%) and D_2 (25%); see Methods. The spectra were collected using a 647.1-nm excitation wavelength. The arrows in **a** and **c** represent the splitting of the L3 mode and the onset of IV′ (for clarity see Extended Data Fig. 4).

[1]School of Physics and Centre for Science at Extreme Conditions, University of Edinburgh, Edinburgh EH9 3JZ, UK. [2]Key Laboratory of Materials Physics, Institute of Solid State Physics, Chinese Academy of Sciences, Hefei 230031, China. †Present address: Center for High Pressure Science & Technology Advanced Research, Shanghai 201203, China.

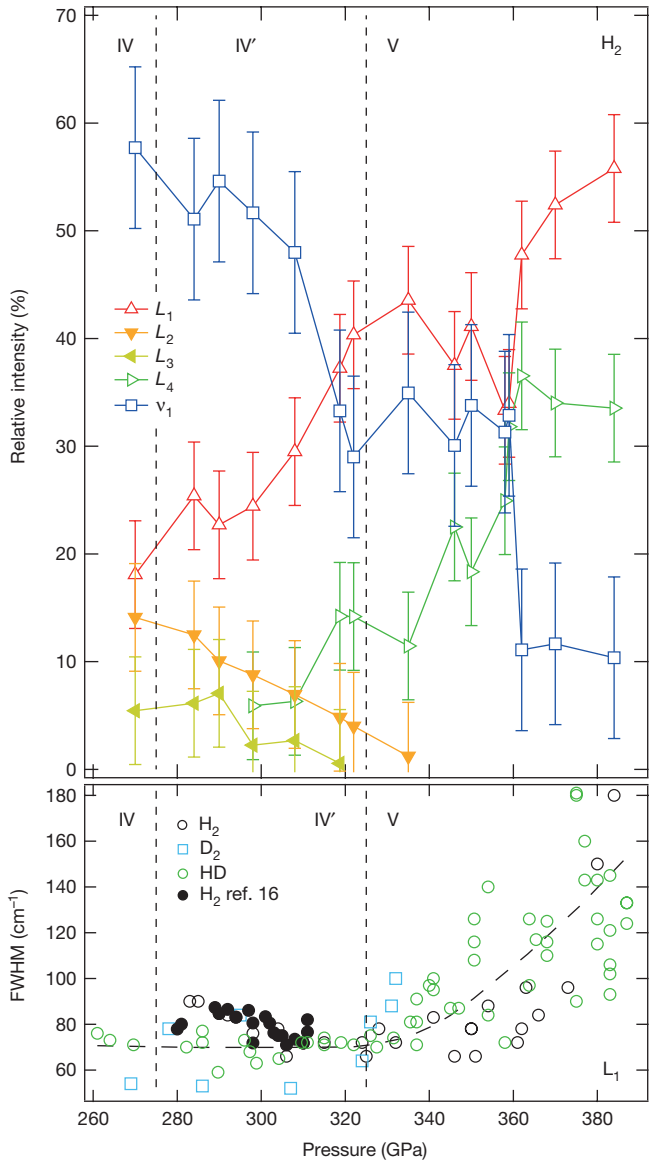

Figure 2 | Relative intensities of the vibrational, low-frequency modes and the full-width at half-maximum of the L_1 mode as a function of pressure. a, Relative intensities of the vibrational (ν_1) and four low-frequency modes (L_{1-4}) of hydrogen represented as a percentage of the total Raman activity of the sample; error bars reflect the accuracy of the measurement (see Methods and Extended Data Fig. 7). The low-frequency modes L_2 and L_3 disappear at around 325 GPa. **b**, The full-width at half-maximum (FWHM) of the low-frequency mode L_1 of H_2, D_2 and HD as function of pressure; the dashed curve is a guide to the eye. The dashed vertical lines in **a** and **b** indicate the transformations to phases IV′ and V.

at pressures (and high temperatures) an order of magnitude higher than that originally proposed[6–14]. Recently, a new solid phase of dense hydrogen—phase IV—was experimentally discovered[15,16] at 300 K and above 230 GPa. This new phase IV exhibits a change in the gradient of the fundamental vibrational-mode frequency ν_1 with respect to pressure P at a constant temperature $T = 300$ K, $(d\nu_1/dP)_T$, which leads to extremely low values of ν_1 above 230 GPa; for example, $\nu_1 \approx 2{,}750\ cm^{-1}$ at 315 GPa (ref. 16). This value is indicative of a much weaker bond, compared to ambient conditions, and is consistent with the bond length of approximately 0.82 Å (ref. 17). It was observed that phase IV could be viewed as a mixed molecular and atomic state and that the complete dissociation of the hydrogen molecule is feasible at even higher compressions[18].

To investigate the states of hydrogen above 320 GPa, we conducted very high pressure studies on H_2, HD (hydrogen deuteride) and D_2, reaching pressures of 384 ± 15 GPa, 388 ± 15 GPa and 380 ± 15 GPa, respectively. These pressures, despite being conservative estimates (see Methods and Extended Data Figs 1 and 2), are still among the highest pressures reported so far in a diamond anvil cell, and the highest pressures hydrogen has so far been subjected to in static experiments. On the basis of the substantial decrease in intensity of vibrational Raman bands, the change of slope of the vibrational-mode frequency with pressure, and changes in position, width and intensity of the low-frequency ($<1{,}300\ cm^{-1}$) modes, we tentatively infer a transition to a new structural configuration—phase V—of H_2 and HD above 325 GPa, while observing phase IV′ of D_2 above 310 GPa. We present experimental information on the physical properties of the dense hydrogen just below 400 GPa and provide some constraints on the P–T space of phase V. On the basis of the optical changes observed through the phase transition, we speculate that the proposed phase V might be the onset of a non-molecular state of hydrogen.

Figure 1 shows the representative Raman spectra of three isotopes of hydrogen compressed at 300 K. (For the full description of the relevant experimental details, see Methods and refs 18 and 19; further information about the intensities of the modes and frequencies of HD as a function of H/D concentration and pressure is provided in ref. 20.) Above 220 GPa, all hydrogen isotopes enter phase IV, which is characterized by sharp, well-defined, low-frequency modes (Fig. 1, marked for clarity as L_1, L_2 and L_3 in all figures; see also ref. 20) and the presence of a second vibrational fundamental mode ν_2. The appearance of the Raman spectra of HD (at similar pressures) is essentially identical to those of H_2 or D_2 (refs 16, 18); see Extended Data Fig. 3. When pressures above 275 GPa are reached (for H_2 and HD), we observe a change in the gradient of the frequency with respect to pressure of the L_3 mode, and its branching to produce a new L_4 mode. These changes mark the appearance of phase IV′, described previously[18]. It was suggested that phase IV′ could structurally resemble phase IV, on the basis of close similarities between the Raman spectra[18]. Above 320 GPa we observe gradual, but profound, modification in the Raman spectra, indicative of the phase transformation to a new phase, phase V (H_2 and HD only). The pressure needed to enter phase IV′ in deuterium is 35 GPa higher, as evidenced by the splitting of L_3 into L_3 and L_4 at 310 GPa (Fig. 1, Extended Data Fig. 4).

In hydrogen, after branching to produce the L_4 mode, the L_3 mode slowly redistributes its intensity into the L_4 mode (Figs 1, 2 and Extended Data Fig. 4). When the suggested phase V is reached, the L_3 mode completely disappears and the intensity of L_4 becomes comparable to that of the L_1 mode (Figs 1 and 2). Meanwhile, the L_1 mode undergoes a marked change itself; Fig. 2b shows the full-width at half-maximum (FWHM) of L_1 as function of pressure. At the same pressure as when the vibrational Raman modes start to become weaker and the L_2 and L_3 modes disappear (>325 GPa; see Figs 1 and 2), the FWHM of the L_1 mode starts to increase rapidly. Between 330 GPa and 388 GPa the width of the L_1 mode increases more than twofold, reaching $180\ cm^{-1}$ by 388 GPa (Fig. 2b). Even though the L_1 mode is very broad at the highest pressures, it remains the dominant feature of the spectra of all isotopes (Fig. 1). We also observe some small but detectable softening of the L_1 frequency with pressure (Fig. 3).

Up to 325 GPa, the total Raman intensity of all modes stays roughly the same (Fig. 2) for all three isotopes, in agreement with previous studies[16] of pure H_2 up to 315 GPa. However, when pressures above 325 GPa are reached, the low-frequency modes L_2 and L_3 disappear and the intensities of both vibrational excitations of H_2 and HD start to decrease rapidly. In the case of hydrogen, the ν_2 modes become almost indistinguishable from the background above 358 GPa, whereas the ν_1 mode becomes broad and weak, overlapping with the second-order diamond band (Fig. 1a); the positions of the hydrogen and deuterium vibrational modes are clearly visible in all spectra (Fig. 1). The second-order diamond mode spanning the approximate range 2,300–$2{,}600\ cm^{-1}$ overlaps in frequency with the ν_1 mode of all isotopes,

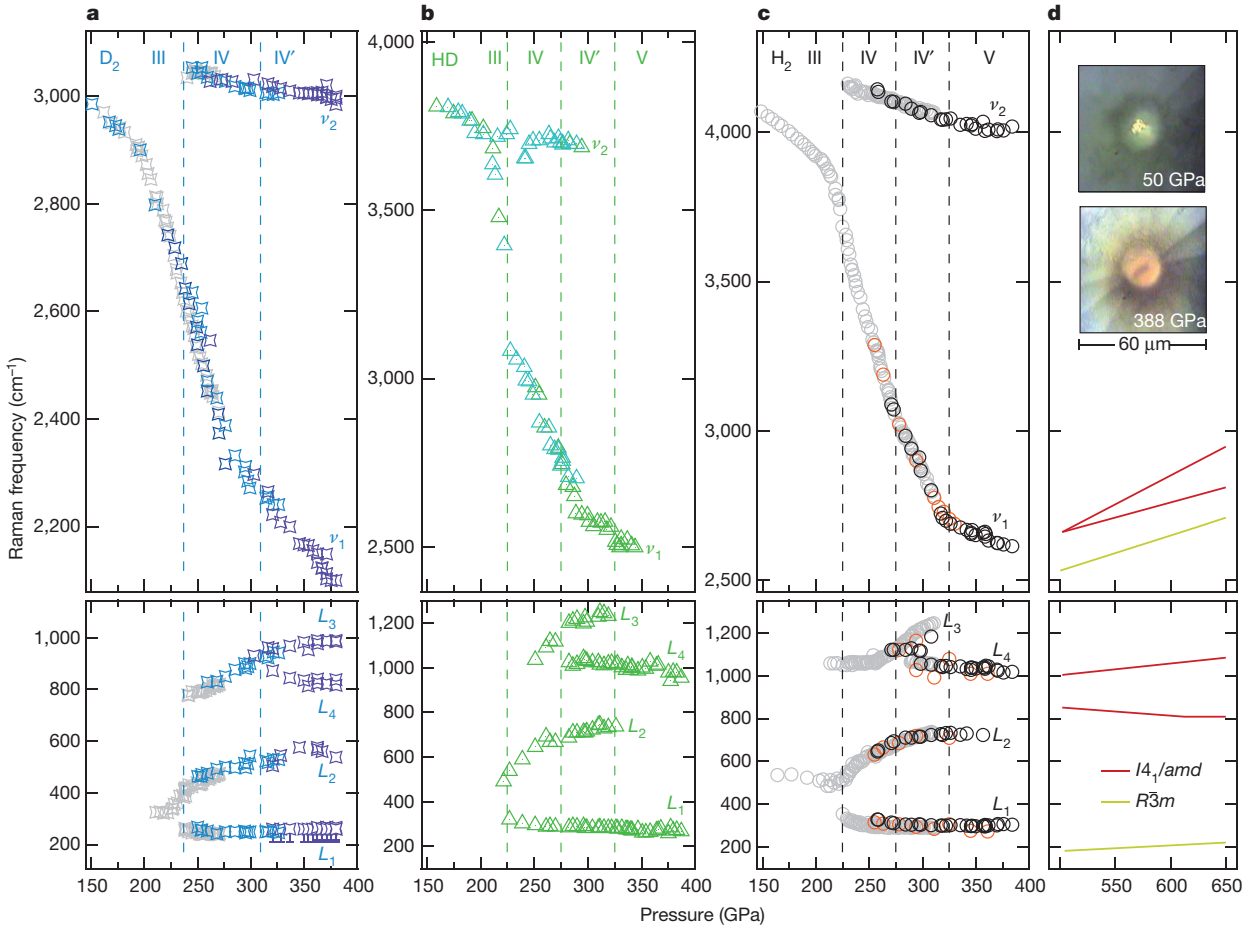

Figure 3 | Frequencies of the vibrational and low-energy modes of the isotopes as functions of pressure. a–**c**, The data for the different isotopes are shown as open stars (D_2; **a**), triangles with centre dots (HD; **b**) and open circles (H_2; **c**), with different colours representing different experimental runs. Data from previous studies[16,18] are shown as grey symbols. The vertical dashed lines denote the phase transitions in the corresponding isotope. **d**, The theoretically calculated frequencies of hydrogen for the metallic and non-molecular (atomic) structures of $I4_1/amd$ (red) and $R\bar{3}m$ (yellow) from ref. 22. The insets are photos of the HD sample at 50 GPa and at 388 GPa, as labelled, taken in transmitted and reflected light.

which makes the estimation of its intensity difficult. In the case of HD, it became impossible to distinguish between the second-order diamond mode and the ν_1 mode above 350 GPa (Fig. 1b). The notable decrease of the vibrational-mode intensity means that the spectra of the suggested phase V looks highly unusual, particularly when compared with those of phase IV, in which the vibrational mode dominates (see >270–320-GPa spectra of all isotopes in Fig. 1). As well as the pronounced drop of the intensities of the vibrational modes, we observe a change in the slope of the ν_1 frequency with pressure $(d\nu_1/dP)_T$ at around 325 GPa for hydrogen and hydrogen deuteride (Fig. 3). The ν_1 mode softens rapidly with pressure in phase IV (average gradient of $-12\,cm^{-1}\,GPa^{-1}$; ref. 16) and changes to a rate of about $-7\,cm^{-1}\,GPa^{-1}$ (refs 16, 18) in phase IV′. When hydrogen is compressed to more than 325 GPa, the softening of the ν_1 mode essentially stops and $(d\nu_1/dP)_T$ becomes almost independent of pressure (equal to $-1.37\,cm^{-1}\,GPa^{-1}$), resembling that of the ν_2 mode ($-1.01\,cm^{-1}\,GPa$); see Fig. 3. The change of slope and the sudden increase of the FWHM of the L_1 mode happen at the same pressure, suggesting that the nature of the bonding is noticeably modified by the transition between phase IV(IV′) and V′. In a recent Raman optical study[21], a small change in the slope of the vibrational mode of the H_2 vibrational mode at 300 GPa was observed, from which three structural phase transitions within 50 GPa (275–325 GPa) were inferred. However, our data do not seem to support these findings (Extended Data Fig. 5).

The pressure at which phase IV of deuterium appears is about 10 GPa higher than that of hydrogen[18], whereas the transition from phases IV to IV′ is shifted by 35–40 GPa. We observe similar qualitative changes in the slope of the deuterium vibrational mode at 310 GPa upon entrance into phase IV′, but the slope remains relatively steep, resulting in the extremely low vibrational frequency of approximately 2,100 cm^{-1} at 380 GPa. The large pressure difference between phase IV′ of hydrogen and that of deuterium suggests that phase V of deuterium will appear at pressures above 380 GPa.

We investigated the *P*–*T* space where phase IV(IV′) and the proposed phase V exist by conducting heating experiments. If hydrogen is heated at 250 GPa, then the phase IV ↔ I transformation happens at 430 K, and at 450 K phase I presumably melts (see Fig. 4 and the figures in ref. 14). In some runs, phase IV(IV′) was heated at pressures above the I-IV-liquid[14] triple point—for example, at 262 GPa to approximately 450 K and at 270 GPa and 290–310 GPa to approximately 375 K—but no transformations to phase V were observed (Fig. 4). Finally, we heated phase V at 350 GPa and did not observe any transformation up to 465 K (Extended Data Fig. 6). These points in *P*–*T* space indicate that phase V is separated from the lower-pressure phase IV(IV′) by a phase line that is probably close to vertical (Fig. 4).

The decrease in the vibrational-mode intensities could indicate the loss of sample, particularly in the case of hydrogen, but the observations described above rule this out and instead indicate a possible phase transition. These observations include: the evolution of the low-frequency modes (that is, broadening and frequency change) with pressure up to 390 GPa, and only a modest drop in the intensity of the L_1 mode; the noticeable change in the slope of the vibrational-mode

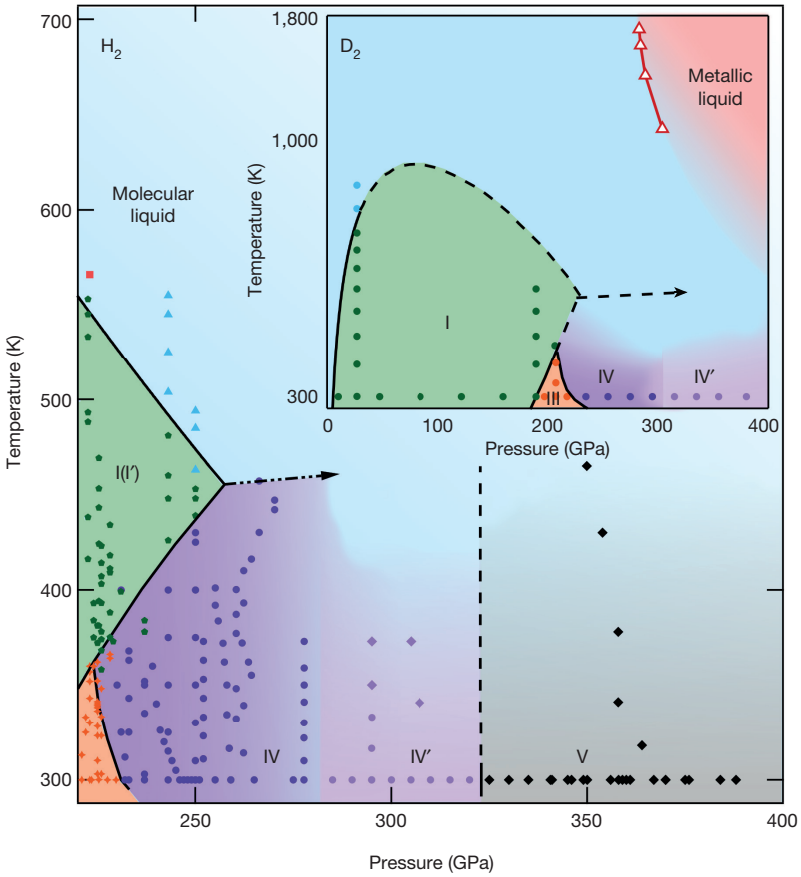

Figure 4 | Proposed phase diagram of hydrogen up to 400 GPa. The coloured, filled symbols and solid phase lines below 300 GPa in the main figure are from ref. 14, and show phases I(I′), III and IV(IV′). The solid black diamonds (phase V) are from this study, the vertical, grey dashed line indicates the transition from phase IV′ to phase V and the dashed-dotted arrow is the proposed continuation of the melting curve. The inset shows a sketch of the phase diagram of D_2. The coloured, filled symbols and solid lines were obtained by us in another, unreported study. The dashed lines are the proposed melting curves of deuterium, which have not been measured experimentally, but are assumed to follow the same trend as those of hydrogen. The red open triangles are from ref. 26 and separate the metallic and semi-conducting liquids.

frequency with pressure at 325 GPa at 300 K; and the lack of sample loss or detection of transformation upon heating at pressures above 320 GPa. In heating experiments, rapid sample loss is observed in the liquid state, which results in the complete disappearance of all hydrogen Raman activity and the resulting spectra resemble those of the gasket (Extended Data Fig. 6).

It is tempting, although highly speculative at this time, to interpret phase V as the onset of the predicted[1] non-molecular and metallic state of hydrogen. *Ab initio* random-structure searches that included zero-point motion estimate that hydrogen should dissociate into atomic and metallic states at around 500 GPa (ref. 22) and 380 GPa (ref. 23), respectively. The possible lowest-energy structural candidates include the tetragonal $I4_1/amd$ and trigonal $R\bar{3}m$ symmetries[22,23]. Both structures have inter-atomic Raman phonons with frequencies of about 2,500 cm^{-1} at 500 GPa, which is close to the frequency of the vibrational mode ν_1 of hydrogen that we observe at 380 GPa (see Fig. 3 and supplementary information in ref. 22). In calculations, these phonons are present up to 4.2 TPa, slowly increasing in energy with increasing pressure[22] as the distance between the atoms decreases. The presence of the extremely weak ν_2 mode at 384 GPa (Fig. 1a) indicates that the purely atomic state was not reached in our experiments and that slightly higher pressures are required to completely dissociate hydrogen. It is plausible that the molecular dissociation commences at pressures above 350 GPa, resulting in the alterations of the Raman spectrum as described here. If the suggested phase V is indeed the beginning of the complete molecular dissociation of partially molecular phase IV′, then it could explain all the optical observations presented here, such as the band gap decreasing with pressure (1.8 eV at 315 GPa in phase IV′, ref. 16). Furthermore, the possible appearance of conducting electrons due to dissociation could explain the very dark appearance of the sample as seen in transmitted and reflected light in the visible region (Fig. 3d, inset), and the overall decrease of the Raman intensities. The relatively simple overall Raman spectrum observed experimentally matches those predicted theoretically rather well (Fig. 3d). The $I4_1/amd$ symmetry does not predict a very prominent L_1 mode, whereas the $R\bar{3}m$ symmetry, which is more energetically favourable at even higher pressures, does not predict the L_4 mode (see Fig. 3b, c), both of which are observed experimentally. However, these discrepancies could be accounted for by the 100-GPa pressure difference between theory and experiment. A minimum in $(d\nu_1/dP)_T$ would indicate the evolution from the intramolecular vibrational mode to an interatomic phonon. This change could require a 100-GPa pressure range to complete and would result in hardening of the phonons at pressures above 500 GPa.

The data from this and a previous melting study[14] provide further insight into the current phase diagram of hydrogen (Fig. 4). It appears that there could be another triple point between the proposed phase V, phase IV(IV′), and a liquid state (not shown) at above 275 GPa and 450 K. If phase V is indeed a precursor to a fully non-molecular, and presumably metallic, solid state, then a question arises about the existence and location of the phase line separating the molecular (insulating) and non-molecular (metallic) liquids and solids. A non-molecular liquid could be expected to exist in the same pressure range as phase V, but at higher temperatures. In fact, theoretical studies have suggested a phase transition from a molecular liquid to an atomic liquid in hydrogen[24,25]. The data presented in refs 24 and 25 suggest the existence of the highly conducting atomic liquid state at pressures as low as about 150 GPa and above 2,000 K (ref. 25). However, shock-wave experiments[26] indicate the existence of the metallic liquid deuterium at higher pressures of 350 GPa, with the corresponding phase line being almost vertical (Fig. 4, inset). These experimental results seem to be in a very good agreement with our current study. Extrapolation of the data from ref. 26 to lower temperatures would imply yet another triple point between the melting curve and the two liquid phases. The presence of two dissimilar liquids would suggest the presence of two solid phases below them, with properties mimicking those of the liquids, for example, non-molecular (insulating) versus atomic (metallic). Experimental confirmation of the location of the phase line(s) and triple points would be very

important for the complete description of phase V, even higher-pressure solid phases and the possible molecular–atomic transition. An understanding of the connection between the proposed metallization and phase V is also required. Such additional data could provide invaluable information about the fundamental physics and chemistry that governs the behaviour of the simplest element at high densities.

Online Content Methods, along with any additional Extended Data display items and Source Data, are available in the online version of the paper; references unique to these sections appear only in the online paper.

Received 16 June; accepted 14 October 2015.

1. Wigner, E. & Huntington, H. B. On the possibility of a metallic modification of hydrogen. *J. Chem. Phys.* **3,** 764–770 (1935).
2. van Kranendonk, J. *Solid Hydrogen* (Plenum Press, 1983).
3. Housecroft, C. E. & Sharpe, A. G. *Inorganic Chemistry* (Prentice Hall, 2007).
4. Langmuir, I. & Mackay, G. M. J. The dissociation of hydrogen into atoms. Part I. Experimental. *J. Am. Chem. Soc.* **36,** 1708–1722 (1914).
5. Langmuir, I. The dissociation of hydrogen into atoms. [Part II.] Calculation of the degree of dissociation and the heat of formation. *J. Am. Chem. Soc.* **37,** 417–458 (1915).
6. Goncharov, A. F., Gregoryanz, E., Hemley, R. J. & Mao, H.-k. Spectroscopic studies of the vibrational and electronic properties of solid hydrogen to 285 GPa. *Proc. Natl Acad. Sci. USA* **98,** 14234–14237 (2001).
7. Loubeyre, P., Occelli, F. & LeToullec, R. Optical studies of solid hydrogen to 320 GPa and evidence for black hydrogen. *Nature* **416,** 613–617 (2002).
8. Gregoryanz, E., Goncharov, A., Matsuishi, K., Mao, H.-k. & Hemley, R. Raman spectroscopy of hot dense hydrogen. *Phys. Rev. Lett.* **90,** 175701 (2003).
9. Eremets, M. I. & Trojan, I. A. Evidence of maximum in the melting curve of hydrogen at megabar pressures. *JETP Lett.* **89,** 174–179 (2009).
10. Subramanian, N., Goncharov, A. F., Struzhkin, V. V., Somayazulu, M. & Hemley, R. J. Bonding changes in hot fluid hydrogen at megabar pressures. *Proc. Natl Acad. Sci. USA* **108,** 6014–6019 (2011).
11. Akahama, Y. *et al.* Evidence from x-ray diffraction of orientational ordering in phase III of solid hydrogen at pressures up to 183 GPa. *Phys. Rev. B* **82,** 060101 (2010).
12. Akahama, Y., Kawamura, H., Hirao, N., Ohishi, Y. & Takemura, K. Raman scattering and x-ray diffraction experiments for phase III of solid hydrogen. *J. Phys. Conf. Ser.* **215,** 012056 (2010).
13. Zha, C.-S., Liu, Z. & Hemley, R. J. Synchrotron infrared measurements of dense hydrogen to 360 GPa. *Phys. Rev. Lett.* **108,** 146402 (2012).
14. Howie, R. T., Dalladay-Simpson, P. & Gregoryanz, E. Raman spectroscopy of hot hydrogen above 200 GPa. *Nature Mater.* **14,** 495–499 (2015).
15. Eremets, M. I. & Troyan, I. A. Conductive dense hydrogen. *Nature Mater.* **10,** 927–931 (2011).
16. Howie, R. T., Guillaume, C. L., Scheler, T., Goncharov, A. F. & Gregoryanz, E. Mixed molecular and atomic phase of dense hydrogen. *Phys. Rev. Lett.* **108,** 125501 (2012).
17. Pickard, C. J. & Needs, R. J. Structure of phase III of solid hydrogen. *Nature Phys.* **3,** 473–476 (2007).
18. Howie, R. T., Scheler, T., Guillaume, C. L. & Gregoryanz, E. Proton tunneling in phase IV of hydrogen and deuterium. *Phys. Rev. B* **86,** 214104 (2012).
19. Howie, R. T., Gregoryanz, E. & Goncharov, A. F. Hydrogen (deuterium) vibron frequency as a pressure comparison gauge at multi-Mbar pressures. *J. Appl. Phys.* **114,** 073505 (2013).
20. Howie, R. T., Magdău, I. B., Goncharov, A. F., Ackland, G. J. & Gregoryanz, E. Phonon localization by mass disorder in dense hydrogen-deuterium binary alloy. *Phys. Rev. Lett.* **113,** 175501 (2014).
21. Zha, C.-s., Cohen, R. E., Mao, H.-k. & Hemley, R. J. Raman measurements of phase transitions in dense solid hydrogen and deuterium to 325 GPa. *Proc. Natl Acad. Sci. USA* **111,** 4793–4797 (2014).
22. McMahon, J. M. & Ceperley, D. M. Ground-state structures of atomic metallic hydrogen. *Phys. Rev. Lett.* **106,** 165302 (2011).
23. Azadi, S., Monserrat, B., Foulkes, W. M. C. & Needs, R. J. Dissociation of high-pressure solid molecular hydrogen: a quantum Monte Carlo and anharmonic vibrational study. *Phys. Rev. Lett.* **112,** 165501 (2014).
24. Tamblyn, I. & Bonev, S. A. Structure and phase boundaries of compressed liquid hydrogen. *Phys. Rev. Lett.* **104,** 065702 (2010).
25. Morales, M., Pierleoni, C., Schwegler, E. & Ceperley, D. M. Evidence for a first-order liquid-liquid transition in high-pressure hydrogen from ab initio simulations. *Proc. Natl Acad. Sci. USA* **107,** 12799–12803 (2010).
26. Knudson, M. D. *et al.* Direct observation of an abrupt insulator-to-metal transition in dense liquid deuterium. *Science* **348,** 1455–1460 (2015).

Acknowledgements We are grateful to M. Frost for assistance during experiments. This work is supported by a Leadership Fellowship from the UK Engineering and Physical Sciences Research Council (EPSRC), reference number EP/J003999/1. P.D-S. acknowledges studentship funding from EPSRC grant number EP/G03673X/1.

Author Contributions R.T.H. and P.D-S. carried out the experiments, analysed the data and wrote the paper. E.G. conceived and designed the project, carried out the experiments, analysed the data and wrote the paper.

Author Information Reprints and permissions information is available at www.nature.com/reprints. The authors declare no competing financial interests. Readers are welcome to comment on the online version of the paper. Correspondence and requests for materials should be addressed to E.G. (e.gregoryanz@ed.ac.uk).

METHODS

Sample loadings. The experimental runs used mostly the same techniques and method described in refs 16, 18, 19 and references therein. For this study we conducted a total of 14 independent experiments up to pressures of 388 ± 15 GPa. In some of the runs we heated the sample, at different pressures, up to temperatures of 465 K. Pressure was generated in long, high-temperature, piston-cylinder diamond anvil cells of our own design equipped with diamonds with culet dimensions ranging from 30 μm to 15 μm. The rhenium foils with thicknesses of 200–250 μm were used as the gasket material to form the sample chamber. The hydrogen gas was clamped at 0.175–0.200 GPa at 300 K and then further compressed to above 150 GPa, usually within 2–3 h after clamping. The HD was produced by mixing the pure isotopes in gas phases (usually <10 MPa) at 300 K. The partial pressures were used to calculate the composition, which, for the experiment on HD described here, was 75% and 25% for hydrogen and deuterium, respectively (see also ref. 20).

Optical measurements. We used 514.15-nm and 647.1-nm excitation wavelengths to collect the spectra. Owing to the quantum efficiency of the visible CCD (charged coupled device) used, the high-energy modes—for example, hydrogen vibrational excitation at above 3,500 cm^{-1}—are much weaker than the low-energy lattice modes if probed using a 647.1-nm wavelength. However, in most of the cases, when 514.15-nm excitation is used, the pressure-induced fluorescence from the stressed diamonds obscures the Raman signal, which leaves 647.1-nm excitation as the only available source, as in Fig. 1.

Pressure and temperature measurements. For pressure measurements, the stressed-diamond-edge frequency was used and, where applicable, cross-referenced with the frequency of the vibrational modes[19] from previous experiments to maintain self-consistency. An example of how the frequency of the stressed diamond edge was determined, and the dependence of the vibrational frequency of hydrogen versus the frequency of the stressed diamond edge is given in Extended Data Fig. 1a. The first-order diamond Raman band becomes elongated in frequency space, composed of two sharp, well-defined peaks: one corresponding to the stressed culet and the other to the unstressed regions of the diamond. The frequency from the stressed culet was determined by the frequency (ω) at which $dI/d\omega$ was minimized (where I is the intensity of the spectrum), a technique proposed in refs 11, 27, and 28.

The calibration data presented in refs 27 and 28 were primarily used here for determining pressure. These two curves agree up to about 200 GPa, but gradually diverge at higher pressures (Extended Data Fig. 2b). For example, at the highest pressure reached, we observed a diamond-edge frequency of 1,936 cm^{-1} (see Fig. 1), which corresponds to pressures of approximately 388 GPa and 403 GPa on the scales proposed by Akahama & Kawamura in 2004[27] and 2006[28], respectively. With their latest calibration in 2010[29], this frequency corresponds to a substantially higher pressure of 449 GPa (Extended Data Fig. 2b). However, the effect of pressures above about 300 GPa on soft samples has yet to be determined; the latest calibration[29] up to 410 GPa needs to be independently verified, particularly for softer samples. To be consistent with previous results, we decided to use the most conservative scale[27], as was used in our previous studies[16,18,19]. This scale provides a smooth continuation of the frequencies of the low-energy and vibrational modes versus pressure observed by us in all experiments.

We therefore stress that the characteristics that provide evidence for the phase V transition are independent of the choice of the previously discussed calibrations, not a direct consequence. Extended Data Figure 2a demonstrates that the discontinuous change in $d\nu_1/dP$ for pure H_2 is present when using any of the stressed-diamond-edge pressure calibrations, and remains just as prominent when using the less-conservative and more-contemporary pressure scales[11,27].

For heating, we used two custom-built resistive heaters placed around the diamonds and the body of the cell. Temperature was determined using one or two thermocouples, attached to one of the diamonds and/or the gasket.

Calculating relative integrated intensities. Calculating the relative Raman intensities in the diamond anvil cell is a difficult task, especially when these intensities are of similar magnitude to the relatively low signal-to-noise ratios. Therefore, the data in Fig. 2 are from the spectrum with the highest signal-to-noise ratio in each run. First, the background caused by the pressure-induced fluorescence of the diamond anvils is subtracted. The residual data are then fitted with Voigt profiles, which produces values for the integrated intensities of each excitation. These values are then summed, and the percentage of total Raman activity is calculated; an example is provided in Extended Data Fig. 7. Owing to the extremely small samples, the second-order Raman band also becomes comparable in magnitude to the excitations from the sample (Extended Data Fig. 7, inset). Consequently, at higher pressures for which the ν_1 excitations overlap with the second-order Raman diamond band, extra care has to be taken. Here, the evolution of the spectra with pressure (which is determined using fits from a previous pressure step as an initial guess) as well as the relationship between the intensity of the first- and second-order diamond bands are used to accurately determine the integrated intensity of ν_1.

27. Akahama, Y. & Kawamura, H. High-pressure Raman spectroscopy of diamond anvils to 250 GPa: method for pressure determination in the multimegabar pressure range. *J. Appl. Phys.* **96,** 3748–3751 (2004).
28. Akahama, Y. & Kawamura, H. Pressure calibration of diamond anvil Raman gauge to 310 GPa. *J. Appl. Phys.* **100,** 043516 (2006).
29. Akahama, Y. & Kawamura, H. Pressure calibration of diamond anvil Raman gauge to 410 GPa. *J. Phys. Conf. Ser.* **215,** 012195 (2010).

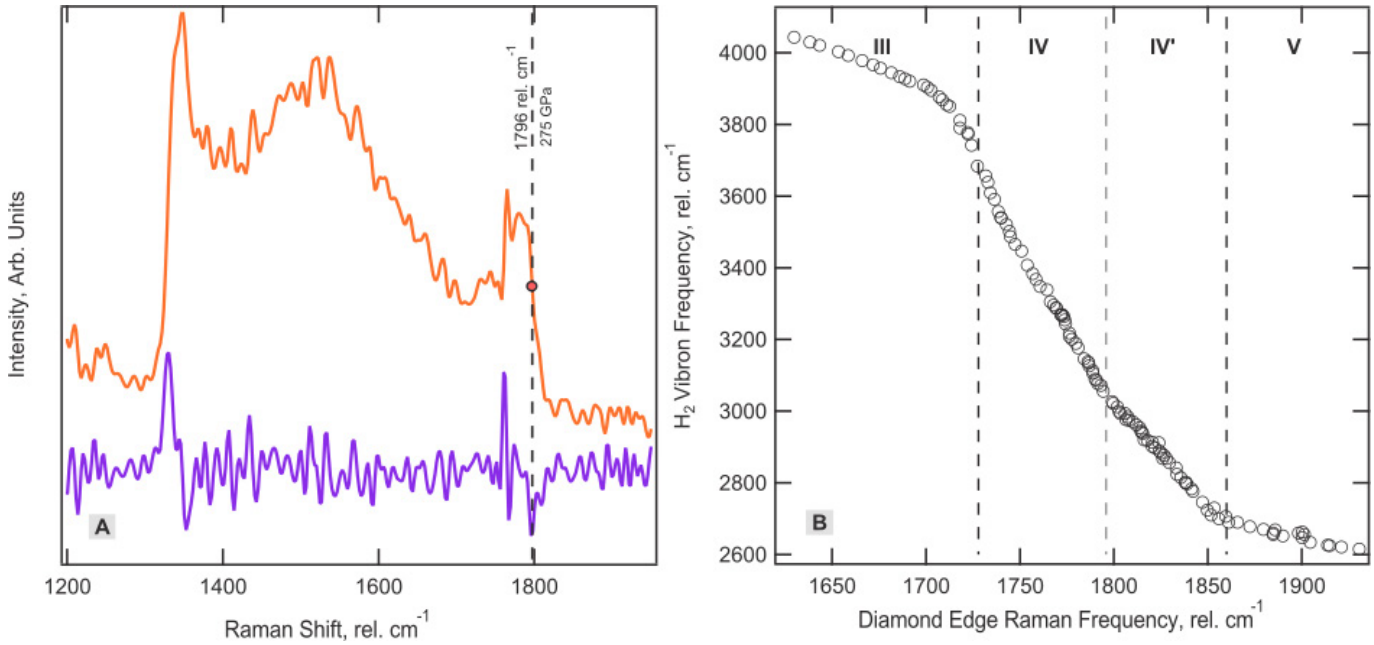

Extended Data Figure 1 | Calculating pressure. a, A typical example of a spectrum from the first-order Raman band of diamond when probing the sample (orange). The frequency edge is given by the vertical dashed line at 1,796 rel. cm^{-1}, which corresponds to a pressure of 275 GPa (ref. 27). This stressed edge is defined as the frequency that minimizes $dI/d\omega$ (purple). **b**, H_2 vibrational-mode (vibron) frequency (ν_1) plotted as a function of the stressed-diamond-edge frequency.

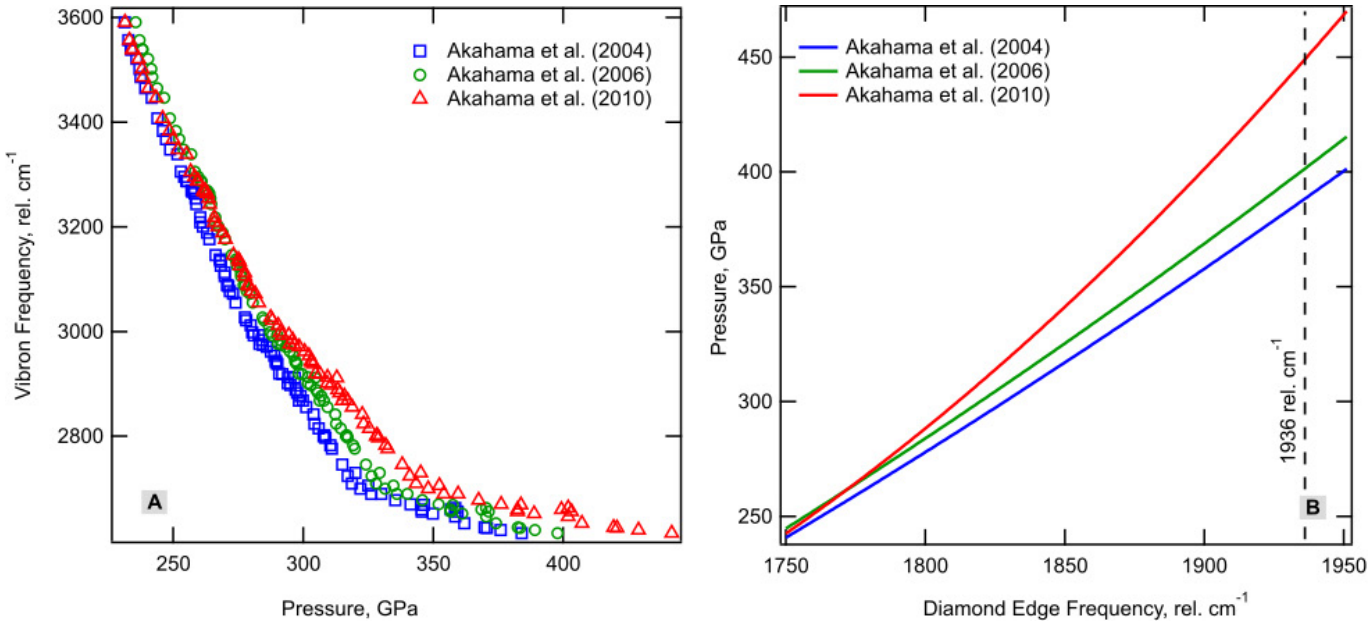

Extended Data Figure 2 | Comparison of pressure calibrations. **a**, Vibration-mode (vibron) frequency plotted using the three pressure gauges of the stressed-diamond frequency proposed by Akahama *et al.*: blue squares[27], green circles[28] and red triangles[11]. **b**, The three pressure gauges plotted as a function of pressure, coloured as in **a**; the dashed line marks the highest frequency of the stressed diamond recorded on a HD sample, 1,936 rel. cm^{-1}.

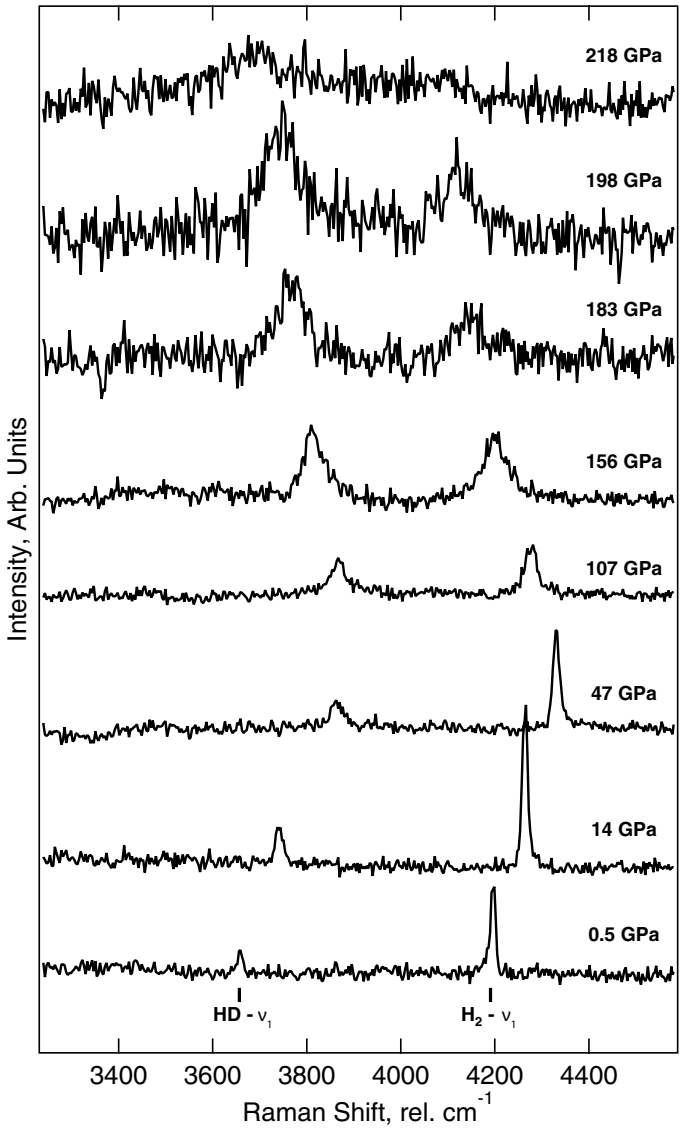

Extended Data Figure 3 | HD compressed to 218 GPa. Representative Raman spectra from HD, a mixture of hydrogen (75%) and deuterium (25%), as a function of pressure at 300 K. The spectra show the evolution of the ν_1 vibrational modes of HD (labelled 'HD-ν_1') and H_2 (labelled 'H_2-ν_1') from loading at 0.5–218 GPa, as labelled. Above 47 GPa, there is an observed transfer of integrated intensity from the ν_1 band of H_2 to the ν_1 band of HD, with the latter vibrational mode becoming stronger than the former at 150 GPa, and the only resolvable ν_1 band above 218 GPa. The spectra were collected using a 514-nm excitation wavelength. The spectra from this run above 218 GPa are shown in Fig. 1b.

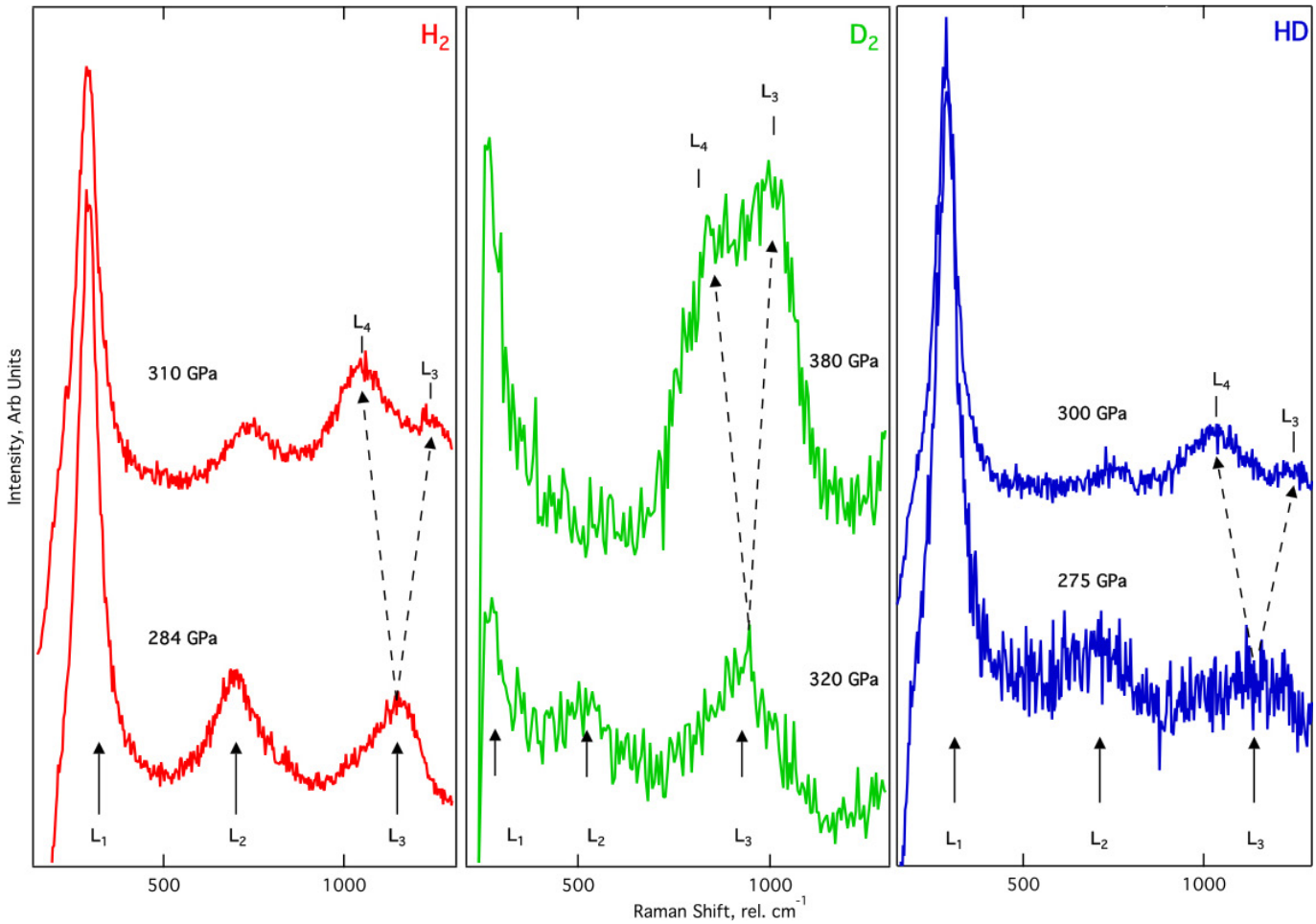

Extended Data Figure 4 | Low-energy-mode splitting from phase IV to phase IV′. Representative Raman spectra of the low-frequency excitations of the three isotopes (left, H_2; centre, D_2; right, HD) as functions of pressure during the transition from phase IV to phase IV′. The low-frequency mode L_3 splits to produce mode L_4.

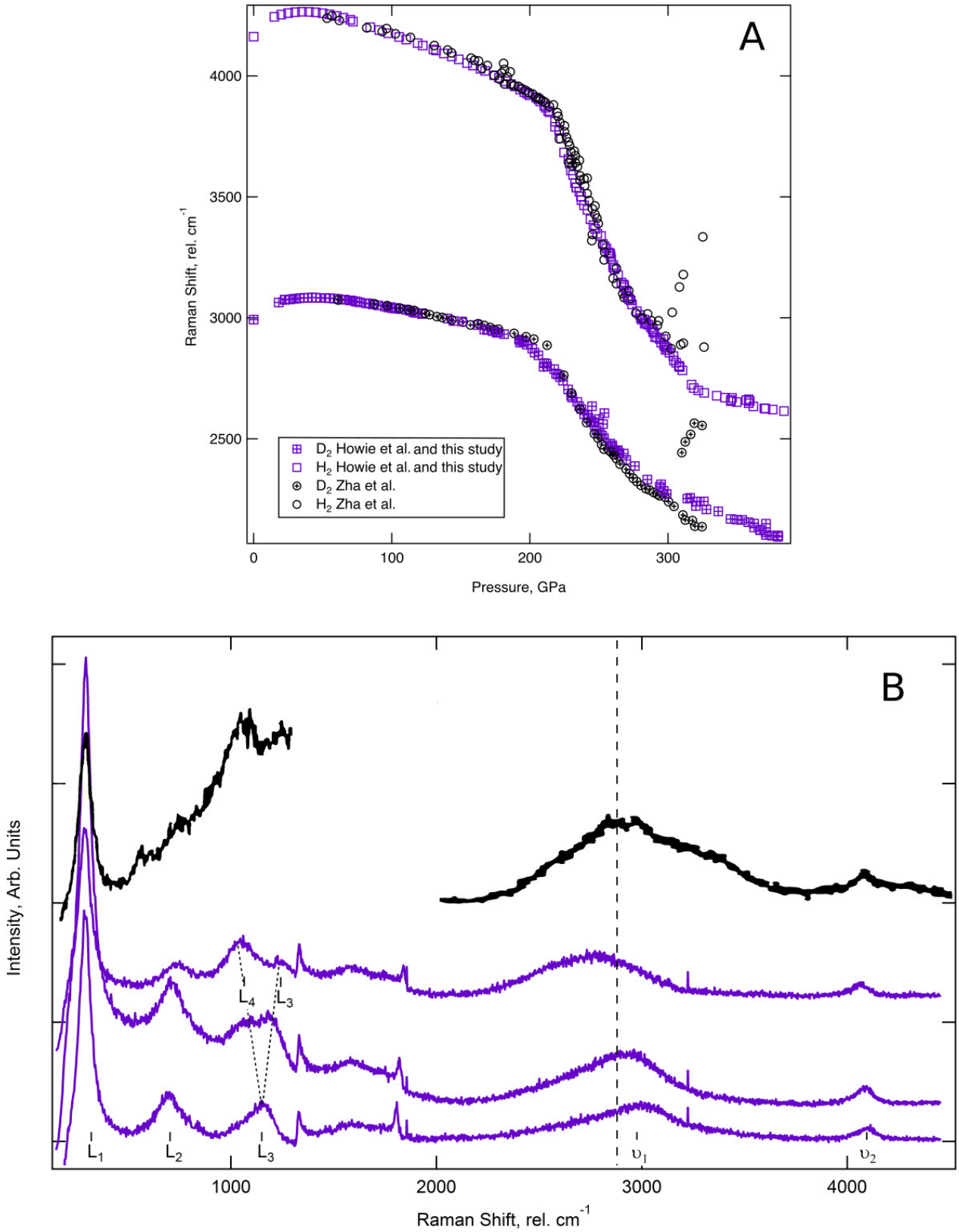

Extended Data Figure 5 | Comparison with previous data. a, Frequencies of the vibrational modes versus pressure from ref. 21 (black circles) and the current study and our previous study[16] (violet squares). The open symbols represent data for H_2; the symbols enclosing pluses represent data for D_2. **b**, Representative Raman spectra of hydrogen from ref. 21 (black) and ref. 16 (violet). The dashed vertical line indicates the lowest vibrational-mode frequency (and therefore the highest pressure) observed in ref. 21.

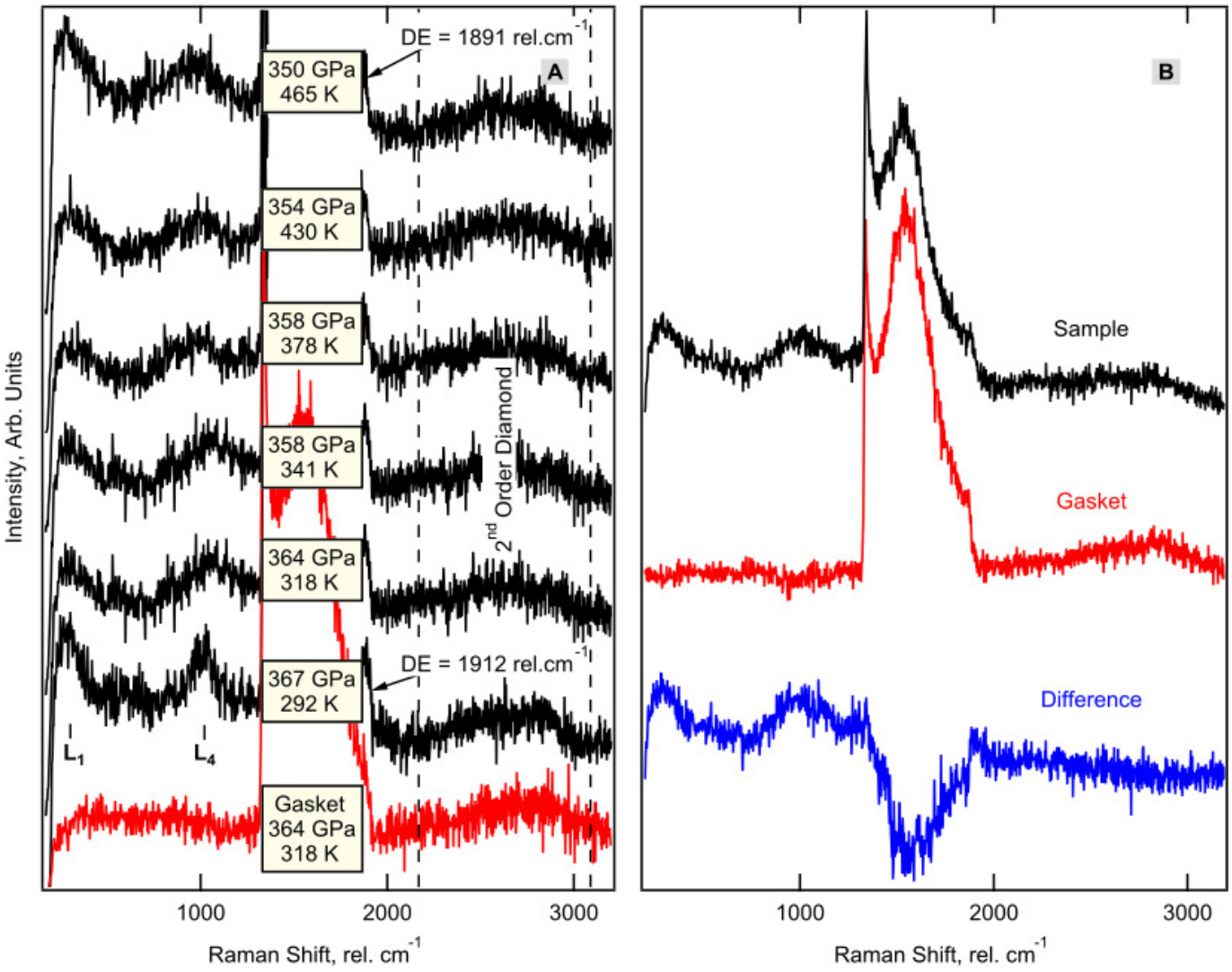

Extended Data Figure 6 | Heating at about 360 GPa. a, Raman spectra for a pure hydrogen sample, taken using a probe laser with a wavelength of 647 nm, as function of temperature at pressures between 367 GPa and 350 GPa (black). The Raman spectrum collected 2 μm away on the rhenium gasket is shown in red. The vertical dashed lines indicate the frequency space occupied by the second-order diamond band. DE, diamond edge. **b**, Example spectrum of the sample (black) and the gasket (2 μm away, red), collected at 361 GPa, and the difference between them (blue).

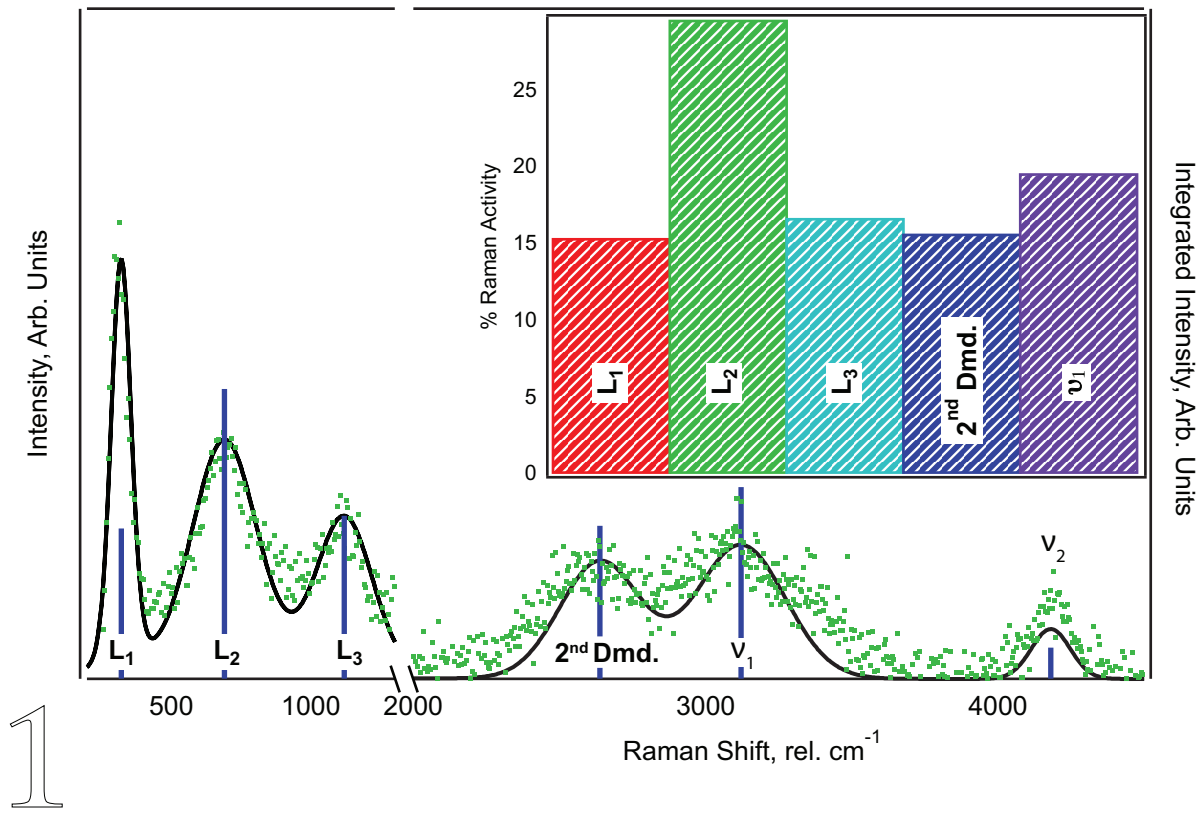

1

Extended Data Figure 7 | Calculating relative integrated intensities. Representative Raman spectrum demonstrating how intensities were calculated for a given spectrum. The best fit (black curve) to the experimental data (green points) is shown (measured by the left axis) along with the integrated intensities for each excitation (indicated by the height of the blue bars, measured by the right axis). The inset shows the raw value of the integrated intensities of each excitation in the main figure as a percentage of the total Raman activity. 2nd Dmd., second-order diamond band (unlabelled in the main figure).

Bibliography

[Akahama 04] Yuichi Akahama & Haruki Kawamura. *High-pressure Raman spectroscopy of diamond anvils to 250GPa: Method for pressure determination in the multimegabar pressure range.* Journal of Applied Physics, vol. 96, no. 7, page 3748, 2004.

[Akahama 06] Yuichi Akahama & Haruki Kawamura. *Pressure calibration of diamond anvil Raman gauge to 310 GPa.* Journal of Applied Physics, vol. 100, no. 4, 2006.

[Akahama 10a] Y Akahama, H Kawamura, N Hirao, Y Ohishi & K Takemura. *Raman scattering and x-ray diffraction experiments for phase III of solid hydrogen.* Journal of Physics: Conference Series, vol. 215, page 012056, 2010.

[Akahama 10b] Yuichi Akahama & Haruki Kawamura. *Pressure calibration of diamond anvil Raman gauge to 410 GPa.* Journal of Physics: Conference Series, vol. 215, page 012195, 2010.

[Akahama 10c] Yuichi Akahama, Manabu Nishimura, Haruki Kawamura, Naohisa Hirao, Yasuo Ohishi & Kenichi Takemura. *Evidence from x-ray diffraction of orientational ordering in phase III of solid hydrogen at pressures up to 183 GPa.* Physical Review B, vol. 82, no. 6, page 060101, 2010.

[Ashcroft 68] N. W. Ashcroft. *Metallic Hydrogen: A High-Temperature Superconductor?* Physical Review Letters, vol. 21, pages 1748–1749, 1968.

[Azadi 14] Sam Azadi, Bartomeu Monserrat, W.M.C. M. C. Foulkes & R.J. J. Needs. *Dissociation of High-Pressure Solid Molecular Hydrogen: A Quantum Monte Carlo and Anharmonic Vibrational Study.* Physical Review Letters, vol. 112, no. 16, page 165501, 2014.

[Babaev 04] Egor Babaev, Asle Sudbo & N. W. Ashcroft. *A superconductor to superfluid phase transition in liquid metallic hydrogen.* Nature, vol. 431, pages 666–668, 2004.

[Babaev 05] E. Babaev, a. Sudbø& N. Ashcroft. *Observability of a Projected New State of Matter: A Metallic Superfluid.* Physical Review Letters, vol. 95, page 105301, 2005.

[Baer 07] Bruce J. Baer, William J. Evans & Choong-Shik Yoo. *Coherent Anti-Stokes Raman Spectroscopy of Highly Compressed Solid Deuterium at 300 K: Evidence for a New Phase and Implications for the Band Gap.* Physical Review Letters, vol. 98, page 235503, 2007.

[Baer 08] Bruce J. Baer, Melanie E. Chang & William J. Evans. *Raman shift of stressed diamond anvils: Pressure calibration and culet geometry dependence.* Journal of Applied Physics, vol. 104, page 034504, 2008.

[Baer 09] Bruce J. Baer, William J. Evans & Choong-Shik Yoo. *Erratum: Coherent Anti-Stokes Raman Spectroscopy of Highly Compressed Solid Deuterium at 300 K: Evidence for a New Phase and Implications for the Band Gap [Phys. Rev. Lett. 98, 235503 (2007)].* Physical Review Letters, vol. 102, page 209901, 2009.

[Boehler 04] Reinhard Boehler & Koen De Hantsetters. *New anvil designs in diamond-cells.* High Pressure Research, vol. 24, pages 391–396, 2004.

[Bonev 04] Stanimir a Bonev, Eric Schwegler, Tadashi Ogitsu & Giulia Galli. *A quantum fluid of metallic hydrogen suggested by first-principles calculations.* Nature, vol. 431, pages 669–72, 2004.

[Brovman 72] Brovman. *Properties of metallic hydrogen under pressure.* vol. 35, no. 4, pages 783–787, 1972.

[Chen 13] Ji Chen, Xin-Zheng Li, Qianfan Zhang, Matthew I J Probert, Chris J Pickard, Richard J Needs, Angelos Michaelides & Enge Wang. *Quantum simulation of low-temperature metallic liquid hydrogen.* Nature communications, vol. 4, page 2064, 2013.

[Chijioke 06] Akobuije Chijioke & Isaac F Silvera. *Megabar-Pressure Infrared Study of Hydrogen Deuteride.* vol. 97, page 255701, 2006.

[Datchi 00] Frédéric Datchi, Paul Loubeyre & René LeToullec. *Extended and accurate determination of the melting curves of argon, helium, ice* (H_2O), *and hydrogen* (H_2). Physical Review B, vol. 61, pages 6535–6546, 2000.

[Dewar 01] James Dewar. *The Nadir of Temperature, and Allied Problems.* Proceedings of the Royal Society, vol. 68, pages 360—-366, 1901.

[Diatschenko 85] V. Diatschenko, C. W. Chu, D. H. Liebenberg, D. A Young, M. Ross & R. L. Mills. *Melting curves of molecular hydrogen and molecular deuterium under high pressures between 20 and 373 K.* Physical Review B, vol. 32, no. 1, pages 381—-389, 1985.

[Drozdov 15] A. P. Drozdov, M. I. Eremets, I. A. Troyan, V. Ksenofontov & S. I. Shylin. *Conventional superconductivity at 203 K at high pressures.* Nature, vol. 525, pages 73–76, 2015.

[Drummond 15] N. D. Drummond, Bartomeu Monserrat, Jonathan H. Lloyd-Williams, P. López Ríos, Chris J. Pickard & R. J. Needs. *Quantum Monte Carlo study of the phase diagram of solid molecular hydrogen at extreme pressures.* Nature Communications, vol. 6, page 7794, 2015.

[Dubrovinsky 12] Leonid Dubrovinsky, Natalia Dubrovinskaia, Vitali B Prakapenka & Artem M Abakumov. *Implementation of micro-ball nanodiamond anvils for high-pressure studies above 6[thinsp]Mbar.* Nature Communications, vol. 3, page 1163, 2012.

[Dunstan 89] D. J. Dunstan. *Theory of the Gasket in Diamond Anvil Cells.* Review of Scientific Instruments, vol. 60, 1989.

[Elkins-Tanton 06] Linda T. Elkins-Tanton. Jupiter and saturn. New York: Chelsea House, 2006.

[Eremets 09] M. I. Eremets & I. A. Trojan. *Evidence of maximum in the melting curve of hydrogen at megabar pressures.* JETP Letters, vol. 89, pages 174–179, 2009.

[Eremets 11] M. I. Eremets & I. A. Troyan. *Conductive dense hydrogen.* Nature Materials, vol. 10, pages 927–931, 2011.

[Faraday 59] M. Faraday. *Not on Regelation.* Proceedings of the Royal Society, vol. 10, pages 440–450, 1859.

[Forman 72] R. Forman, G. Piermarini, J. Barnett & S. Block. *Pressure Measurement Made by the Ulilization of Ruby Sharp-Line Luminescence.* Science, vol. 176, pages 284–285, 1972.

[Goncharov 11] Alexander F Goncharov, Russell J Hemley, Ho-kwang Mao, Alexander F Goncharov, Russell J Hemley & Ho-kwang Mao. *Vibron frequencies of solid H2 and D2 to 200 GPa and implications for the P T phase diagram Vibron frequencies of solid H 2 and D 2 to 200 GPa and implications for the P T phase diagram.* The Journal of chemical physics, vol. 134, page 174501, 2011.

[Goncharov 12] Alexander F. Goncharov. *Raman Spectroscopy at High Pressures.* International Journal of Spectroscopy, vol. 2012, pages 1–16, 2012.

[Gregoryanz 03] Eugene Gregoryanz, Alexander F. Goncharov, Kiyoto Matsuishi, Ho-kwang Mao & Russell J. Hemley. *Raman Spectroscopy of Hot Dense Hydrogen.* Physical Review Letters, vol. 90, page 175701, 2003.

[Gregoryanz 05] Eugene Gregoryanz, Olga Degtyareva, Maddury Somayazulu, Russell J. Hemley & Ho-kwang Mao. *Melting of Dense Sodium.* Physical Review Letters, vol. 94, page 185502, 2005.

[Guillaume 11] Christophe L. Guillaume, Eugene Gregoryanz, Olga Degtyareva, Malcolm I. McMahon, Michael Hanfland, Shaun Evans, Malcolm Guthrie, Stanislav V. Sinogeikin & H-K. Mao. *Cold melting and solid structures of dense lithium.* Nature Physics, vol. 7, pages 211–214, 2011.

[Haken 95] H. Haken & H. C. Wolf. Molecular physics and elements of quantum chemistry. Springer-Verlag, Berlin, 1995.

[Hanfland 85] M. Hanfland, K. Syassen, S. Fahy, S. G. Louie & M. L. Cohen. *Pressure dependence of the first-order Raman mode in diamond.* Physical Review B, vol. 31, pages 6896–6899, 1985.

[Hazen 87] R. M. Hazen, H. K. Mao, L. W. Finger & R. J. Hemley. *Single-crystal x-ray diffraction of n-H_2 at high pressure.* Physical Review B, vol. 36, pages 3944–3947, 1987.

[Hemley 88] R. Hemley & H. Mao. *Phase Transition in Solid Molecular Hydrogen at Ultrahigh Pressures.* Physical Review Letters, vol. 61, no. 7, pages 857–860, 1988.

[Herzberg 60] G. Herzberg. Molecular spectra and molecular structure. D. Van Nostrand Company, New York, 1960.

[Hill 29] L Hill & E Kemble. *On The Raman Effect In Gases.* Proceedings of the National Academy of Sciences of the United States of America, vol. 15, pages 387—-392, 1929.

[Howie 12a] Ross T. Howie, Christophe L. Guillaume, Thomas Scheler, Alexander F. Goncharov & Eugene Gregoryanz. *Mixed Molecular and Atomic Phase of Dense Hydrogen.* Physical Review Letters, vol. 108, page 125501, 2012.

[Howie 12b] Ross T. Howie, Thomas Scheler, Christophe L. Guillaume & Eugene Gregoryanz. *Proton tunneling in phase IV of hydrogen and deuterium.* Physical Review B, vol. 86, page 214104, 2012.

[Howie 13a] Ross T. Howie, Eugene Gregoryanz & Alexander F. Goncharov. *Hydrogen (deuterium) vibron frequency as a pressure comparison gauge at multi-Mbar pressures.* Journal of Applied Physics, vol. 114, no. 7, page 073505, 2013.

[Howie 13b] R.T. Howie. *Optical Studies of Dense Hydrogen at Multi-Megabar Pressures.* PhD thesis, The University of Edinburgh, 2013.

[Kapitza 38] P. Kapitza. *Viscosity of Liquid Helium below the λ-Point.* Nature, vol. 141, no. 3558, pages 74–74, 1938.

[Kechin 01] Vladimir Kechin. *Melting curve equations at high pressure.* Physical Review B, vol. 65, page 052102, 2001.

[Knudson 15] M. D. Knudson, M. P. Desjarlais, A. Becker, R. W. Lemke, K. R. Cochrane, M. E. Savage, D. E. Bliss, T. R. Mattsson & R. Redmer. *Direct observation of an abrupt insulator-to-metal transition in dense liquid deuterium.* Science, vol. 384, pages 1455–1460, 2015.

[Landsberg 28] Gr. Landsberg & L. Mandelstam. *Über die Lichtzerstreuung in Kristallen.* Zeitschrift fur Physik, vol. 50, pages 769–780, 1928.

[Liu 00] Ming Liu, Les Bursill, S Prawer & R Beserman. *Temperature dependence of the first-order Raman phonon line of diamond.* Physical Review B, vol. 61, pages 3391–3395, 2000.

[Liu 13] Hanyu Liu, Eduardo R. Hernández, Jun Yan & Yanming Ma. *Anomalous Melting Behavior of Solid Hydrogen at High Pressures.* The Journal of Physical Chemistry C, vol. 117, pages 11873–11877, 2013.

[Loa 12] I. Loa, R. J. Nelmes, L. F. Lundegaard & M. I. McMahon. *Extraordinarily complex crystal structure with mesoscopic patterning in barium at high pressure.* Nature Materials, vol. 11, pages 627–632, 2012.

[Loubeyre 96] P. Loubeyre, R. LeToullec, D. Hausermann, M. Hanfland, R. J. Hemley, H-K. Mao & L. Finger. *X-ray diffraction and equation of state of hydrogen at megabar pressures.* Nature, vol. 383, pages 702–704, 1996.

[Loubeyre 13] Paul Loubeyre, Florent Occelli & Paul Dumas. *Hydrogen phase IV revisited via synchrotron infrared measurements in H 2 and D2 up to 290 GPa at 296 K.* Physical Review B, vol. 87, page 134101, 2013.

[Ma 09] Yanming Ma, Mikhail Eremets, Artem R. Oganov, Yu Xie, Ivan Trojan, Sergey Medvedev, Andriy O. Lyakhov, Mario Valle & Vitali Prakapenka. *Transparent dense sodium.* Nature, vol. 458, pages 182–185, 2009.

[Magdău 13] Ioan B. Magdău & Graeme J. Ackland. *Identification of high-pressure phases III and IV in hydrogen: Simulating Raman spectra using molecular dynamics.* Physical Review B, vol. 87, pages 1–8, 2013.

[Mao 76] H. K. Mao & P. M. Bell. *High-Pressure Physics: The 1-Megabar Mark on the Ruby R1 Static Pressure Scale.* Science, vol. 191, pages 851–852, 1976.

[Mao 78] H. K. Mao & P. M. Bell. *Observations of Hydrogen at Room Temperature (25° C) and High Pressure (to 500 Kilobars).* Science, vol. 203, pages 1004–1006, 1978.

[Mao 94] H-K. Mao & R. J. Hemley. *Ultrahigh-pressure transitions in solid hyrdogen.* Reviews of modern Physics, vol. 6, pages 671–692, 1994.

[McMahon 11] Jeffrey M. McMahon & David M. Ceperley. *Ground-State Structures of Atomic Metallic Hydrogen.* Physical Review Letters, vol. 106, page 165302, 2011.

[Minsky 57] M Minsky. *Microscopy Apparatus.* US Patent 3013467, vol. 3013467, no. 3013467, page 5, 1957.

[Mitra 69] S. Mitra, O. Brafman, W. Daniels & R. Crawford. *Pressure Induced Phonon Frequency Shifts Measured by Raman Scattering.* Physical Review, vol. 186, pages 942–944, 1969.

[Monserrat 15] Bartomeu Monserrat. *Private Correspondance.* email, August 2015.

[Morales 10] Miguel A. Morales, Carlo Pierleoni, Eric Schwegler & D. M. Ceperley. *Evidence for a first-order liquid-liquid transition in high-pressure hydrogen from ab initio simulations.* Proceedings of the National Academy of Sciences, vol. 107, pages 12799–12803, 2010.

[Narygina 11] O. Narygina, E. E. McBride, G. W. Stinton & M. I. McMahon. *Melting curve of potassium to 22 GPa.* Physical Review B, vol. 84, page 054111, 2011.

[Newton 87] Issac. Newton. Philosophiæ naturalis principia mathematica. 1687.

[Onnes 11] H. K. Onnes. *The resistance of pure mercury at helium temperatures.* Commun. Phys. Lab. Univ. Leiden, vol. 12, page 120, 1911.

[Orloff 00] Jon Orloff, Chandrabhas Narayana & Arthur L. Ruoff. *Use of focused ion beams for making tiny sample holes in gaskets for diamond anvil cells.* Review of Scientific Instruments, vol. 71, pages 216–219, 2000.

[Pérez 06] Fernando Rull Pérez & Jesus Martinez-frias. *Raman spectroscopy goes to Mars.* Spectroscopy Europe, vol. 18, pages 18–21, 2006.

[Perkins 26] J. Perkins. *On the Progressive Compression of Water by High Degrees of Force, with Some Trials of Its Effects on Other Fluids.* Philosophical Transactions of the Royal Society of London, vol. 116, pages 541–547, 1826.

[Pickard 07] Chris J. Pickard & Richard J. Needs. *Structure of phase III of solid hydrogen.* Nature Physics, vol. 3, pages 473–476, 2007.

[Pickard 11] Chris J Pickard & R J Needs. *Ab initio random structure searching.* Journal of Physics: Condensed Matter, vol. 23, no. 5, page 053201, 2011.

[Pickard 12] Chris J. Pickard, Miguel Martinez-Canales & Richard J. Needs. *Density functional theory study of phase IV of solid hydrogen.* Physical Review B, vol. 85, page 214114, 2012.

[Raman 28a] C.V. Raman & Krishnan K.S. *A new type of secondary radiation.* Nature, no. 121, page 501, 1928.

[Raman 28b] C.V. Raman & Krishnan K.S. *The Optical Analogue of the Compton Effect.* Nature, vol. 121, page 711, 1928.

[Ramaswamy 30] C Ramaswamy. *Infra-red Spectrum of Diamond by Infra-red Spectrometer and Raman Methods.* Nature, vol. 125, no. 3158, page 704, 1930.

[Rasetti 29] F. Rasetti. *Incoherent Scattered Radiation in Diatomic Molecules.* Physical Review, vol. 34, pages 367–371, 1929.

[Sanloup 13] Chrystèle Sanloup, James W E Drewitt, Zuzana Konôpková, Philip Dalladay-Simpson, Donna M Morton, Nachiketa Rai, Wim van Westrenen & Wolfgang Morgenroth. *Structural change in molten basalt at deep mantle conditions.* Nature, vol. 503, pages 104–107, 2013.

[Scandolo 03] Sandro Scandolo. *Liquid-liquid phase transition in compressed hydrogen from first-principles simulations.* Proceedings of the National Academy of Sciences of the United States of America, vol. 100, pages 3051–3, 2003.

[Scheler 11] Thomas Scheler, Olga Degtyareva & Eugene Gregoryanz. *On the effects of high temperature and high pressure on the hydrogen solubility in rhenium.* The Journal of Chemical Physics, vol. 135, page 214501, 2011.

[Smekal 23] A. Smekal. *Zur Quantentheorie der Dispersion.* Naturwissenschaften, vol. 11, page 873, 1923.

[Smith 14] R. F. Smith, J. H. Eggert, R. Jeanloz, T. S. Duffy, D. G. Braun & J. R. Patterson. *Ramp compression of diamond to five terapascals.* Nature, vol. 511, pages 330–333, 2014.

[Subramanian 11] Natarajan Subramanian, Alexander F Goncharov, Viktor V Struzhkin, Maddury Somayazulu & Russell J Hemley. *Bonding changes in hot fluid hydrogen at megabar pressures.* Proceedings of

the National Academy of Sciences of the United States of America, vol. 108, pages 6014–6019, 2011.

[Tamblyn 10] Isaac Tamblyn & Stanimir A. Bonev. *Structure and Phase Boundaries of Compressed Liquid Hydrogen.* Physical Review Letters, vol. 104, page 065702, 2010.

[Thomson 50] William Thomson. *The Effect of Pressure in Lowering the Freezing Point of Water Experimentally Demonstrated.* vol. 37, pages 123—-127, 1850.

[Vestel 12] Michael Vestel, Caterina Netti, Erkinjon Nazarov, Gareth Dobson, Stephen Coy, Richard Copeland, Michael Coggiolo, Lawrence Dubios, Alexander Hallock & Joseph Setter. *Surface Enhanced Raman Sepctroscopy Detection with Ion Seperation Pre-Filter*, 2012.

[Weir 59] C. E. Weir, E. R. Lippincott, a Van Valkenburg & E. N. Bunting. *Infrared studies in the 1- to 15-micron region to 30,000 atmospheres.* Journal of Research of the National Bureau of Standards Section A: Physics and Chemistry, vol. 63A, no. 1, page 55, 1959.

[Weir 63] C. E. Weir, E. R. Lippincott & A. Van Valkenburg. *High Pressure Optical Cell*, 1963.

[Wigner 35] E. Wigner & H. B. Huntington. *On the Possibility of a Metallic Modification of Hydrogen.* The Journal of Chemical Physics, vol. 3, page 764, 1935.

[Xu 86] J. A. Xu, H. K. Mao & P. M. Bell. *High-Pressure Ruby and Diamond Fluorescence: Observations at 0.21 to 0.55 Terapascal.* Science, vol. 232, pages 1404–1406, 1986.

[Yang 91] Bijun Yang, Michael D. Morris & Harry Owen. *Holographic Notch Filter for Low-Wavenumber Stokes and Anti-Stokes Raman Spectroscopy.* Applied Spectroscopy, vol. 45, no. 9, pages 1533–1536, 1991.

[Zha 03] Chang-Sheng Zha & W. A. Bassett. *Internal resistive heating in diamond anvil cell for in-situ x-ray diffraction and Raman scattering.* Review of Scientific Instruments, vol. 74, page 1255, 2003.

[Zha 12] Chang-Sheng Zha, Zhenxian Liu & Russell J. Hemley. *Synchrotron Infrared Measurements of Dense Hydrogen to ∼360 GPa.* Physical Review Letters, vol. 108, page 146402, 2012.

[Zha 14] Chang-Sheng Zha, R E Cohen, Ho-Kwang Mao & Russell J Hemley. *Raman measurements of phase transitions in dense solid hydrogen and deuterium to 325 GPa.* Proceedings of the National Academy of Sciences of the United States of America, pages 1–6, 2014.

Publications

P. Dalladay-Simpson; R. T. Howie; E.Gregoryanz. "Evidence for a new phase of dense hydrogen above 325 gigapascals." *Nature*, **529**, 63–67 (2016).

M. Frost; R. T. Howie; P. Dalladay-Simpson; A. Goncharov; E. Gregoryanz. "Novel high-pressure nitrogen phase formed by compression at low temperature." *Physical Review B* (Awaiting publication).

R. T. Howie; P. Dalladay-Simpson; E.Gregoryanz. "Raman spectroscopy of hot hydrogen above 200 GPa." *Nature Materials*, **14**, 495-499 (2015).

C. Sanloup; J. Drewitt; Z. Konopkova; P. Dalldaday-Simpson; D. Morton; R. Nachiketa; W. van Westrenen; W. Morgenroth. "Structural change in molten basalt at deep mantle conditions." *Nature*, **503**, 104-107. (2013)

K. -A Lorenzer; P. Dalladay-Simpson; F. Kubel; A. Siderenko; A. Prokofiev; S. Paschen. "Structural, magnetic and transport properties of the rare-earth cage compound Ce4Pd12Sn25." *Solid State Phenomena*, **194**, 31-34. (2013)